SRI International

Final Technical Report • July 1998

INSTRUMENTATION FOR AEROSOL AND GAS SPECIATION

Prepared by:

Michael J. Coggiola
Molecular Physics Laboratory

SRI Project 7383
MP 98-059

Prepared for:

NASA Ames Research Center
Earth System Science Division, 239-20
Moffett Field, CA 94035-1000

Approved by:

David R. Crosley, Director
Molecular Physics Laboratory

333 Ravenswood Avenue • Menlo Park, CA 94025-3493 • (650) 859-2000

EXECUTIVE SUMMARY

SRI International, under NASA Grant No. NAG 2-963 (SRI Project 7383), from 1 February, 1995 through 31 January, 1998, designed, fabricated, tested, and deployed a real-time aerosol speciation instrument in NASA's DC-8 aircraft during the Spring 1996 SUbsonic Aircraft: Contrail and Cloud Effects Special Study (SUCCESS) mission. Post-mission laboratory calibrations and data reduction and analysis were also included in the effort.

This new instrument provides real-time chemical analysis of the composition of individual aerosol particles with diameters greater than approximately 0.3 μm. During the SUCCESS mission, this instrument chemically characterized more than 25,000 individual aerosol particles sampled directly from the upper troposphere (UT) during 19 flights. Of these aerosols, approximately 140 were found to contain interesting chemical species, identified as sulfates, nitrates, carbonates, and sulfuric acid. The remaining aerosols showed only evidence of water with no other chemically interesting species present above our detection limit. These represent the first examples of aerosol particles chemically speciated in real-time from an airborne platform in the UT.

As a result of a non-optimum external aerosol sampler, we likely oversampled larger particles. The large amount of water associated with these larger particles and the high ambient humidity encountered during cloud transits where our spectra were taken resulted in the majority of particles appearing to contain only water. Despite these limitations, we were able to chemically characterize many individual aerosol particles. Laboratory studies have largely confirmed the assignment of these aerosol spectra measured in the UT. The paucity of chemically interesting experimental results obtained using this new instrument during its first deployment as part of the SUCCESS mission does not admit making statistically significant observations about the chemical composition of UT aerosol particles. Straightforward changes to the sampling inlet and the instrument will permit such upper tropospheric aerosol compositional observations to be made on future deployments. However, even in its current configuration, this new instrument has demonstrated the ability to chemically characterize in real-time single aerosol particles sampled directly from the troposphere.

CONTENTS

FIGURES

TABLES

INTRODUCTION

Using support from NASA Grant No. NAG 2-963, SRI International successfully completed the project, entitled, "Instrumentation for Aerosol and Gas Speciation." This effort (SRI Project 7383) covered the design, fabrication, testing, and deployment of a real-time aerosol speciation instrument in NASA's DC-8 aircraft during the Spring 1996 SUbsonic aircraft: Contrail and Cloud Effects Special Study (SUCCESS) mission. This final technical report describes the pertinent details of the instrument design, its abilities, its deployment during SUCCESS and the data acquired from the mission, and the post-mission calibration, data reduction, and analysis.

CHEMICAL CHARACTERIZATION OF AEROSOLS

A critical requirement in accurately assessing the effects on the atmosphere of the worldwide subsonic fleet of aircraft is a complete, accurate, chemical characterization of all kinds of aerosols by simple and reliable means. Whether the issue is ozone concentrations or radiation transfer and its climatic consequences, aerosols play an important role, yet detailed understanding of their behavior is noticeably lacking. An important component in understanding and predicting the effects of the large fleet of subsonic aircraft is the ability to readily make accurate *in-situ,* chemical composition measurements of atmospheric aerosols, correlated with their size and abundance as well as with the location, altitude, and time of collection. The chemical composition of aerosols in the region near the tropopause will dictate their chemical reactivity, transport, and transformation and will significantly influence meteorology.

To achieve chemical speciation of individual aerosol particles researchers have used a variety of experimental techniques, including optical (infrared) spectroscopy [Sageev-Grader et al., 1987], micro-beam methods [Gorzelska et al., 1994; Post and Buseck, 1984; Kim and Hopke, 1988; Hoffer and Van Grieken, 1993; Xhoffer et al., 1993], and numerous mass spectrometric approaches [Johnston and Wexler, 1995]. The mass spectrometric methods can be divided into two broad categories: those that employ a laser for volatilization/ionization, and those that use thermal vaporization combined with conventional electron impact ionization (EI). Our instrument is of the latter type. The use of this approach offers several advantages over laser ionization schemes. Laser methods must rely on a precisely timed laser trigger and spatially localized aerosol beam to ensure adequate overlap of the photon pulse with the moving particle. These constraints often lead to a low probability of obtaining ions from an individual particle. In contrast, virtually all of the particles that exit the differentially pumped aerosol inlet of our instrument enter the

analysis region where their trajectory necessarily brings them into contact with the thermal vaporization surface. EI is a universal ionization method that produces predictable ion products from most all vapor species. The specific ion species (both parent molecular ions and fragments) and their relative abundances produced by EI are determined largely by the electron energy, universally chosen to be 70 eV. Conversely, the ion species generated by laser ionization schemes are known to vary widely depending on the wavelength, pulse energy, pulse duration, geometric overlap with the aerosol particle, focal properties of the laser beam, details of the energy transfer from the laser to the particle, vaporization of the particle, and subsequent ionization of the vapor plume by plasma or multiphoton processes [Murphy and Thomson, 1995; Neubauer et al., 1995; Mansoori et al., 1994].

Under grant NAG 2-963, SRI developed an instrument that provides real-time chemical analysis of the composition of aerosol particles with diameters down to approximately 0.3 μm or smaller in the general tropopause region. This *in-situ* aerosol measuring instrument determines abundances, and chemical composition of upper tropospheric (UT) and lower stratospheric (LS) aerosols. The instrument is based largely on commercially available technology, including a time-of-flight mass spectrometer (TOFMS), coupled with a sampling system and a laser scattering particle detector. A direct sampling method and differential vacuum pumping scheme is used to introduce the aerosols into the mass spectrometer. Volatilization of aerosols on a heated surface within the ion source volume followed by complete mass spectrometric analysis of the resulting vapors using electron impact ionization yields the information required.

CONTRIBUTION TO OVERALL MISSION GOALS

The need for greater, more detailed characterization and quantification of tropospheric aerosols has been well documented. For example, in a 1993 report prepared for the Department of Energy (Quantifying and Minimizing Uncertainty of Climate Forcing by Anthropogenic Aerosols, DOE/NBB-0092T, March, 1993.), the authors reviewed existing data, as well as the required data and the types of experiments that would be required to obtain that information. They noted that *in-situ* measurements of the physical properties of aerosols was, by itself, not sufficient to fully understand the aerosols' role in climate forcing. They concluded that chemical information was essential to identify and quantify aerosol types and to relate these properties to the aerosol and precursor gas sources. They recommended that aircraft-based instruments be used to obtain vertical and horizontal profiles of key aerosol properties, and to provide *in-situ* observations of cloud microphysical and chemical properties. We anticipate that the deployment of our instrument will provide exactly those types of observations.

A recent review by J. Heintzenberg [1989] pointed out that despite the importance of the particulate composition and abundance in the troposphere above the boundary layer, only minimal data exist. He notes that serious shortcomings in that data limit the data's usefulness in radiative and cloud models. More recently, some limited chemical speciation of aerosols has been reported as part of the Global Backscattering Experiment (GLOBE) and the Global Tropospheric Experiment/Arctic Boundary Layer Expedition (GTE/ABLE). In both missions, bulk collection of the aerosols was followed by chemical analysis using HPLC and ion chromatography in the former case, and energy dispersive x-ray analysis in the latter case. The GLOBE measurements provide chemical speciation of aerosols. However, they represent only an average because of the bulk collection method required to provide sufficient sample volume. The GTE/ABLE measurements were particulate specific, but provided only limited elemental composition.

Only a real-time, *in-situ,* analytical method can provide single-particle chemical composition information of the type required. Real-time single-particle analysis also allows correlation of the size and type of aerosol particles with other tropospheric species, such as ozone and nitrogen oxides. The instrument developed from an airborne platform and deployed as a result of this project represents the first attempt to measure in real-time and the chemical composition of upper tropospheric aerosols.

PROJECT ACCOMPLISHMENTS

INSTRUMENT DESIGN

Our design for the particulate mass spectrometer consists of a differentially pumped aerosol inlet; a small, diode-laser-based, optical particle counter (OPC) that provides a timing trigger; a heated surface for rapid vaporization of the particle under vacuum conditions; a reflectron, time-of-flight (TOF) mass spectrometer using EI to ionize the vaporized species; and a computer for data acquisition and experiment control. Figure 1 shows a schematic representation of our instrument in its SUCCESS mission configuration.

Many of the design choices were dictated by the strict time deadline imposed by the mission aircraft integration schedule. Although SRI was notified of the grant award in the middle of 1994, funding was not available to us until February 1995. As a result, we had only 13 months to complete the entire instrument design, assembly, testing, and aircraft integration. Of necessity, this very short time period resulted in a number of design shortcomings and compromises that limited instrument performance. Despite these shortcomings, and the fact that this was the first airborne deployment of a real-time aerosol characterization instrument, it functioned successfully.

EXTERNAL AEROSOL INLET

The main criterion for the design of an aircraft aerosol sampling inlet is to acquire particles with minimum sampling bias or distortion of the size distribution, and minimum evaporative loss of volatile components. Losses due to turbulent deposition or inertial impaction are of concern as well. To eliminate size discrimination, we must use an isokinetic probe in which the velocity of the sample stream relative to the probe tip remains the same inside the probe as it is outside the aircraft [Porter et al., 1992; Daum and Springton, 1993].

The inlet system that was used to sample aerosols directly from the upper troposphere under flight conditions and transfer them to the instrument for speciation consisted of three components: (1) the external aerosol sampler, (2) the aerosol transfer line, and (3) the differentially pumped, capillary, sampling system.

Because of the experimental configuration and location of our instrument on the DC-8, and the use of the forward-most window on the port side of the aircraft (station 290), we were restricted in our choice of external samplers to a simple, forward-facing probe. This probe was

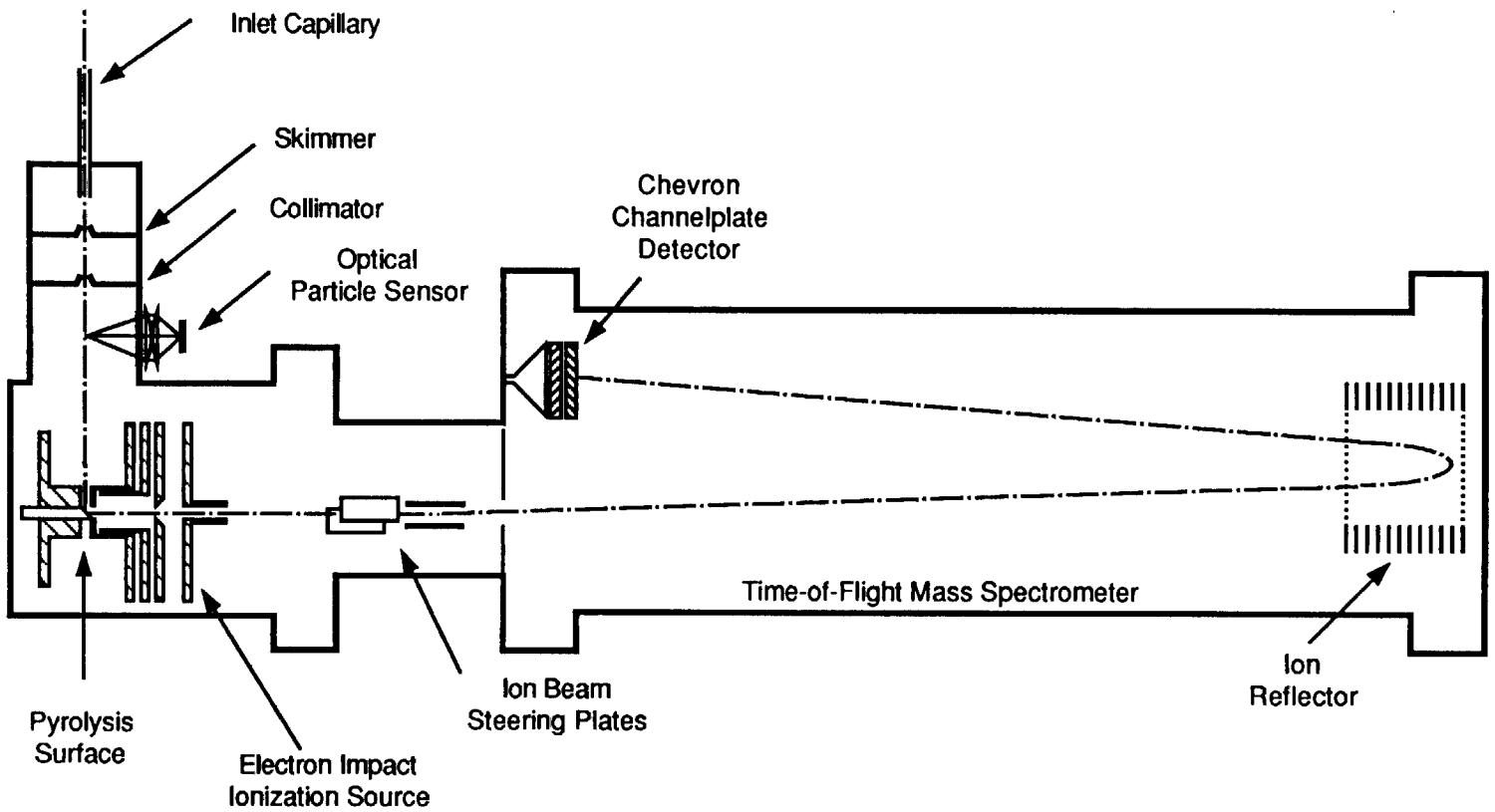

Figure 1. Schematic diagram of the real-time aerosol mass spectrometer instrument.

supplied by ARC, and is shown in their drawing 4237474. The probe consists of a metal tube 3.175 cm in diameter that extends approximately 30 cm beyond the aircraft exterior, mounted on a curved, passenger port plate. The probe turns 45° with a bend radius of approximately 42 cm. A conical diffuser probe tip with a 0.635 cm sample orifice and a 20.2° half-angle was added to the end of the probe. The conical diffuser probe tip design was provided by the Desert Research Institute, and is the same as used by that group on previous, DC-8 based, aerosol sampling experiments. The centerline of the sampling orifice tilted 6° down with respect to the fuselage centerline to account for the aircraft angle of attack during flight. The approximate Stokes number in the inlet ranged from 0.014 to 2.2 for particles in the size range from 0.4 to 5 μm.

Aerosols sampled through this probe were transported through approximately 1 m of 0.635-cm-id, conductive silicone tubing (TSI, St. Paul, Minnesota) to the instrument inlet. Figure 2 shows the configuration of the DC-8 sample inlet and vent lines. Approximately half of the 4 L/min air stream was drawn inside the instrument via the particle beam generator for analysis by the mass spectrometer. The resulting aerosol inlet was far from ideal, operating in a subisokinetic regime that oversampled larger particles relative to smaller ones [Rader and Marple, 1988]. To a significant degree, this non-ideal aerosol sampling inlet dictated the ultimate lack of success in acquiring large numbers of chemically interesting, small particles. Rather, the subioskinetic operation of the probe resulted in primarily very large particles entering the instrument. Because these large particles were most likely ice particles, our chemical analysis of these aerosols overwhelmingly and not suprisingly showed only water.

As an alternative to the dedicated aerosol inlet described above, we also had the option of directing the sample stream from the NCAR counterflow virtual impactor (CVI) [Twohy and Gandrud, 1998] into our instrument. Although this configuation was used sporatically during the mission, none of the results presented here were obtained using the CVI inlet. In general, we observed that aerosols sampled using the CVI inlet did not appear markely different from those sampled using the dedicated aerosol probe.

PARTICLE BEAM GENERATOR

The second component of the aerosol inlet is the particle beam generator (PBG). The PBG causes the particles in the sampled air stream to take the form of a beam that ultimately strikes the heated surface within the ion source of the mass spectrometer. Our PBG design was adapted from the system developed by Murphy (NOAA, Boulder, Colorado) for direct aerosol sampling from the stratosphere. Figure 3 shows a cross-sectional view of the PBG. This design uses a glass-lined, stainless steel, capillary to restrict the volumetric gas flow entering the vacuum system, and to aerodynamically focus the particles near the centerline of the flow. The inner diameter and

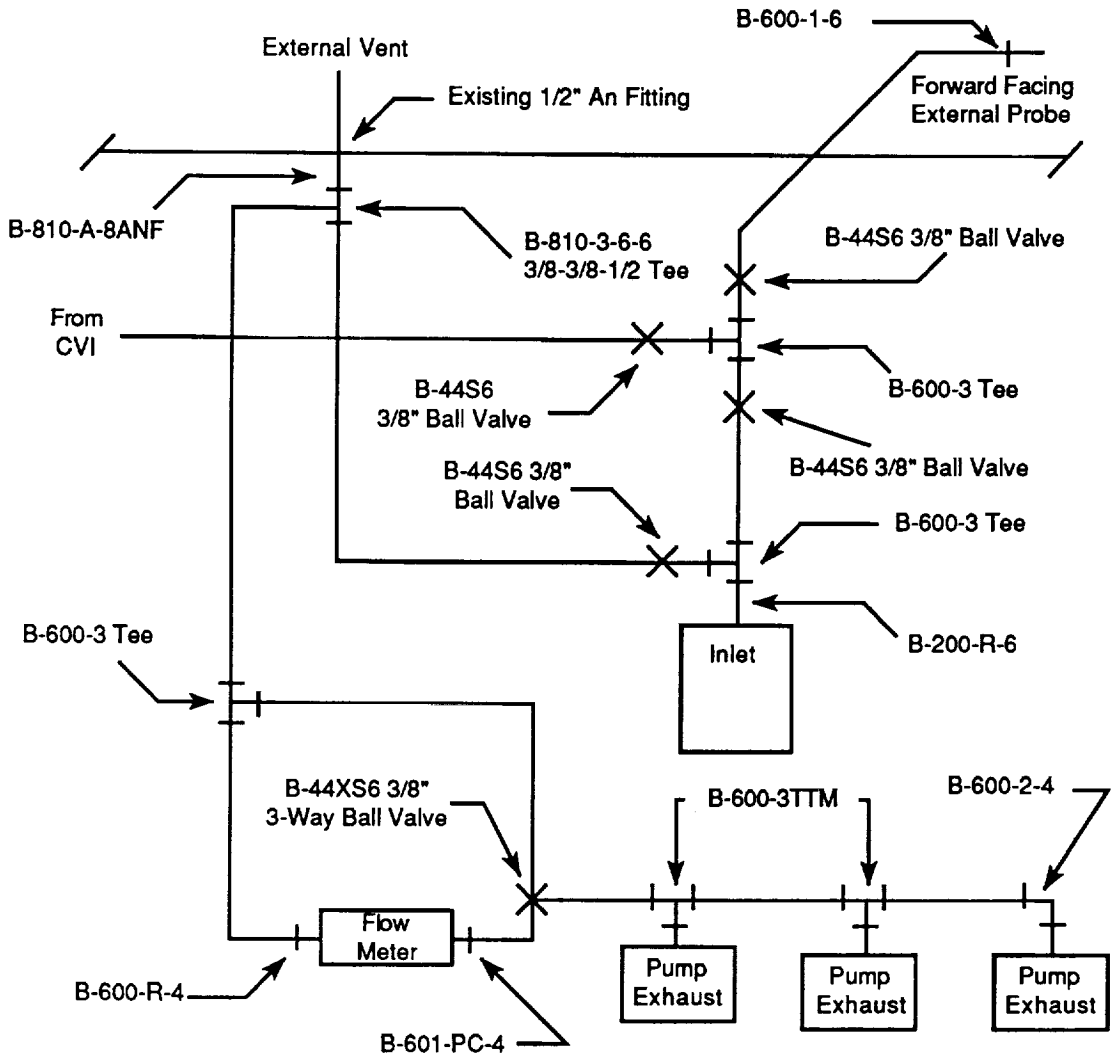

All Lines Are 3/8" OD
X 0.035" Wall Type 3003
Aluminum Tubing

All Fittings Are Swagelok
Unless Otherwise Noted

Figure 2. SUCCESS Mission configuration for sample transfer and vent lines.

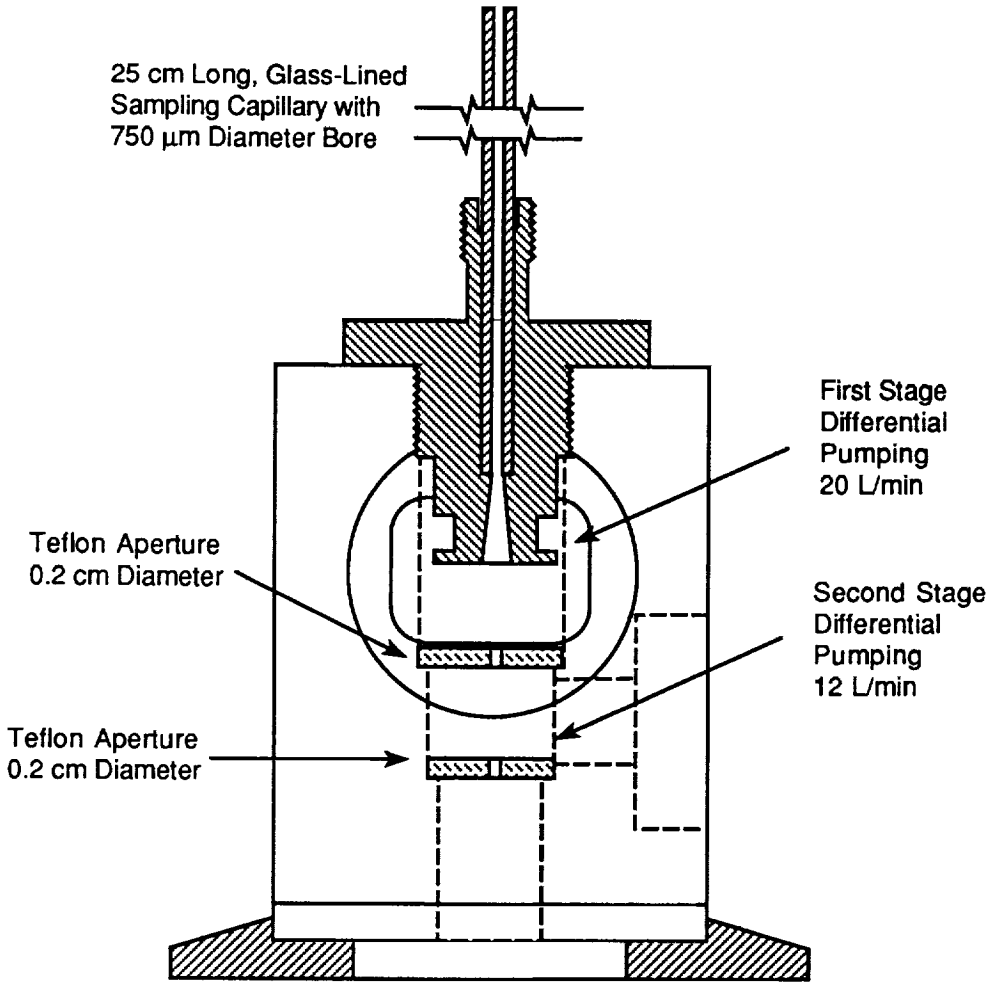

Figure 3. Detailed view of capillary inlet and differential pumping region.

length of the tubing are selected to restrict the volumetric gas flow through the sampler, and thus depend on the ambient pressure from which particles are being sampled. Our design incorporates interchangeable capillaries to accommodate laboratory testing at 760 Torr ambient pressure, and tropospheric sampling at subambient pressures of 150-300 Torr. For the former application, the capillary has a diameter of 750 µm and a length of 25 cm. For the latter case, the corresponding dimensions are 1.5 mm and approximately 15 cm.

Figure 4 illustrates the interface between the sample transfer line connected to the external probe tip and the glass-lined capillary inlet restrictor tube, as well as the details of the differentially pumped aerosol inlet. In actual use, the connection between the conductive silicone tubing and the glass-lined capillary tube was formed using a Swagelok "tee." The capillary tube was inserted into the "tee" until it extended above the side arm leading to the external vent. This configuration was intended to avoid sampling from the turbulent zone produced by the abrupt 90-degree turn in the flow path.

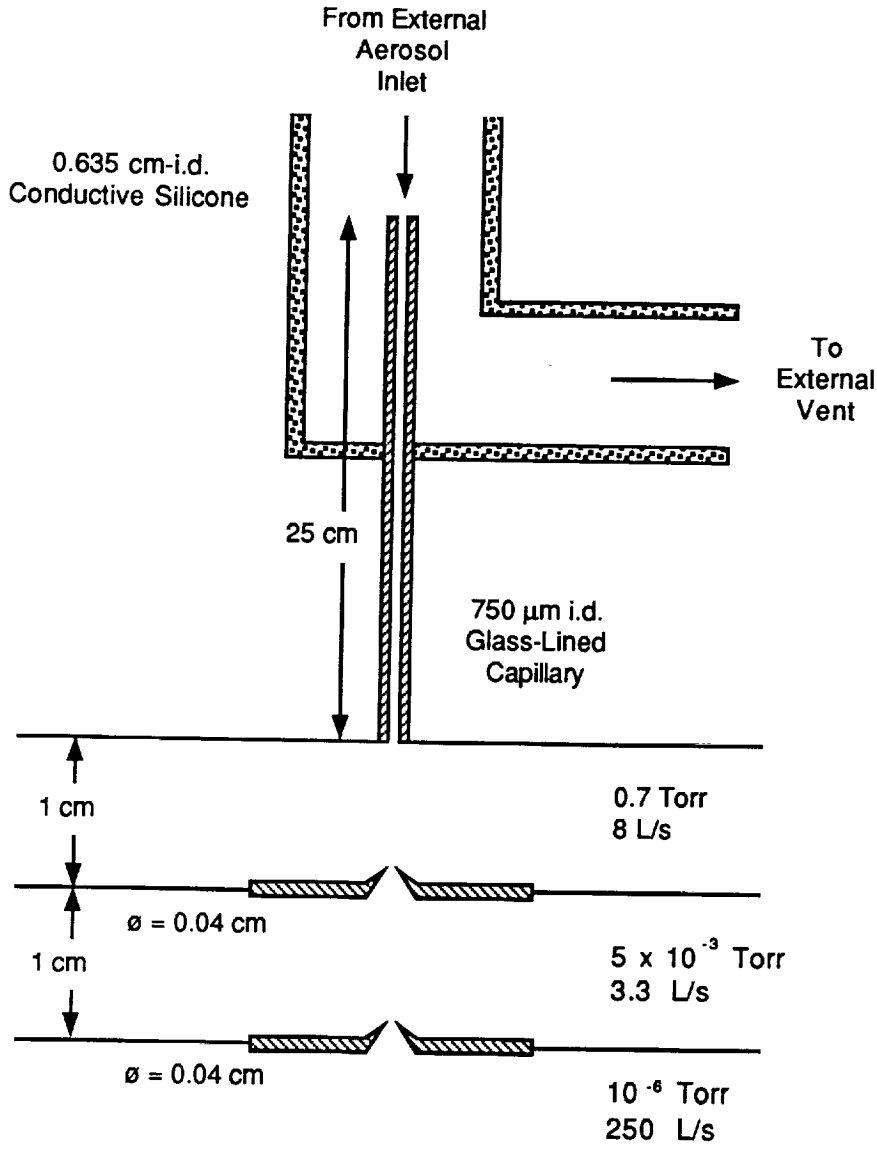

Figure 4. Schematic diagram of the sample transfer system and the differentially pumped aerosol inlet.

Under the typical operating conditions encountered during SUCCESS, a 25 cm length of 750 μm in diameter capillary produced a pressure drop of approximately a factor of 200 from an ambient pressure of 150 Torr to a pressure in the first differential region of 0.7 Torr. The first differential pumping region was defined by the exit of the capillary and a Teflon disk with a sampling orifice 0.04 cm in diameter located 1 cm from the capillary. An 8 L/s mechanical pump was used to remove the excess gas flow from this region. Aerosols and background gas entering the second differential pumping region again traversed a distance of 1 cm before encountering a second Teflon disk with an orifice 0.04 cm in diameter. Pumping in this region was provided by a 3.3 L/s mechanical pump, yielding a typical operating pressure of 5×10^{-3} Torr. The overall effect of the differentially pumped PBG is to significantly enhance the particle/air ratio.

Through the use of a capillary inlet and two stages of differential pumping, the volumetric gas flow at the exit of the aerosol sampler is reduced by approximately four orders of magnitude, while a reasonable fraction of the aerosol particles are retained. Recently, other aerosol inlet designs have been demonstrated based on aerodynamic focusing [Liu et al., 1995]. Although these new designs provide enhanced aerosol transmission as compared with the one used in our instrument, how they would function under the conditions encountered during typical DC-8 flights is not clear.

OPTICAL PARTICLE COUNTER

Upon exiting the second differential pumping region, the aerosol particles pass through the observation region of an optical particle counter. The OPC used on this instrument is a commercial device (Vaculaz-2), manufactured by Particle Measuring Systems (PMS, Boulder, Colorado). This OPC is specifically designed to operate at reduced pressures. The system includes the vacuum interface module, the sensor module, and the control electronics. The vacuum interface module, which couples to the exit of the aerosol sampler, contains the necessary optical windows to admit laser diode radiation from the sensor module and to transmit light scattered from particles to a photodetector also located in the sensor module. The PBG, the OPC vacuum interface module, and the electron impact ionization source are all shown diagrammatically in Figure 5 along with the source region vacuum chamber. The sensor module contains the diode laser, photodiode, and signal preamplifier. The sensor module is driven by the main electronics module that includes a microprocessor to determine the particle size based on the intensity of the scattered laser light.

Our Vaculaz system was modified by PMS to provide a very narrow (100 ns) pulse for each particle that passes through the unit. This pulse is used to trigger the chemical analysis following a time delay corresponding to the aerosol flight time from the OPC to the vaporization

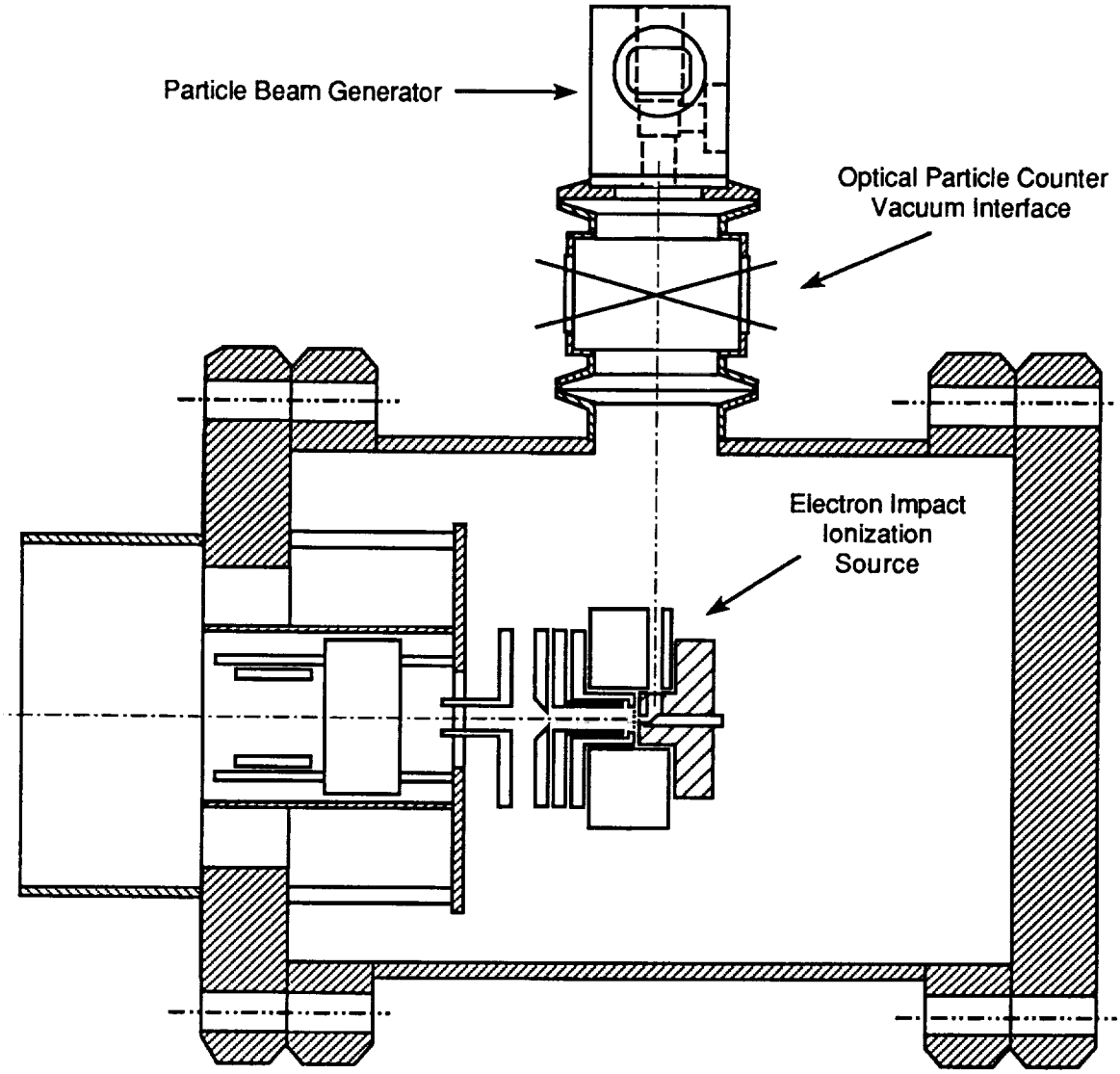

Figure 5. Cross-sectional view of the source chamber showing the differentially pumped capillary inlet, the laser-based particle detector, the ion source with integral thermal vaporization, the ion extraction and focusing lens elements, and the ion deflectors.

region. In addition to the trigger pulse, we planned to have the Vaculaz provide approximate aerosol size information based on the magnitude of the scattered light signal. Normally, the Vaculaz instrument provides four size channels, > 1.0 μm, < 0.50 μm, < 0.35 μm, and a selectable lower size limit that ranges between 0.20 μm and 0.30 μm. Because of the modification of our unit by PMS to provide the prompt trigger pulse, the four-channel sizing feature did not function. Instead, the size threshold for which a trigger pulse is generated can be set to two ranges; particles between 0.20 and 1.0 μm in diameter, and particles greater than 1.0 μm in diameter.

Particles that pass through the OPC then enter the vacuum chamber, directly above the electron impact ion source (see Figure 5). Before to installing the ion source, the aerosol inlet and OPC were temporarily installed onto the vacuum chamber, along with a turbomolecular pump to evacuate the chamber and two mechanical pumps to evacuate the differentially pumped inlet. The smaller capillary inlet was installed on the aerosol sampler, and the entire system evacuated after a grease-covered glass slide was placed in the vacuum chamber at the approximate location of the ion source. Once the pressure in the system was reduced appropriately, a small amount of 3-μm-diameter sodium fluoresceine powder was introduced into the open end of the capillary. These particles were entrained in the ambient gas flow, passed through the differential pumping region and the OPC, and entered the vacuum chamber where they impinged onto the glass slide. The thin layer of vacuum grease captured the particles, allowing a determination of both the spot size (3-4 mm diameter) and the location relative to the nominal center line. This information was used to locate the ion source directly in the path of the particle beam.

AEROSOL VOLATILIZATION

Our instrument uses an indirectly heated, stainless steel surface inclined 45° with respect to the incident aerosol beam to vaporize the particles. The heated target can be seen in Figure 6, which depicts the details of the ion source region. Spot welded onto the front of the target surface are multiple layers of nickel mesh (Buckbee-Meers, Minnesota). The mesh provides numerous wells, wherein aerosols are trapped, forcing them to undergo multiple collisions with the heated surfaces. This technique significantly enhances the probability that an aerosol particle accommodates on the surface long enough to be heated to the nominal target temperature of 600° C, and hence long enough to volatilize. Experiments have shown that at this temperature, most volatile or semi-volatile particles are vaporized within 0.5 ms. The upper temperature limit of 600° C was found experimentally to be restricted by the operating limit of the 0.3-cm-diameter cartridge heater. This temperature is sufficient to volatilize most tropospheric aerosols, with the exception of refractory materials and elemental carbon (soot) [Smith and O'Dowd, 1996].

Attempts to increase the volatilization temperature beyond 600° C resulted in failure of the machinable ceramic (Macor) insulator that held the heater. Because this ceramic piece also forms an integral part of the ionization source, its design could not be easily altered without having a significant impact on the overall source design. It should be possible, however, to change the source design to accommodate a larger heater that could yield a higher volatilization temperature. Alternatively, the indirectly heated volatilization method could be replaced by a directly heated ribbon-like target [Sinha et al., 1982 ; Allen and Gould, 1981]. While the latter approach offers the possibility of achieving vaporization temperatures above 1400° C, our initial attempts to implement this approach resulted in a significant distortion of the electric fields within the ion source, to the point where it would no longer function correctly. Hence, the direct ribbon heater approach was abandoned in favor of the indirect method. It appears that with only a modest amount of additional effort, a directly heated ribbon vaporizer could be incorporated into the present instrument, albeit with a modified ion source.

By design, a large portion of the vapors produced during the volatilization enter directly into the ionization region of the instrument. This is apparent in Figure 6 from the close proximity of the vaporization target to the ionization region located between the two grid structures. The ion optical axis of the source is also at a 45° angle to the volatilization target surface, and hence perpendicular to the aerosol beam.

Mass Spectrometry

The mass spectrometric requirements of our instrument are modest: an upper mass range of 500 amu, with unit mass resolution or better. Due to the significantly wider spatial, temporal, and energy spread of the nascent ions formed by EI as compared to laser ionization, it was necessary to use an ion mirror, or reflectron-type TOF. A significant improvement in resolution and signal level was also obtained through the careful design of the ion source itself [Grix et al., 1989]. Our ion source is based on the design of Wollnik and coworkers at the University of Giessen, Germany. This source is an electron-impact ion source that operates in a space charge mode. Because of the high electron density within the ionization volume, a negative space charge well is generated that traps any positive ions formed. The nominal trapping time is many tens of milliseconds. A combined extraction and ion bunching scheme is then used to produce a narrow ion burst of ~10 ns duration. As a result of the ion bunching, however, the ion burst has a wide energy spread (typically 100 eV). The use of a reflecting ion mirror provides sufficient energy compensation to achieve the required resolution. Once extracted, the ions are spatially focused and deflected so as to enter the flight tube in line with the entrance to the ion mirror.

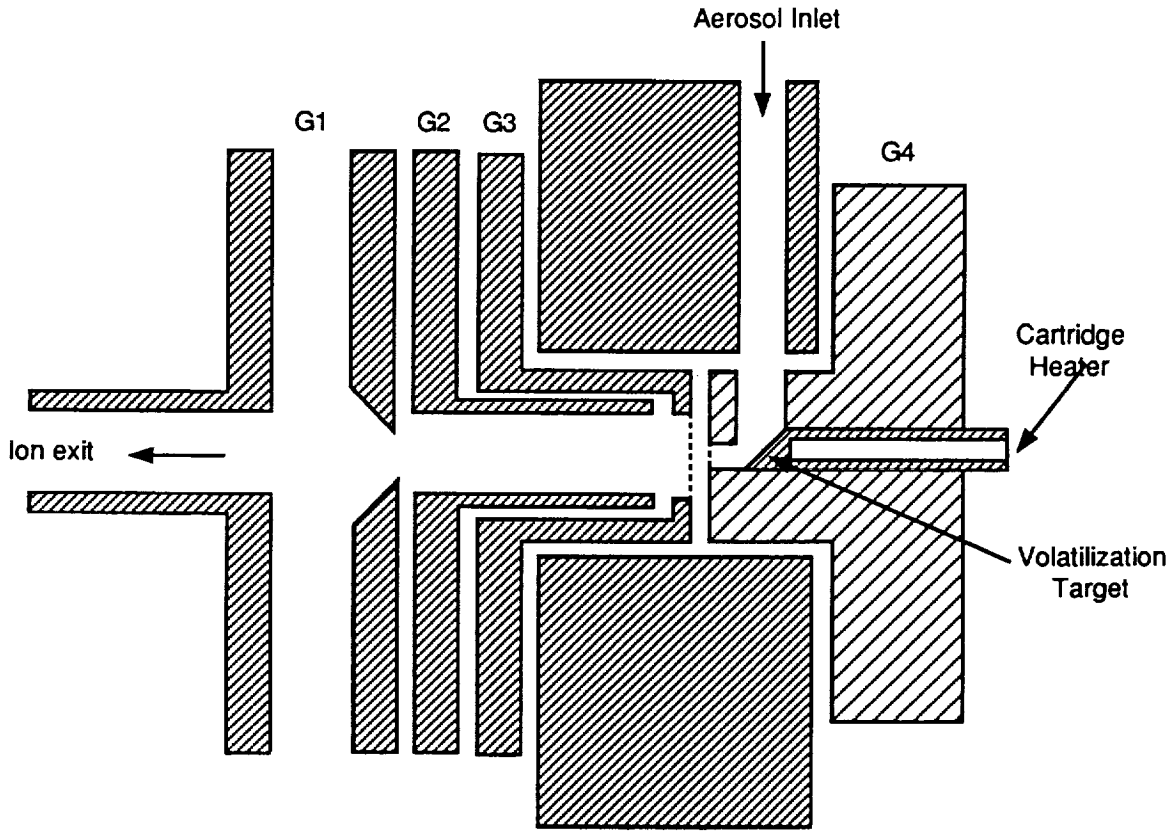

Figure 6. Cross-sectional view of the electron impact ionization source as modified to allow aerosol particles to impinge upon the indirectly heated volatilization surface.

The electrode naming convention follows that of Wollnik [Grix et al., 1989].

Electron Impact Ion Source

The ion source chamber shown in Figure 5 is pumped by a 250 L/s turbomolecular pump. All source components are fabricated either from stainless steel, alumina, Teflon, Vespel, or Macor. In operation, the potentials on the various source elements are adjusted to produce a negative space-charge well between the two electrodes, G2 and G4. Within this small volume, positive ions are formed by 70-eV electron impact and temporarily trapped by the negative well. Not shown in Figure 6 are the two filaments used to generate the intense electron ionization beam. The filaments are located on either side of the source (above and below the plane of Figure 6) with the electrons entering the ionization volume through small slits in the region between electrodes G2 and G4. The electron beams are focused using pairs of small permanent magnets (~300 Gauss) positioned near the filaments. In addition, a pair of small repeller electrodes is located on either side of each filament to further enhance the flux of electrons entering the ionization region. Only one filament is used at any given time, with the other filament assembly biased to act as a collector for monitoring the electron (trap) current. The trapping efficiency and duration are functions of the well strength (depth), local pressure, and most importantly, the local ion density.

We chose this ion source design as based on two of its major characteristics: its high ionization efficiency as compared with more conventional EI sources, and its ability to trap nascent positive ions on a millisecond timescale. The former characteristic is of obvious benefit when dealing with a very limited (neutral) sample size, as would be produced by the volatilization of a submicron particle. The latter characteristic is important in the present application because the volatilization process can occur over a variable time period of up to one millisecond. In a conventional EI source, ions formed from a pulse of neutrals produced over this time period time would be lost unless they were ejected from the source by pulsing it rapidly (10 kHz or faster). Such rapid pulsing is possible, however, it has the disadvantage of yielding many spectra, each of which exhibits poor ion statistics due to the relatively low number of ions in each pulse. Moreover, even when pulsed rapidly, a significant number of ions will not be extracted and detected due to the lack of electrostatic containment within the source during the time between extraction pulses. Conversely, the Giesen design allows the majority of ions formed during the full vaporization period to be stored within the source and extracted together in a single ion packet. The total number of ions in each extracted packet is thus higher, producing a mass spectrum of higher statistical quality.

During operation, the voltages applied to electrodes G1, G2, and G3 are maintained at fixed, optimal values. When we want to record a mass spectrum, the potential on G4 is pulsed positive by 200 V to repel ions from the source. The duration of this extraction pulse is typically 100 ns, with very sharply defined rising and falling edges to maintain the high temporal resolution needed to achieve a correspondingly high mass resolution. The magnitude and duration of this pulse is enough to extract essentially all of the ions from the source in a single ion packet. As soon as the potential on G4 returns to its quiescent level, ions immediately begin filling the now empty volume defined by electrodes G2 and G4.

Although the above cited advantages of this source are critical for maximizing the signal levels produced from the limited amount of neutral vapor resulting from the aerosol vaporization, they also lead to a serious limitation in instrument operation. As noted above, the trapping time and efficiency are largely determined by the number of ions within the trapping volume. As the trapping region fills with positive ions, they begin to effectively neutralize the trapping potential, which in turn allows the more energetic ions to escape from the trap. As the ion density increases further, the resulting positive space charge will begin to actively repel ions from the region.

Given the size of the trapping region, the static electrode potentials, and the typical electron flux, one can estimate that the region can hold approximately 10^4 to 10^5 ions before the space charge effects begin to influence the source operation. If these ions were only associated with the vaporized aerosol molecules, then one would not anticipate much loss in sensitivity as the trap

began to fill, because the expected yield from a 0.5 μm aerosol in on the order of 10^5 ions. Unfortunately, however, the trapping region is always filled with positive ions formed by ionization of the background vapors that are present within the source volume. Thus, when an aerosol particle is vaporized and the nascent neutral molecules enter the source volume and become ionized, they must displace the background ions already within the trapping region. Although this ion displacement can and does occur, it is equally likely that the desired signal ions arising from the aerosol vapors will be displaced by the undesirable background ions. The net effect of this action is to limit both the dynamic range of the source and the signal-to-background ratio.

The dynamic range limitation imposed by the ion source design can be understood by estimating the signal levels associated with an aerosol particle whose bulk composition is water with a minor constituent (say 1% by weight) of ammonium sulfate. The number of neutral water molecules produced by vaporization of a 0.5 μm diameter particle, for example, is on the order of 2×10^9, and the corresponding number of ions produced by this source would be approximately 10^5. The literature suggests that the vaporization of aqueous aerosol particles initially produces water vapor followed by vapors of the minor components. Because of the space-charge imposed limit of 10^5 ions in the trapping region, the initial production of ions from water vapor would fill the trapping region and effectively prevent the storage of ammonium sulfate ions. Therefore, although the 1% ammonium sulfate constituent could potentially generate 10^3 ions from 2×10^7 vaporized neutral molecules, the actual number of ammonium sulfate ions that would remain trapped could be substantially less. Furthermore, because the extent of this discrimination due to space-charge effects is strongly dependent on the local neutral vapor density, the discrimination would vary with the cube (volume) of the particle size.

Time-of-Flight Mass Spectrometer

The mass spectrometer includes the flight tube, the ion mirror ("reflectron"), and the detector. The latter three components were purchased as a commercial unit from the R. M. Jordan Company, Grass Valley, California. The flight tube is a 61 cm long, 20 cm in diameter stainless steel chamber evacuated by a 250 L/s turbomolecular pump. The pressure under operating condition is 10^{-7} Torr. Ions entering the flight tube from the source chamber travel the length of the flight tube in a field-free region before entering a two-grid ion mirror. Potentials on the ion mirror cause the ions to decelerate, stop, reverse direction, and reaccelerate toward the detector. The detector is a dual, microchannel plate (MCP), electron multiplier with a 50 Ω terminated electron collector. The signal from the collector is fed directly into the analog-to-digital converter where it is digitized to generate the arrival time spectrum.

During laboratory calibration, we could routinely observe characteristic mass spectra of single polystyrene latex particles with diameters of 0.482 μm. Based on the magnitude of the observed ion signals, we estimated that fully vaporized particles with diameters down to approximately 0.25 μm could be detected above the background level, although this was not verified experimentally before deployment. Subsequent post-flight tests showed this lower limit to be true, at least for polystyrene latex particles. Because we lacked the ability to dynamically size laboratory-generated particles, we could not verify the lower size limit for any other particle composition.

DATA ACQUISITION SYSTEM

Given the fixed ion flight path and a nominal ion energy of 1.7 keV, and the desired mass range of 500 amu, an analog-to-digital converter (ADC) speed of 500 MHz is required. This capability is provided by a DA500A ADC (Signatec, Inc. Corona, California). This unit plugs into an IBM-compatible computer, and provides 8-bit digitization with 256 kB of local data storage. Once triggered by the data acquisition sequence (see below), the ADC acquires 32,768 data points at 2 ns intervals, thus covering arrival times up to 64 μs, and requiring 32 kB of data storage space. Custom instrument control software was responsible for transferring the raw spectral data from the DA500A local storage and storing the results in a disk file along with selected instrument and flight parameters. The former included the operating pressures in the aerosol inlet, and the vaporization temperature, while the latter included location, altitude, and true ground speed as supplied by the DC-8 data network.

The 8-bit digitization provided by the DA500A ADC yields a maximum signal dynamic range of only 1 part in 256. In reality, a constant noise level of several ADC "counts" reduces the usable dynamic range to less than 2 orders of magnitude. The net result of this limitation is that in order to observe the small signals corresponding to chemically interesting species present at low levels in bulk water, the raw signal must be amplified until the former signals are detectable, resulting in the latter signal exceeding the available dynamic range of the ADC. As will be apparent in the raw data shown below, the ion signals associated with the bulk water is off scale as a result of this limited dynamic range. Having the water signal exceed the input range of the ADC does not preclude its mass identification; however, it makes any quantitation of the particle composition impossible. Moreover, the integrated ion signal is no longer directly related to the particle volume, and hence cannot be used to provide a size estimate.

Currently, all ADCs above 250 MHz are limited to 8-bits, so only three options are available to mitigate the limited dynamic range: (1) the raw signal can be directed through a logarithmic amplifier (log amp); (2) multiple arrival time spectra can be recorded and averaged; and

(3) two digitizers can be operated in parallel, each with a different input gain. The log amp approach extends the effective dynamic range at the expense of linearity. Transforming the data back into a linear scale can produce undesirable distortion in the measured intensities. The addition of an amplifier to the signal path also introduces possible electronic noise and unwanted electrical interference. Nonetheless, this approach has been used by others [Murphy and Thomson, 1995]. Signal averaging under our single particle detection conditions is not straightforward owing to the very limited time during which vapors, and hence ions, are available for measurement. Our detection electronics did incorporate a "burst mode" feature whereby a single OPC trigger pulse would initiate 16 sequential digitization events, each of 64 μs duration. The total digitized sequence of 1 ms corresponds to the expected width of the vaporization event, so that summation of the 16 separate arrival time spectra would be justified and might be expected to yield an improvement of a factor of 4 in the signal-to-background ratio.

Laboratory tests, however, did not show a noticeable improvement in the signal-to-background ratio, possibly because of a combination of other factors, including the inherent nonlinearity of the ion source and distortion of the raw signal amplitude produced by the MCPs when exposed to a rapid sequence of very intense ion bursts. Because the burst mode approach offered no significant advantage, and resulted in a much slower data acquisition rate (particles per second), it was not used during the SUCCESS mission. The use of parallel digitizers offers the possibility of achieving an effective dynamic range of 12- to 13-bits. Taking into account the noise background and slight errors involved in adding together the two properly scaled spectra, a dynamic range of 4000-to-1 is possible. The three drawbacks to this approach are: (1) cost of an additional ADC ($6,500); (2) added processing time to add the raw spectra in real time, or double the data storage space for post processed spectra; and (3) the raw signal must be split evenly using a properly terminated, 1:1 50 Ω pulse divider so that each resulting signal pulse is attenuated by 50%. We have recently implemented the latter approach in our laboratory, and we have demonstrated a significant improvement in the overall dynamic range of the instrument.

Figure 7 shows the sequence of events that results in the acquisition of a particle mass spectrum. The sequence begins with the trigger pulse generated by the OPC as a result of particle passing within its viewing window that exceeds its preset threshold size. This pulse is used to trigger a delay generator whose output is a single, narrow pulse delayed from the trigger pulse by a fixed time of 1.2 ms. This time corresponds to the average transit time of an aerosol particle from the OPC to the vaporization target. In practice, this time will vary with the size of the particle and should be adjusted dynamically based on some independent measure of the particle velocity.

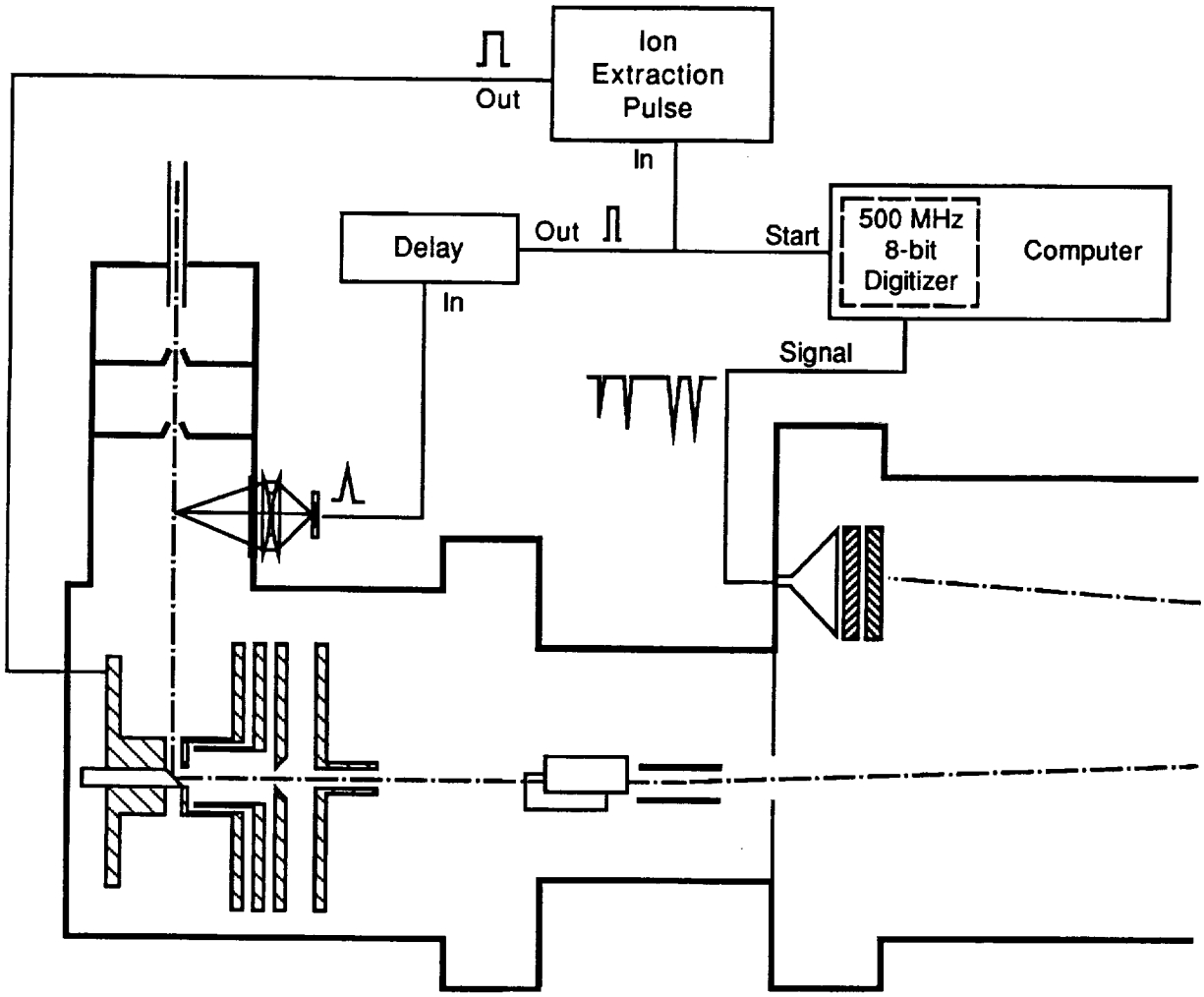

Figure 7. Data acquisition sequence triggered by a particle.

Such a dynamic delay adjustment has been used by other [Sinha, 1984; Salt et al., 1996]. Measuring the particle's velocity makes it possible, to simultaneously adjust the delay appropriately and to obtain information on the particle's aerodynamic size. Such a system requires two independent OPCs and custom electronics, neither of which could be made available for the SUCCESS mission. Laboratory tests showed that our compromise solution of a fixed delay of 1.2 ms would capture the majority of particles up to approximately 10 μm in diameter. Although the smaller particles will reach the vaporization target up to 500 μs sooner than the larger particles, the trapping ability of the ion source helps to capture the mass spectrum of the corresponding ions even after a delay exceeding 700 μs.

The output pulse from the delay generator simultaneously triggers the source extraction pulse applied to G4 and initiates analog-to-digital conversion. This pulse, therefore, represents "time zero" of the arrival time spectra. If a second particle arrives within the OPC before the complete arrival time spectrum from the previous particle has been recorded and transferred to a disk file, its trigger pulse is ignored, and it generates no data. However, the "missed" particle still impacts the vaporization target and thus produces a burst of both neutral molecules and ions within the ion source region. These additional neutral and ion species will not affect subsequent particle spectra as long as there is enough time to remove them from the source by diffusion (neutrals) and by the finite trapping time (ions). These times are on the order of 1 to 2 ms, so that the maximum particle arrival rate that can be accommodated is between 500 and 1000 s^{-1}.

DC-8 INTEGRATION

The SRI-developed instrument was completed on schedule to begin the DC-8 integration in March, 1996, prior to the SUCCESS mission. A number of engineering problems arose during the integration, related primarily to the weight and turning moment of the instrument. As originally configured, the time-of-flight mass spectrometer was mounted on the top of a NASA medium rack, with the support electronics below, and the three mechanical vacuum pumps on the base of the rack. This configuration exceeded the allowable turning moment for a medium rack, so the spectrometer was separated from the rack. To accommodate the larger instrument footprint that resulted from this separation, the spectrometer was bolted directly to the floor rails of the DC-8 at station 320, with the rack just forward at station 280, as depicted in Figure 8. This mounting configuration required the control electronics rack to be mounted facing aft, that is with the operator position forward of the rack. Fortunately, because this was the forward most rack on the aircraft, we could operate the instrument while sitting in the forward entry door area.

Also shown in Figure 8 is the approximate position of the external probe relative to the instrument, and the inlet transfer line that transported both vapor and aerosol samples to the PBG.

SUCCESS DEPLOYMENT

During the SUCCESS mission, our instrument was operational on 18 of the 19 flights, suffering only a computer board failure during one of the flights. Although the instrument was able to acquire aerosol spectra during the majority of the available flight time, the quality of the data was not uniformly good. A primary difficulty encountered during the field deployment was the inability to maintain an adequate vacuum in the spectrometer between flights.

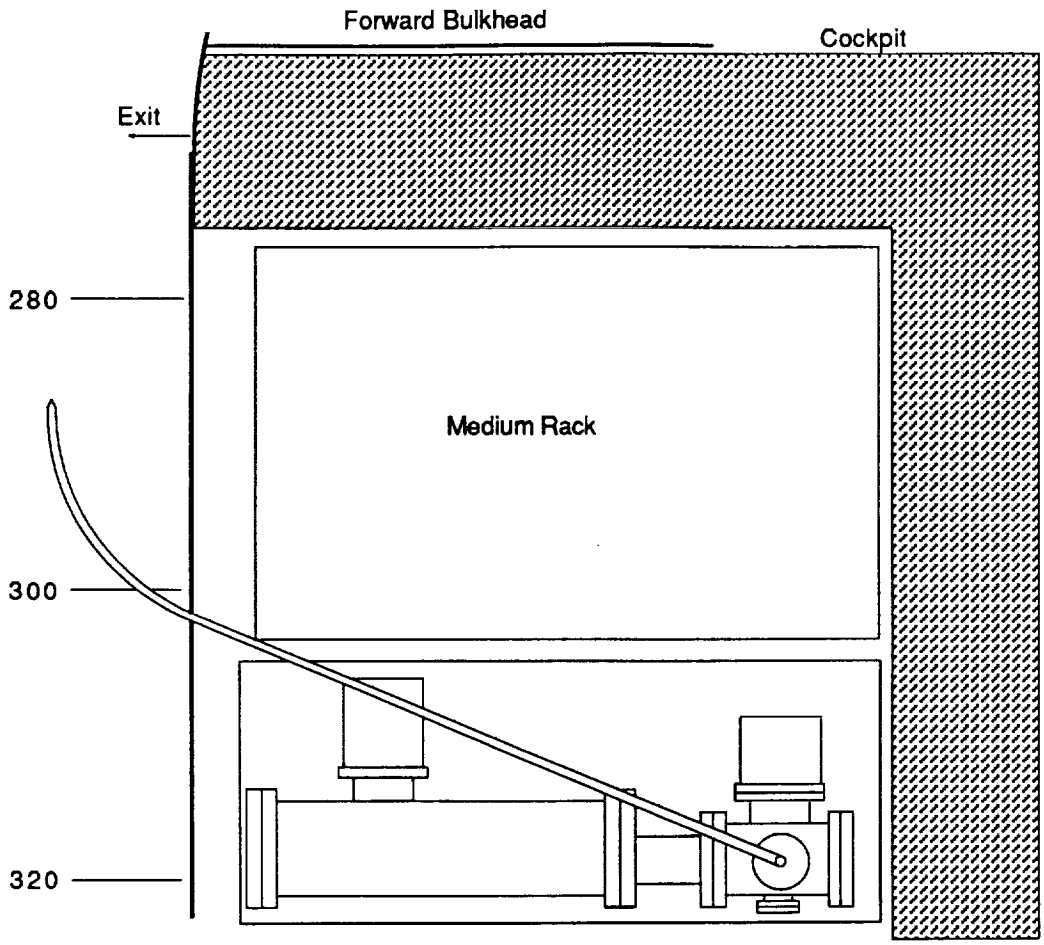

Figure 8. Relative position of the electronics rack and vacuum chamber as installed on the DC-8.

Between flights, power was not continuously available on the DC-8, and hence our vacuum pumps could not be operated for extended periods of time. During those periods when the pumps could not be operated, the vacuum within the mass spectrometer rose from the typical base pressure of 5×10^{-8} Torr to 100 mTorr, or greater, depending on the length of time without pumping. As a result of this pressure rise, water vapor accumulated on the two microchannel plate detectors used to measure the ion signal. Although water vapor itself does not damage the microchannel plates, it must be removed before applying the high voltage required for plate operation. Normally, this removal process requires 10-12 hours of continuous exposure to a high vacuum. Unfortunately, with the typical DC-8 operational schedule, we were only able to evacuate the instrument for 1-2 hours before beginning measurements on a flight. As a result of this reduced pumping time, the microchannel plate detectors steadily lost sensitivity over the first half of the deployment such that much of the data acquired during those missions was not usable.

As soon as time was available, we changed the microchannel plates and restored the instrumental sensitivity. At the same time, we made several modifications to the vacuum system and our operating procedures to minimize the pressure rise between flights. These measures were at least partially successful, so that data from the remaining flights was of an acceptable quality.

Table 1 summarizes the 19 flights of the mission, including a pre-deployment test flight, 2 transit flights, 14 field flights, and 2 post-deployment science flights. For each flight, the total number of mass spectra was recorded. Each recorded spectrum was examined, at least cursorily, to determine if it contained data that was both useable and chemically interesting. If a spectrum showed potentially interesting signal peaks, it was more carefully analyzed by converting the measured ion arrival times to the corresponding mass-to-charge ratio. Peak heights were then measured and used to establish the relative ion abundances. From these abundance ratios, it was generally possible to determine the chemical composition of the aerosol particle.

Table 1. Summary of SUCCESS Mission Flights

Date	Flight	Conditions	Location	Aerosol Spectra	
				Recorded	Analyzed
Apr 10	96201	Test-flight over water	OR, WA	260	0
Apr 13	96202	Transit / cirrus over pacific	CA	72	0
Apr 15	96203	Clear-sky coordination	OK - cart	840	0
Apr 16	96204	Thin cirrus / T-39 exhaust ?	OK - cart	2390	0
Apr 18	96205	Clear sky, low cirrus uncinus	OK, TX	880	0
Apr 20	96206	Patchy fast cirrus [no lows]	OK - cart	3040	0
Apr 21	96207	Conv.in-/outflow / thick ci	TX, OK	1850	0
Apr 24	96208	High cirrus cells [no lows]	OK - cart	2100	2
Apr 27	96209	Thick cirrus cloud	OK - cart	2500	0
Apr 29	96210	Low stratus	OK - cart	325	2
Apr 30	96211	757 exh.>30 mi / wave-cloud	NM	620	12
May 02	96212	Wave-cloud [over Boulder]	CO	1000	25
May 03	96213	757 exh/con <10 mi microphys.	OK - cart	1350	43
May 04	96214	757 exhaust/con mic.+radiation	OK - cart	675	20
May 07	96215	757 exhaust/con mic.+radiation	NE	1450	5
May 08	96216	Convective outflow / contrails	IO, WI	1550	6
May 10	96217	Transit / aerosol profiling	CA	300	0
May 12	96218	Persistent contrail over water	OR	2100	3
May 15	96219	Cirrus over water	OR, WA	2400	2
			Totals	25702	120

SUCCESS RESULTS

Of the more than 25,000 aerosol mass spectra obtained during the 19 SUCCESS mission flights, approximately 8,100 were more closely examined. These spectra were chosen based on two criteria: (1) a normally functioning instrument with good sensitivity and (2) an integrated ion intensity that was significantly above the average. The former criterion eliminated data obtained when the instrument was not producing quantifiable data due to an operational problem described above. The latter criterion allowed us to rapidly sort through the raw data and identify those spectra that likely contained chemically interesting results.

The examined spectra were classified as to their likely chemical composition based on the observed ions, their distribution, and their relative intensities. Of the 8,100 spectra included in the evaluation, 120 were found to have significant ion intensities associated with materials other than water. All of the remaining spectra showed only evidence of water, with no significant other chemical species apparent above the background. The distribution of chemical compositions that were assigned to these 120 aerosol particles is: sulfate 60%, carbonate 13%, nitrate 6%, sodium 4%, potassium 1%, sulfuric acid 9%, and unassigned 6%. In many cases, the counter-ion could also be inferred from the mass spectra. For example, the majority of sulfate aerosols were ammonium sulfate, while the carbonate aerosols appeared to be both ammonium(bi) carbonate and calcium carbonate. We saw no evidence for particles containing mixtures of chemical species, such as ammonium sulfate and nitrate.

Several typical examples of the mass spectra of chemically identified aerosol particles are shown below to illustrate the nature of the recorded data. More detailed information on each of the analyzed mass spectra is included in the SUCCESS mission data archive, as well as on the CD-ROM produced by NASA Ames Research Center [Gains and Hipskind, 1997].

The majority of chemically interesting aerosol particles were measured on four consecutive flights beginning on May 2 (96212) and continuing until May 7, 1996 (96215). Tables 2-5 summarize the aerosol characterization data for each of these flights, including the aerosol type as determined by examination of the mass spectra, the time at which the data was recorded, and the aircraft position at that time as provided by the DC-8 flight data archive. Appendices A-D show all of the chemically interesting mass spectra for these four flights, along with a tabular summary of the intensities for the most important ion species in each spectrum.

Based on visual observation, less than 1% of the measured particle spectra were collected in clear air, and this included none of the chemically interesting spectra. All of the remaining spectra were recorded while traversing clouds in the middle and upper troposphere.

Table 2. DC-8 Flight Data Corresponding to Analyzed Aerosols for May 2, 1996

Aerosol Type	Time (UTC)	Latitude (NMS) +N (degrees)	Longitude (NMS) +E (degrees)	True Air Speed (m/s)	True Heading (degrees)	Radar Altitude (m)
Sulfate	61846	40.773	-101.928	235.1	290.4	9695.1
Nitrate	61895	40.805	-102.028	236.1	290.2	9670.4
Sulfate	62155	40.972	-102.570	238.7	290.1	9621.3
Sulfate	62409	41.105	-103.115	239.2	276.0	9476.5
Sulfate	62501	41.120	-103.323	240.2	276.3	9365.3
Sulfate	62533	41.125	-103.395	240.2	276.0	9333.9
Sulfate	62542	41.127	-103.417	239.7	275.9	9336.3
Sulfate	62544	41.127	-103.420	239.7	275.9	9338.5
Sulfate	64120	41.507	-106.838	235.6	287.9	9894.1
Nitrate	64261	41.588	-107.142	236.6	287.4	9836.5
Sulfate	65090	42.025	-107.633	228.4	118.6	9850.2
Nitrate	66075	41.448	-105.597	229.4	234.3	10016.0
Sulfate	69655	41.358	-104.503	228.9	–	8970.9
Sulfate	73114	39.592	-105.188	232.5	29.9	10501.6
Sulfate	73133	39.557	-105.157	232.0	167.6	10934.7
Sulfate	73722	40.380	-105.082	227.4	283.7	11279.1
Sulfate	73981	40.348	-104.952	225.8	213.2	10495.8
Sulfate	73992	40.330	-104.962	226.4	213.1	10499.1
Sulfate	74072	40.192	-105.042	225.8	213.1	10498.8
Sulfate	74507	39.470	-105.118	231.5	66.8	10408.0
Sulfate	74706	39.645	-105.245	234.6	264.0	9187.3
Sulfate	76370	39.755	-106.335	231.5	99.6	7631.6
Sulfate	76810	39.515	-104.993	241.3	149.9	9677.4
Sulfate	77949	40.310	-105.003	225.3	215.0	10519.6
Sulfate	78697	39.775	-104.388	233.0	100.1	10393.7

Table 3. DC-8 Flight Data Corresponding to Analyzed Aerosols for May 3, 1996

Aerosol Type	Time (UTC)	Latitude (NMS) +N (degrees)	Longitude (NMS) +E (degrees)	True Air Speed (m/s)	True Heading (degrees)	Radar Altitude (m)
Nitrate	67584	36.507	-99.902	208.9	329.4	–
Sulfate	67707	36.687	-99.783	205.3	79.0	10255.0
Sulfate	67746	36.688	-99.685	208.3	88.5	10160.5
Sulfate	67853	36.692	-99.415	205.3	89.3	10352.5
Nitrate	68044	36.693	-98.927	205.8	88.3	10403.1
Sulfate	69240	36.555	-96.015	212.5	212.6	11246.5
Magnesium	69330	36.497	-96.163	217.6	269.0	11476.9
Unknown	69333	36.497	-96.168	217.6	269.2	11482.4
Sulfate	70698	36.500	-98.740	205.8	264.5	11347.1
Nitrate	71052	36.487	-99.453	231.5	266.8	11188.9
Sulfate	72728	36.700	-96.228	193.9	90.0	11511.1
Sulfuric Acid	73611	36.510	-97.420	202.7	267.3	11486.7
Sulfate	74273	36.498	-98.672	199.1	265.7	11282.2
Nitrate	74434	36.492	-99.000	205.3	267.7	10162.6
Sulfate	75013	36.612	-99.905	189.3	14.2	8702.3
Sulfate	75607	36.698	-98.610	179.0	88.0	8947.1
Sulfate	76100	36.702	-97.490	180.1	88.4	9022.7
Ammonium Sulfate	76380	36.700	-96.847	186.2	89.9	8997.7
Sulfuric Acid	76869	36.670	-95.735	212.0	95.6	9482.6
Sulfate	76978	36.645	-95.440	234.6	94.2	9514.9
Sulfate	77407	36.385	-95.180	214.5	341.2	10766.8
Sulfate	77474	36.507	-95.188	204.2	331.1	–
Carbonate	78184	36.602	-96.562	201.1	269.1	12457.8
Carbonate	78227	36.602	-96.640	201.1	269.2	12431.0
Carbonate	78246	36.602	-96.673	201.7	268.9	12467.8
Carbonate	78281	36.602	-96.737	201.7	268.8	12488.9
Carbonate	78300	36.603	-96.770	202.2	269.0	12481.3
Carbonate	78350	36.603	-96.860	203.7	269.1	12468.5
Carbonate	78532	36.605	-97.192	203.2	268.8	12491.9
Carbonate	78628	36.605	-97.367	205.3	268.4	12464.2
Sulfate	78644	36.605	-97.395	205.8	268.5	12448.3
Carbonate	78650	36.605	-97.407	205.8	268.5	12459.0
Carbonate	78704	36.605	-97.507	205.8	268.0	12465.7
Carbonate	78819	36.605	-97.722	208.3	267.8	12449.6
Sulfate	78912	36.605	-97.898	210.9	269.1	12444.7
Carbonate	78948	36.603	-97.968	212.5	268.7	12424.0
Carbonate	78951	36.603	-97.973	212.5	268.7	12422.7
Carbonate	79052	36.603	-98.170	214.5	268.4	12397.7
Carbonate	79113	36.602	-98.288	215.6	268.5	12368.5
Carbonate	79332	36.598	-98.720	217.6	268.0	12321.2
Carbonate	79394	36.597	-98.843	217.6	267.0	12304.2
Sulfate	80010	36.687	-100.012	213.0	20.6	–
Carbonate	80095	36.815	-99.863	205.8	34.6	12118.2

Table 4. DC-8 Flight Data Corresponding to Analyzed Aerosols for May 4, 1996

Aerosol Type	Time (UTC)	Latitude (NMS) +N (degrees)	Longitude (NMS) +E (degrees)	True Air Speed (m/s)	True Heading (degrees)	Radar Altitude (m)
Sulfate	67234	36.750	-97.807	217.1	99.8	11897.0
Sulfate	67250	36.745	-97.760	214.5	100.1	11914.6
Sulfate	67256	36.742	-97.743	214.5	99.6	11911.9
Sulfate	67277	36.735	-97.687	214.0	100.6	11910.7
Nitrate	67312	36.722	-97.593	212.0	100.4	11925.6
Nitrate	67385	36.695	-97.400	209.4	100.5	11907.6
Sulfate	67393	36.693	-97.380	208.9	99.7	11921.3
Sulfate	67403	36.690	-97.353	208.3	100.2	11934.4
Unknown	67449	36.673	-97.233	208.3	100.9	11952.1
Unknown	67495	36.657	-97.115	209.4	102.4	11940.8
Nitrate	68150	36.343	-96.402	209.9	282.0	12117.3
Sulfate	68166	36.348	-96.432	207.3	281.7	12181.3
Sulfuric Acid	69014	36.590	-98.085	217.6	277.6	11947.6
Sulfate	69857	36.822	-99.835	207.8	300.4	–
Sulfuric Acid	70057	36.987	-99.567	208.9	100.9	12006.4
Sulfuric Acid	70219	36.933	-99.147	206.8	99.6	11959.4
Sulfate	71155	36.595	-96.708	207.3	101.1	12153.0
Sulfate	71405	36.437	-96.095	236.1	188.0	–
Sulfate	71556	36.328	-96.297	218.1	281.6	12146.0
Sulfate	71711	36.375	-96.597	208.9	279.2	12202.7

Table 5. DC-8 Flight Data Corresponding to Analyzed Aerosols for May 7, 1996

Aerosol Type	Time (UTC)	Latitude (NMS) +N (degrees)	Longitude (NMS) +E (degrees)	True Air Speed (m/sec.)	True Heading (degrees)	Radar Altitude (m)
Sulfate	68153	42.508	-100.013	217.1	304.1	10084.0
Sulfate	68589	42.743	-100.835	209.4	253.3	10002.0
Sulfuric Acid	71524	42.412	-102.123	219.7	250.7	9656.4
Sulfuric Acid	71936	42.497	-102.477	209.9	65.7	9671.6
Sulfate	73230	42.583	-101.517	241.3	250.8	10341.3
Sulfate	73442	42.452	-101.995	215.6	249.4	10155.0
Sulfate (Sodium)	73836	42.298	-102.757	220.7	305.7	10021.8
Sulfuric Acid	78980	42.902	-101.077	205.8	72.6	11012.4
Sulfate	79244	43.010	-100.353	218.6	172.5	–
Sulfuric Acid	80047	42.483	-101.813	204.7	244.8	9696.6
Sulfate	80524	42.272	-102.747	211.4	292.6	11152.6
Sulfuric Acid	82009	42.275	-99.545	173.9	144.2	10145.3

Figure 9 is a histogram plot of the number of sulfate aerosol particles measured as a function of the radar altitude of the DC-8. The bulk of the sulfate aerosols appears to be located in two bands, ranging from 9.25 to 10.50 km, and from 11.75 to 12.50 km.

Figure 10a shows an example of an aerosol particle that likely contains ammonium sulfate. Characteristic peaks are seen at nominal m/z 14 (N^+), 16 (NH_2^+, O^+), 17 (NH_3^+, OH^+), 18 (NH_4^+, H_2O^+), 32 (S^+), 48 (SO^+), 64 (SO_2^+), 80 (SO_3^+), and 96 (SO_4^+). The isobaric species at m/z 16, 17, and 18 cannot be readily attributed to either the water background or the presence of ammonium ions in the aerosol. However, the intensity distribution of these three ions in Figure 10a makes an interesting comparison with the distribution in Figure 10b. In the latter example, presumed to be calcium nitrate, the m/z 17 peak is not apparent, while in the former case, it is off scale indicating that its origin is different in the two particles. These differences are consistent with the presence of ammonium in the sulfate particle, but not in the nitrate particle.

Figure 10b shows an example of an aerosol particle most probably containing calcium nitrate. Characteristic peaks are seen at nominal m/z 14 (N^+), 16 (O^+), 17 (OH^+), 18 (H_2O^+), 28 (N_2^+), 30 (NO^+), 32 (O_2^+), 40 (Ca^+), 46 (NO_2^+), and 62 (NO_3^+). Despite having a mass resolution ($M/\Delta M$) in excess of 1000, the ion peak at m/z 40 cannot be assigned unambiguously to Ca+ alone (atomic mass 39.9626) because of the isobaric argon ion (atomic mass 39.948).

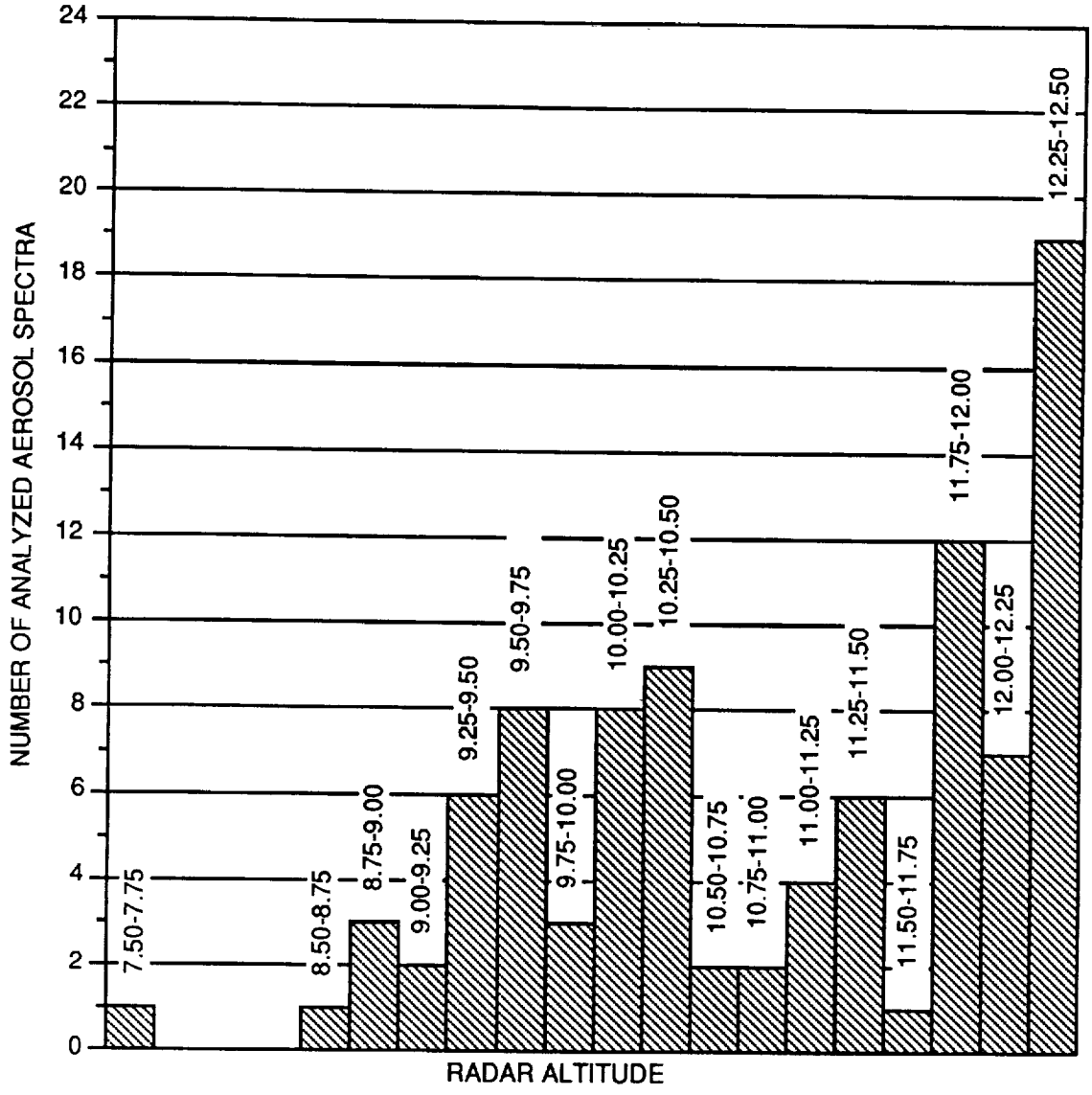

Figure 9. Histogram plot of the number of sulfate-based aerosol particles measured as a function of the DC-8 (radar) altitude.

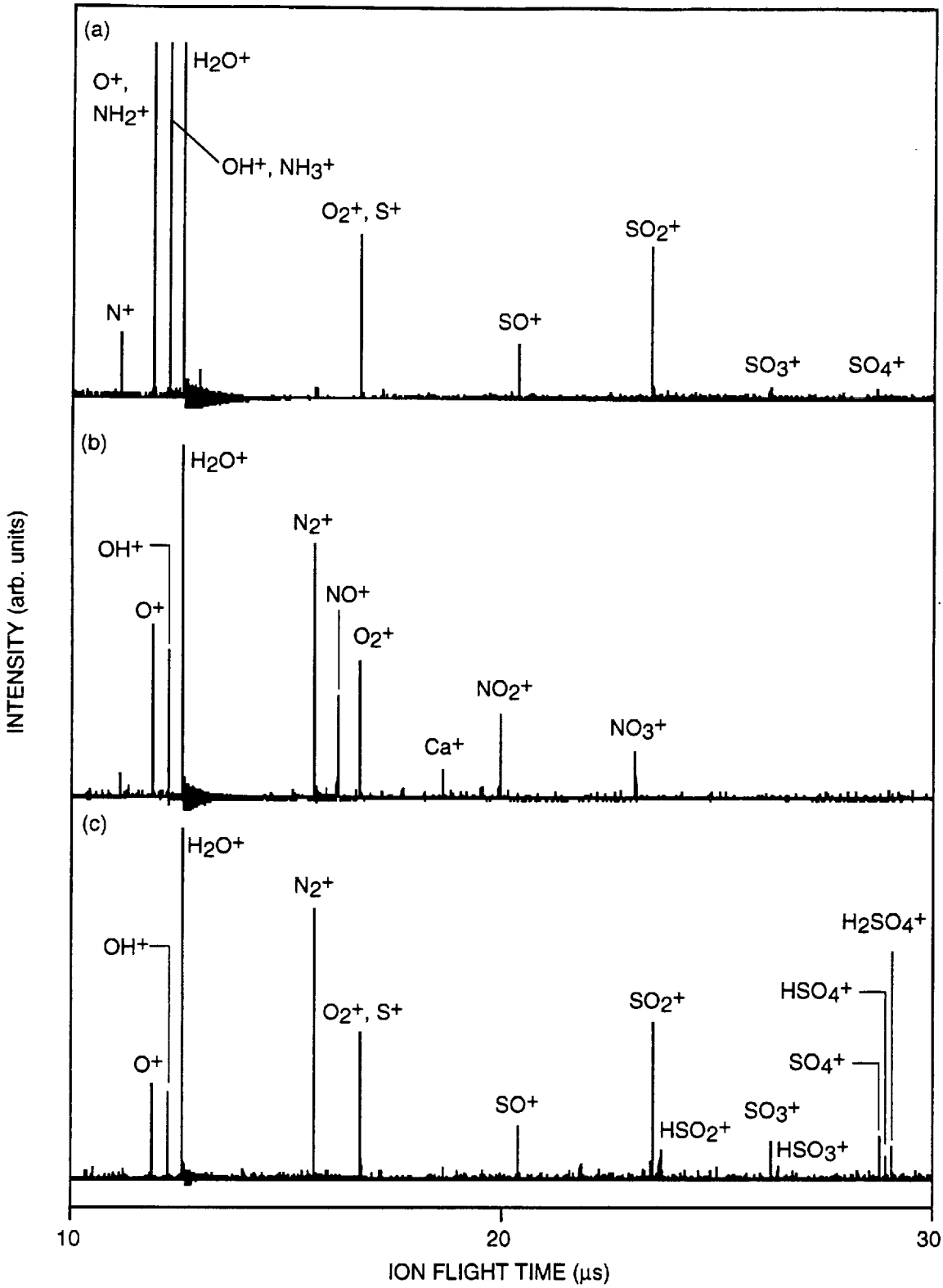

Figure 10. Time-of-flight mass spectra of single aerosol particles recorded during SUCCESS flights: (a) ammonium sulfate (Flight 960212, 17:20:09 UTC); (b) calcium nitrate (Flight 960212, 18:21:15 UTC); (c) sulfuric acid (Flight 960213, 20:26:51 UTC).

Separation of these ions would require a mass resolution in excess of 2,500. However, because this spectrum was obtained in a single scan, the m/z 40 intensity due to background argon would be very much lower than observed here.

The characteristic spectral pattern in Figure 10a is very similar to spectra of ammonium sulfate aerosols measured in the laboratory, both with regard to the ion species present, and their relative intensity ratios. In general, the mass spectra of aerosols generated in the laboratory by nebulizing a dilute aqueous solution of the calibrant showed peak ratios that were constant to within ±10%, while the absolute peak intensities varied by an order of magnitude. The later variation likely resulted from the variation in aerosol size. The ion species of particles classified as sulfate observed in all mass spectra recorded during SUCCESS were essentially the same as those shown in Figure 10a.

Figure 10c shows an example of what appears to be an aerosol particle containing a significant amount of sulfuric acid. This particle was sampled in the wake of the NASA 757 at a separation distance of 5-10 km, corresponding to a plume age of 1 min. In fact, most, if not all of the aerosol particles tentatively assigned as sulfuric acid were sampled under similar conditions, lending support to the theory that they were formed in the engine exhaust. The spectra in Figure 10c show characteristic peaks at nominal m/z 16 (O^+), 17 (OH^+), 18 (H_2O^+), 28 (N_2^+), 32 (O_2^+, S^+), 48 (SO^+), 64 (SO_2^+), 65 (HSO_2^+), 80 (SO_3^+), 81 (HSO_3^+), 96 (SO_4^+), 97 (HSO_4^+), and 98 ($H_2SO_4^+$).

Although many aerosol mass spectra were classified as having arisen from a sulfate-based particle, these mass spectra did not show uniform peak intensities. Figure 11 shows the peak intensities for the three major characteristic sulfate ions; m/z 48 (SO^+), m/z 64 (SO_2^+), and m/z 80 (SO_3^+) as measured from 22 selected spectra. These data show that the SO_2^+ peak exhibits the smallest intensity variation on a particle-to-particle basis. The corresponding SO_3^+ peaks show considerably more variation, while the relatively low intensity of the SO^+ peaks makes them less reliable as an indicator of the presence of sulfate. In post-mission studies with laboratory generated ammonium sulfate aerosols, a similar degree of variability was found, indicating that it is an instrument response characteristic. The source of this response behavior is not clear, however, it is likely related to the limited dynamic range of the instrument leading to non-linear ion signals as a function of aerosol size and composition.

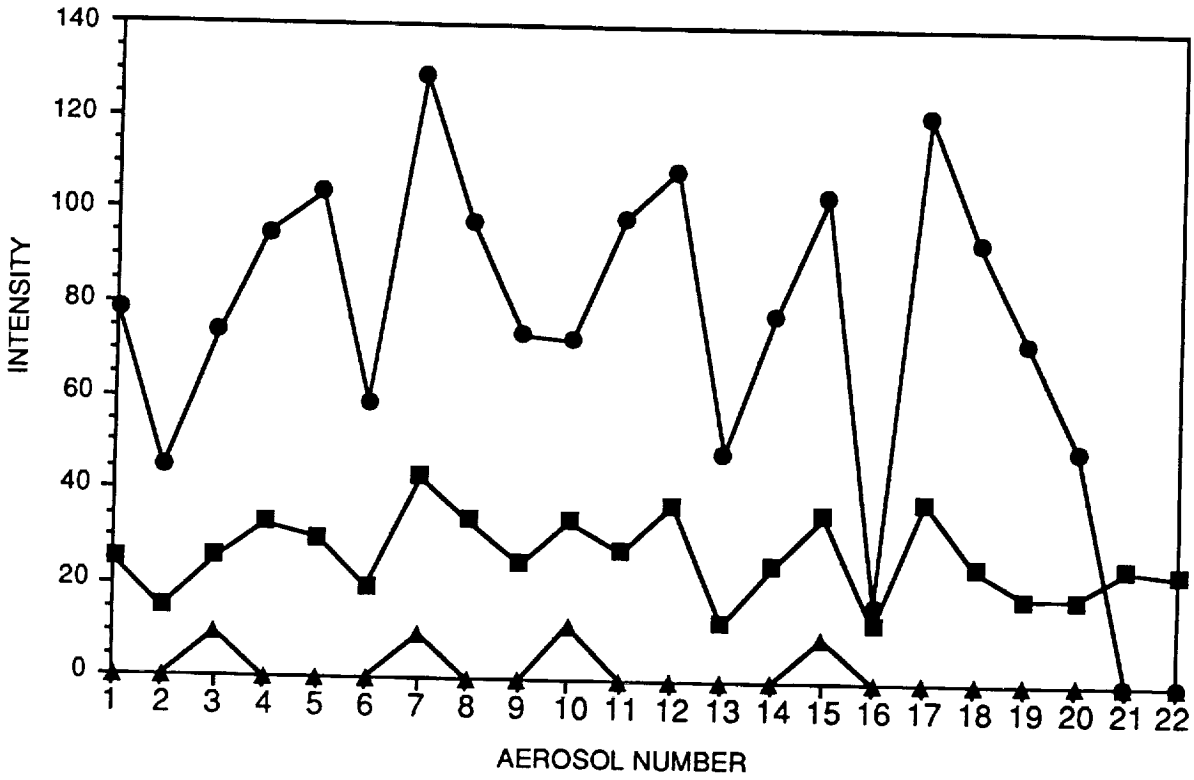

Figure 11. Variation in the peak heights of SO^+ (m/z 48, ■), SO_2^+ (m/z 64, ●), and SO_3^+ (m/z 80, ▲) measured from 22 different sulfate-based aerosols.

POST-MISSION CALIBRATION AND ANALYSIS

Following the field deployment portion of the SUCCESS mission, we undertook a comprehensive laboratory calibration program. During this effort, we generated aerosols of those species that had been identified in our raw data. These aerosols were sampled into the instrument, and the resulting mass spectra compared with our previously acquired field data. Although it is most desirable to generate and sample the aerosols under conditions that closely approximate those encountered during the mission flights, owing to the unusual combination of low temperature, low relative humidity, reduced pressure, high aerosol water content, and high flow velocity make this a difficult task . Duplication of all of these conditions would require that a special calibration chamber be built, combining aspects of a small wind tunnel with an aerosol generator. This configuration is beyond the scope of the present effort. However, lacking these facilities, we were was still able to acquire aerosol spectra that aided in the interpretation, assignment, and verification of our SUCCESS data.

A second goal of our calibration effort was to determine if our inlet and sampling system introduce any significant size bias. The high percentage of particles that show only water is at odds with the generally accepted distribution of aerosol particles in the UT/LS. One possible source of this discrepancy is a size bias in our instrument that allows only large ice particles to be detected while missing the smaller, nonwater particles. We therefore performed a systematic study of the sampling efficiency of our instrument as a function of the aerosol particle size. These laboratory tests verified that our PBG was able to sample particles in the size range from approximately 0.2 μto > 5.0 μm.

The typical transmission efficiency measured in the laboratory for 0.502-μm-diameter polystyrene latex spheres (Duke Scientific, Palo Alto, California) through the aerosol inlet to the ion source region was 0.2%. This was determined gravimetrically whereby a known mass of particles was placed in a 1-L spherical glass bulb and a stream of dry nitrogen was used to maintain them airborne where they were sampled through the capillary inlet protruding into the bulb. A glass slide coated with vacuum grease was placed within the vacuum chamber at the location of the aerosol inlet aperture to the ion source. After sampling for a time sufficient to noticeably reduce the original particle level within the bulb, the mass of particles remaining in the bulb and deposited on the slide was measured to determine the transmission efficiency. The 0.2% overall efficiency found for 0.5 μm particles is comparable to the efficiencies measured by others for similar, capillary-based aerosol inlets [Murphy and Thomson, 1995; Sinha et al., 1982; Yang et al., 1996; Hinz et al., 1994].

The transmission efficiency was not measured over the full particle size range, nor was any attempt made to determine the efficiency under conditions more representative of the actual DC-8 sampling. Although these laboratory studies did not measure the ability of our PBG sampling system to acquire aerosols without size bias, it is most probable that the greastest influence on the sampling characteristics of the instrument was imposed by the external probe. As discussed above in the description of this probe, its sub-isokinetic sampling almost certainly resulted in a serious undersampling of smaller aerosols. Furthermore, since we could not measure our sampling efficiency or sampling size bias in the laboratory under conditions that were characteristic of actual flight conditions, the information from any such studies would not be useful in assessing the mission results.

Although we are tempted to compare our results with other tropospheric aerosol composition data measured previously and during the SUCCESS mission, such comparison presents difficulties. The ionic composition results obtained by Talbot et al. [1998] during SUCCESS correspond to 10-minute averages of a very large number of particles sampled under varying atmospheric conditions. In general, we would not have measured a statistically significant

number of individual particles during the same 10-minute period, and thus it is not reasonable to compare single particle and bulk composition data. Similar data obtained during ABLE 3B [Grozelska et al., 1994] for middle and upper tropospheric aerosol composition corresponded to 20-60 minute sampling averages. Those data showed that the bulk ionic composition was dominated by ammonium and sulfate, with lesser amounts of nitrate. Although quantitatively different from the present results, the qualitative trend is similar.

Individual particles were collected during various SUCCESS flights by Pueschel et al. [1998] and by Chen et al. [1998] using a wire impactor and a TEM grid, respectively, and subsequently analyzed for chemical composition. Analysis of these particles occurred after a considerable time interval and after prolonged exposure to air followed by vacuum exposure during electron microscopic examination. These conditions are markedly different from those under which we sampled and vaporized the single particles reported here, making any direct comparison problematic.

Similarly, Sheridan et al. [1994] have reported on the elemental composition of single particles collected on impactors in the UT. Greater than 90% of those aerosols contained sulfate, while the remainder were classified as carbon-rich, crustal, metallic, and marine. Of the latter types, most carbon-rich (soot) materials would not be vaporized under our conditions, nor would most metallic particles. Some crustal materials and most marine aerosols would be vaporized in our instrument. However, a large proportion of the chemically interesting particles that we observed can be classified as sulfate, in general agreement with both Talbot et al. [1998] and Sheridan et al. [1994].

Because the chemical composition of UT aerosol particles is not expected to be dominated by water, the present results are not easily explained. Several possible factors can be considered to account for the observed results. Because the majority of particles analyzed by our instrument were sampled during cloud transits, we can reasonably conclude that high humidity levels prevailed throughout the unheated sampling line. This condition could lead to the condensation of additional water onto smaller particles, both after entering the probe, and within the capillary inlet. Under these conditions, one might expect these particles to contain a relatively large proportion of water compared with the core material (such as ammonium sulfate or sulfuric acid). In our instrument, such particles could yield mass spectra showing only water-related peaks.

The cause of this discrimination results from the design of the ion source. The ion source was designed to provide the highest possible ionization efficiency to maximize sensitivity. This high efficiency is achieved by operating the source in a space-charge regime, which results in limiting the total number of ions that can reside in the source at any given time. Our laboratory studies using this source have shown that the range over which a linear increase in sample vapor

concentration within the source yields a linear ion response is approximately two orders of magnitude. The result of this limited linear response range is that a dominant species, such as water vapor, will generate enough ion density within the source to preclude the ionization of minor species. This problem is further exacerbated by the dynamic range of the digitization electronics, which is limited to approximately 7-bits of resolution due to the detector noise.

In addition to the possible existence of excess water vapor condensed on the incoming aerosol particles, the ambient gas phase water vapor could also contribute a large background signal. Although the total pressure in the ion source region in the absence of a vaporizing particle is 10^{-6} Torr, the partial pressure due to water will be a significant fraction of this under conditions of high relative humidity within the inlet. Because the ion source operates continuously, this high partial pressure of water will lead to the continuous presence of a large number density of water ions within the source volume. Thus, the material arising from the vaporization of an aerosol particle will not be efficiently ionized due to the space-charge limit extant within the source. The result is an aerosol mass spectrum dominated by water. When the instrument is operated in the laboratory, the background signal associated with water is very much smaller than under flight conditions, and wet aerosol particles are readily detected and chemically speciated. This laboratory functionality verifies the fundamental viability of the thermal vaporization electron impact ionization scheme for single particle analysis demonstrated previously by Sinha et al. [1982].

Several readily implemented changes to the instrument will mitigate the difficulties exhibited when this system was used under flight conditions in the UT. A properly designed external sampling probe that provides more nearly isokinetic conditions would significantly reduce the inlet size bias [Porter et al., 1992]. Temperature and humidity control within the inlet could reduce the ambient water levels, although possibly at the expense of some composition information. Sizing of each analyzed particle would provide information on the correlation of composition with size, as well as giving some measure of the sampling and transmission efficiency of the inlet. Changes in the design and operation of the EI source would substantially increase its linear response range. These changes coupled with logarithmic detection electronics [Murphy and Thomson, 1995] will result in an instrument with significantly enhanced capabilities.

CONCLUSIONS

A new instrument was developed and deployed on the SUCCESS mission. This effort was the first use of a real-time aerosol characterization instrument on an airborne platform. As a result of the non-optimum external aerosol sampler, however, we likely oversampled larger particles. The large amount of water associated with these particles and the high ambient humidity encountered during cloud transits where our spectra were taken, resulted in the majority of particles appearing to contain only water. Despite this limitation, we were able to chemically characterize a number of individual aerosol particles. Laboratory studies have largely confirmed the assignment of these aerosol spectra measured in the UT. The paucity of chemically interesting experimental results obtained using this new instrument during its first deployment as part of the SUCCESS mission does not admit making statistically significant observations about the chemical composition of UT aerosol particles. Straightforward changes to the sampling inlet and the instrument will permit such upper tropospheric, aerosol compositional observations to be made on future deployments. However, even in its current configuration, this new instrument demonstrated an ability to chemically characterize in real-time single aerosol particles sampled directly from the troposphere.

ACKNOWLEDGEMENTS

The authors would like to thank Dr. D. M. Murphy, NOAA, Boulder, CO, for providing us with his aerosol inlet design, Dr. Hermann Wollnik, University of Giessen, for his assistance in the design of the ion source, and Dr. Christopher H. Becker, SRI International, for his advice and encouragement during this effort.

REFERENCES

Allen, J., and R. K. Gould, Mass spectrometric analyzer for individual aerosol particles, *Rev. Sci. Instrum.*, 52, 804-809, 1981.

Chen, Y., S. M. Kreidenweis, L. M. McInnes, D. C. Rogers, and P. J. DeMott, Single particle analyses of ice nucleating particles in the upper troposphere and lower stratosphere, *Geophys. Res. Letts.*, to be published, 1998.

Daum, P. H., and S. R. Springton, *Measurement Challenges in Atmospheric Chemistry*, Chap. 4, American Chemical Society, 1993.

Gaines, S., and S. Hipskind, eds., Subsonic aircraft: contrail and cloud effects special study, NASA/SASS-001 Edition 1, NASA Ames Research Center, December, 1997.

Gorzelska, K., R. W. Talbot, K. Klemm, B. Lefer, O. Klemm, G. L. Gregory, B. Anderson, and L. A. Barrie, Chemical composition of the atmospheric aerosol in the troposphere over Hudson Bay lowlands and Quebec-Labrador regions of Canada, *J. Geophys. Res.* 99, 1763 (1994).

Grix, R., U. Grüner, G. Li, H. Stroh, and H. Wollnik, An electron impact storage ion source for time-of-flight mass spectrometers, *Int. J. Mass Spectrom. Ion Proc.*, 93, 323-330, 1989.

Heintzenberg, J., Fine particles in the global troposphere: A review, *Tellus*, 41B, 149-160, 1989.

Hinz, K-P., R. Kaufmann, and B. Spengler, Laser-induced mass analysis of single particles in the airborne state, *Anal. Chem.*, 66, 2071-2076, 1994.

Johnston, M. V., and A. S. Wexler, MS of individual aerosol particles, *Anal. Chem.*, 67, 721A-726A, 1995.

Kim, D., and P. K. Hopke, Classification of individual particles based on computer-controlled scanning electron microscopy data, *Aerosol Sci.Technol.*, 9, 133-151, 1988.

Liu, P., P. J. Ziemann, D. B. Kittleson, and P. H. McMurry, Generating particle beams of controlled diemsnions and divergence. 2. Experimental evaluation of particle motion in aerodynamic lenses and nozzle expansions, *Aerosol Sci. Technol.*, 22, 314-324, 1995.

Mansoori, B. A., M. V. Johnston, and A. S. Wexler, Quantitation of ionic species in single microdroplets by on-line laser desorption/ionization, *Anal. Chem.*, 66, 3681-3687, 1994.

Murphy. D. M., and D. S. Thomson, Laser ionization mass spectroscopy of single aerosol particles, *Aerosol Sci.Technol.*, 22, 237-249, 1995.

Neubauer, K. R., M. V. Johnston, and A. S. Wexler, Chromium speciation in aerosols by rapid single-particle mass spectrometry, *Int. J. Mass Spectrom. Ion Proc.*, 151, 77-87, 1995.

Porter, J. N., A. D. Clarke, G. Ferry, and R. F. Pueschel, Aircraft studies of size-dependent aerosol sampling through inlets, *J. Geophys. Res.*, 97, 3815-3824, 1992.

Post, J. E., and P. R. Buseck, Characterization of individual particles in the Phoenix urban aerosol using electron-beam instruments, *Environ. Sci. Technol.*, 18, 35-42, 1984.

Pueschel, R. F., *et al.*, Sulfuric acid and soot particle formation in aircraft exhaust, *Geophys. Res. Letts.*, to be published, 1998.

Rader, D. J., and V. A. Marple, A study of the effects of anisokinetic sampling, *Aerosol Sci.Technol.*, 8, 283-299, 1988.

Sageev-Grader, G., R. C. Flagan, J. H. Seinfeld, and S. Arnold, Fourier transform infrared spectrometer for a single aerosol particle, *Rev. Sci. Instrum.*, 58, 584-587, 1987.

Salt, K., Noble, C. A., and Prather, K. A., Aerodynamic particle sizing versus light scattering intensity measurements as methods for real-time particle sizing coupled with time-of-flight mass spectrometry, *Anal. Chem.*, 68, 230-234, 1996.

Sheridan, P. J., C. A. Brock, and J. C. Wilson, Aerosol particles in the upper troposphere and lower stratosphere: elemental composition and morphology of individual particles in northern midlatitudes, *Geophys. Res. Letts.*, 21, 2587-2590, 1994.

Sinha, M. P., C. E. Giffin, D. D. Norris, T. J. Estes, V. L. Vilker, and S. K. Friedlander, Particle analysis by mass spectrometry, *J. Colloid Interface Sci.*, 87, 140-153, 1982.

Sinha, M. P., Laser-induced volatilization and ionization of microparticles, *Rev. Sci. Instrum.*, 55, 886-891, 1984.

Smith, M. H., and C. D. O'Dowd, Observations of accumulation mode aerosol composition and soot carbon concentrations by means of a high-temperature volatility technique, *J. Geophys. Res.*, 101, 19583-19591, 1996.

Talbot, R. W., J. E. Dibb, and M. Loomis, Influence of vertical transport on free tropospheric aerosols over the central USA in springtime, *Geophys. Res. Letts.*, to be published, 1998.

Twohy, C. H., and B. Gandrud, Ice-forming particles in aircraft exhaust, *Geophys. Res. Letts.*, to be published, 1998.

Xhoffer, C., and R. Van Grieken, *Environmental Particles*, Vol. 2, Chap. 5, Lewis Publishers, Boca Raton, Florida, 1993.

Xhoffer, C., L. Wouters, P. Artaxo, A. Van Put, and R. Van Grieken, *Environmental Particles*, Vol. 1, Chap. 3, Lewis Publishers, Boca Raton, Florida, 1993.

Yang, M., P. T. A. Reilly, K. B. Boraas, W. B. Whitten, and J. M. Ramsey, Real-time chemical analysis of aerosol particles using an ion trap mass spectrometer, *Rapid Commun. Mass Spectrom.*, 10, 347-351, 1996.

APPENDIX A

SELECTED AEROSOL MASS SPECTRA FROM SUCCESS MISSION

FLIGHT 09212

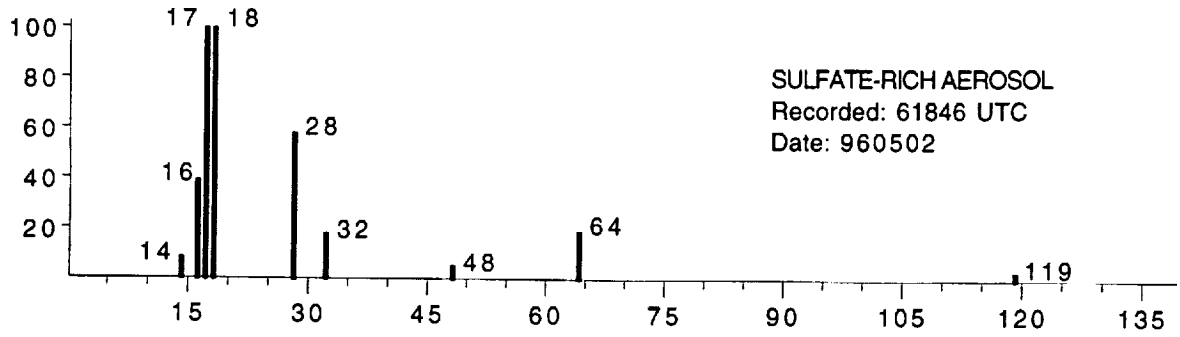

m/z	Rel. Abund.	m/z	Rel. Abund.	m/z	Rel. Abund.
14	8	16	39	17	100
18	100	28	58	32	18
48	5	64	19	119	4

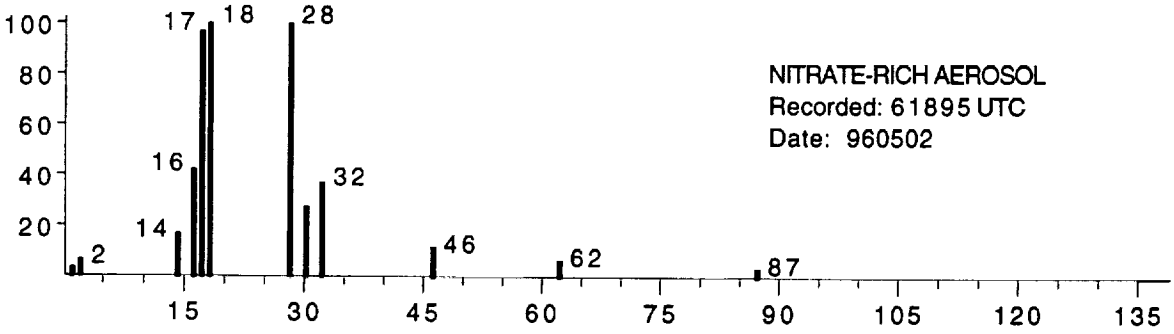

m/z	Rel. Abund.	m/z	Rel. Abund.	m/z	Rel. Abund.
1	3	2	6	14	16
16	42	17	96	18	100
28	100	30	27	32	37
46	12	62	6	87	3

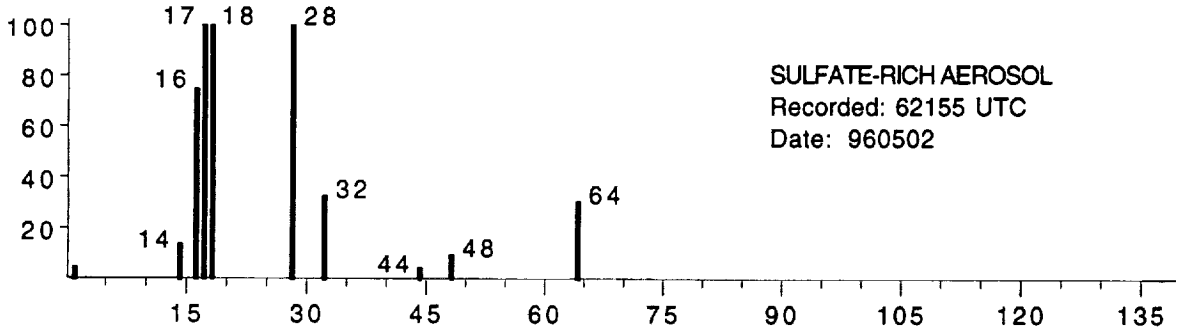

m/z	Rel. Abund.	m/z	Rel. Abund.	m/z	Rel. Abund.
1	5	14	13	16	75
17	100	18	100	28	100
32	33	44	4	48	10
64	31				

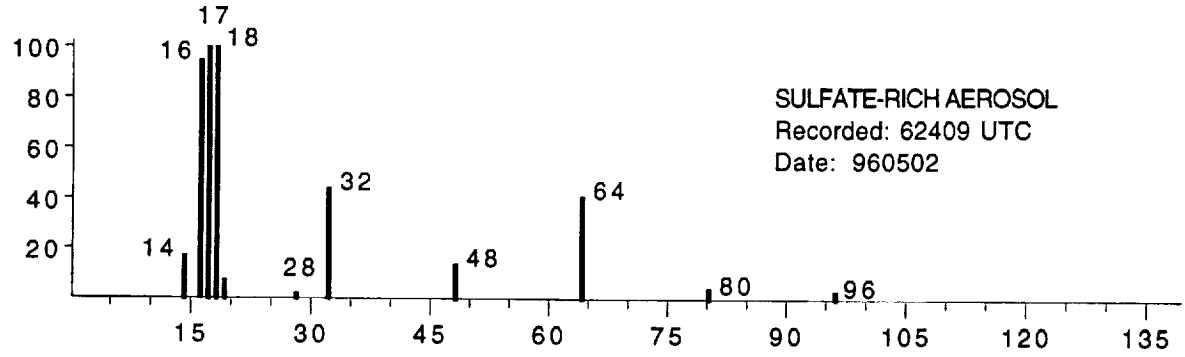

m/z	Rel. Abund.	m/z	Rel. Abund.	m/z	Rel. Abund.
14	17	16	95	17	100
18	100	19	7	28	2
32	44	48	14	64	41
80	4	96	3		

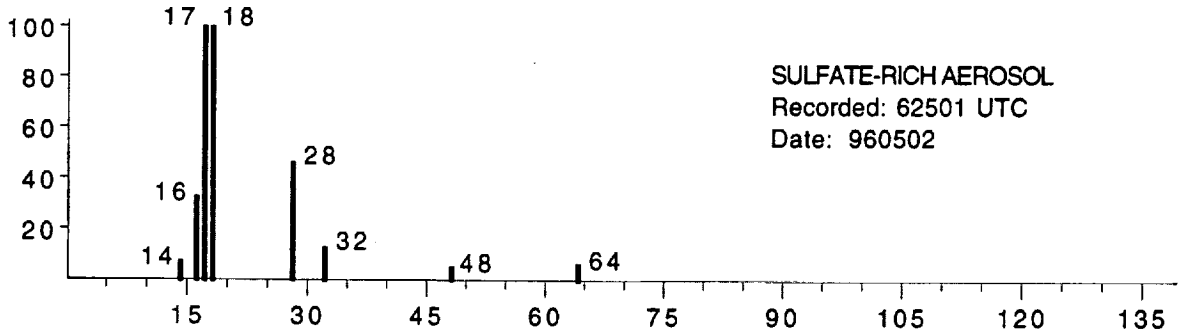

m/z	Rel. Abund.	m/z	Rel. Abund.	m/z	Rel. Abund.
14	7	16	32	17	100
18	100	28	46	32	13
48	5	64	7		

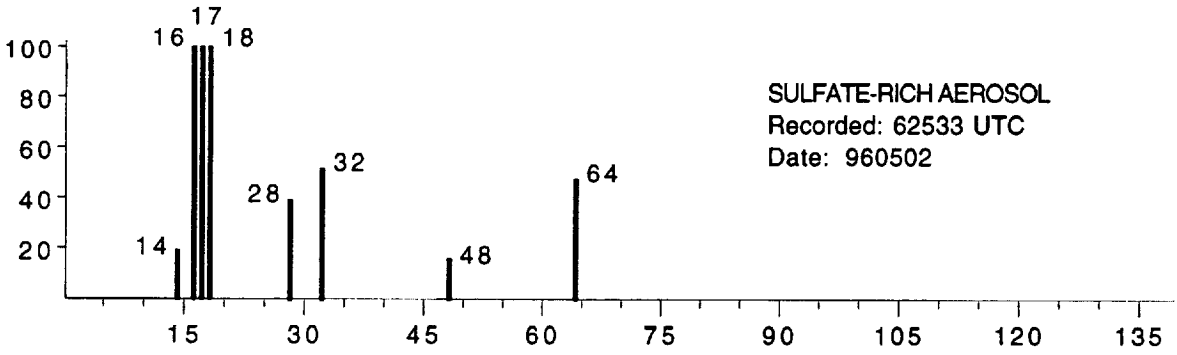

m/z	Rel. Abund.	m/z	Rel. Abund.	m/z	Rel. Abund.
14	18	16	100	17	100
18	100	28	39	32	52
48	15	64	47		

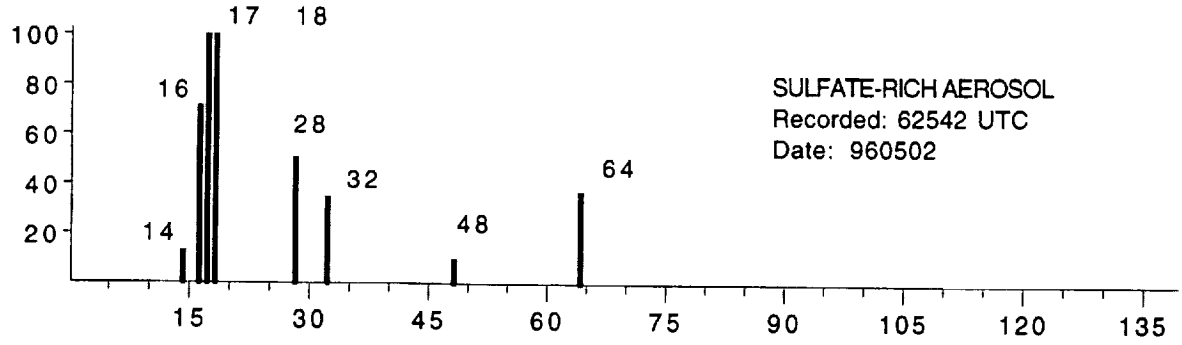

SULFATE-RICH AEROSOL
Recorded: 62542 UTC
Date: 960502

m/z	Rel. Abund.	m/z	Rel. Abund.	m/z	Rel. Abund.
14	13	16	72	17	100
18	100	28	50	32	35
48	10	64	37		

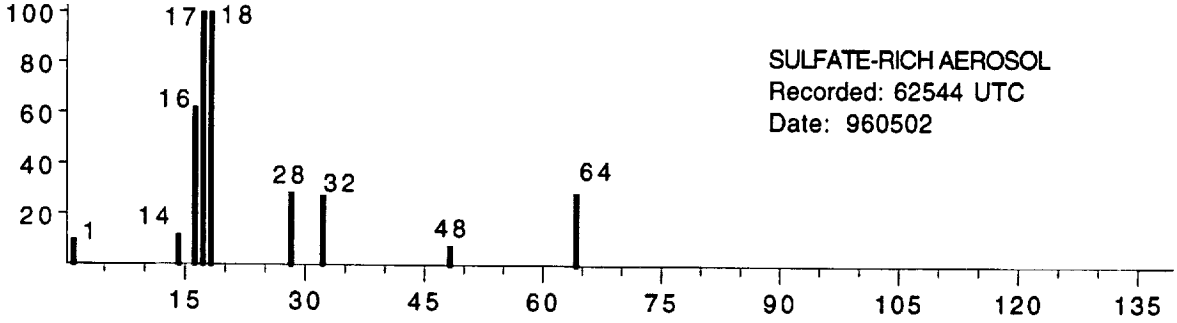

SULFATE-RICH AEROSOL
Recorded: 62544 UTC
Date: 960502

m/z	Rel. Abund.	m/z	Rel. Abund.	m/z	Rel. Abund.
1	9	14	11	16	62
17	100	18	100	28	29
32	27	48	7	64	29

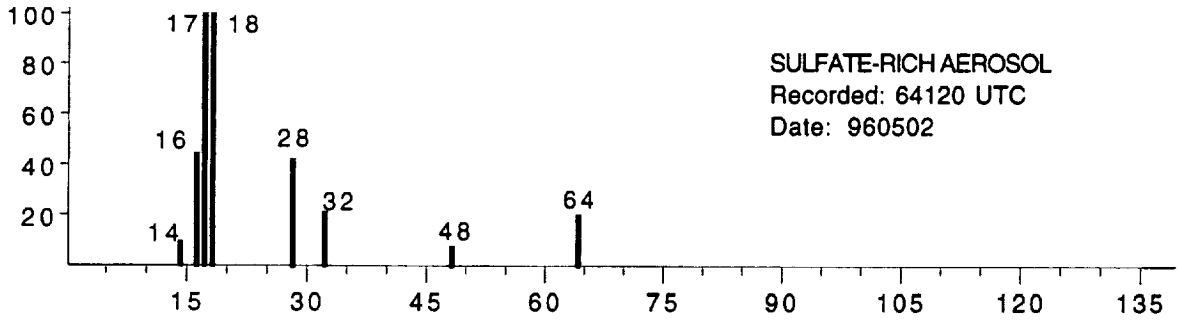

SULFATE-RICH AEROSOL
Recorded: 64120 UTC
Date: 960502

m/z	Rel. Abund.	m/z	Rel. Abund.	m/z	Rel. Abund.
14	9	16	44	17	100
18	100	28	42	32	21
48	7	64	20		

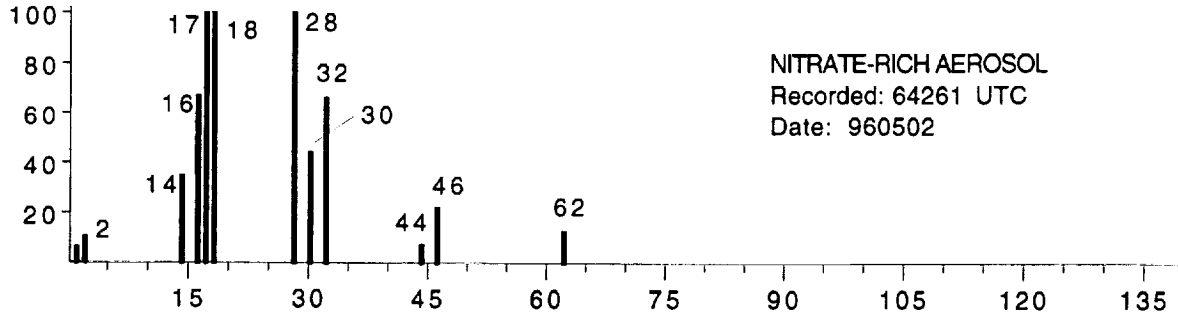

NITRATE-RICH AEROSOL
Recorded: 64261 UTC
Date: 960502

m/z	Rel. Abund.	m/z	Rel. Abund.	m/z	Rel. Abund.
1	7	2	11	14	35
16	68	17	100	18	100
28	100	30	44	32	66
44	7	46	22	62	12

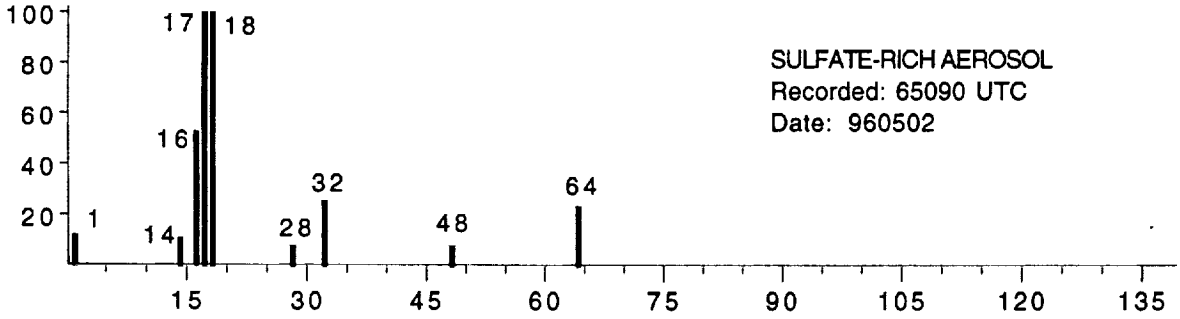

SULFATE-RICH AEROSOL
Recorded: 65090 UTC
Date: 960502

m/z	Rel. Abund.	m/z	Rel. Abund.	m/z	Rel. Abund.
1	12	14	11	16	53
17	100	18	100	28	7
32	25	48	8	64	23

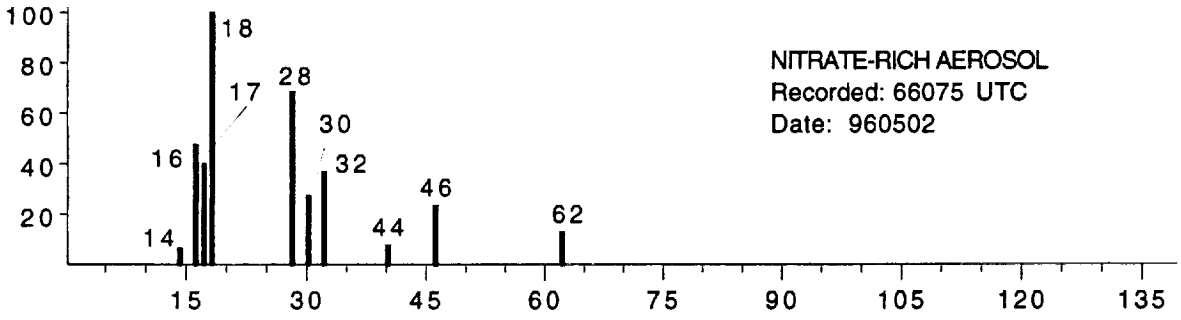

NITRATE-RICH AEROSOL
Recorded: 66075 UTC
Date: 960502

m/z	Rel. Abund.	m/z	Rel. Abund.	m/z	Rel. Abund.
14	7	16	47	17	40
18	100	28	69	30	28
32	37	40	8	46	23
62	13				

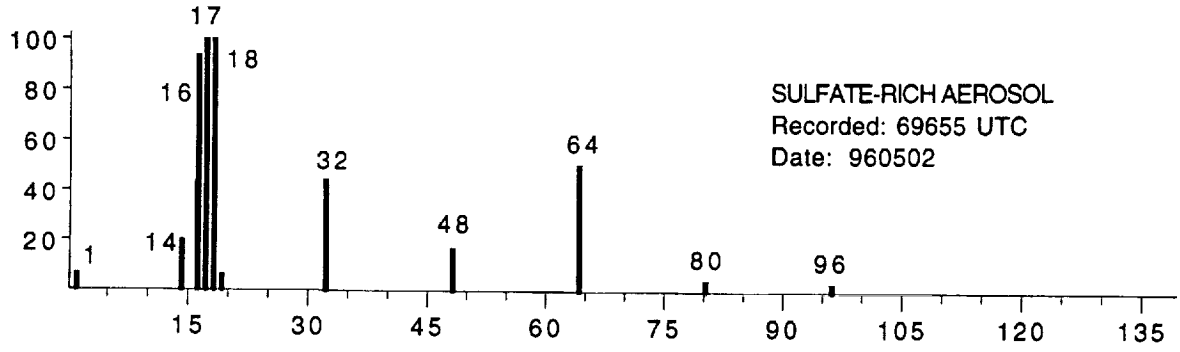

m/z	Rel. Abund.	m/z	Rel. Abund.	m/z	Rel. Abund.
1	7	14	20	16	94
17	100	18	100	19	6
32	44	48	17	64	51
80	4	96	4		

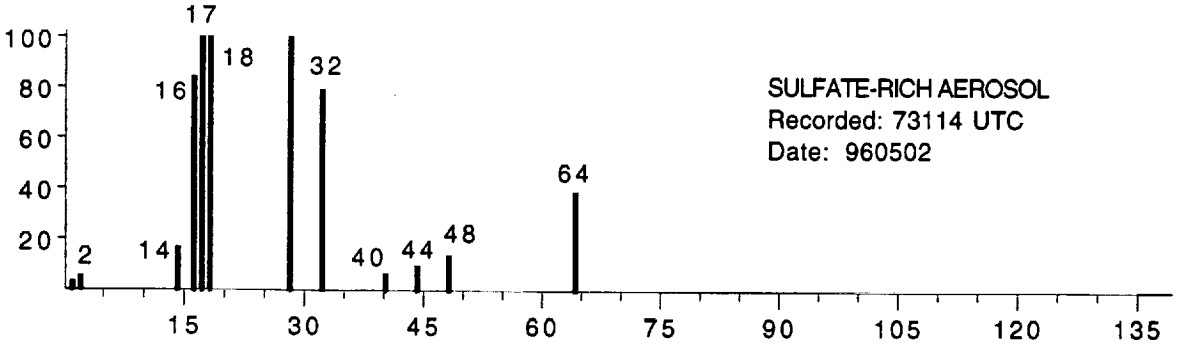

m/z	Rel. Abund.	m/z	Rel. Abund.	m/z	Rel. Abund.
1	3	2	5	14	17
16	84	17	100	18	100
28	100	32	79	40	6
44	9	48	13	64	38

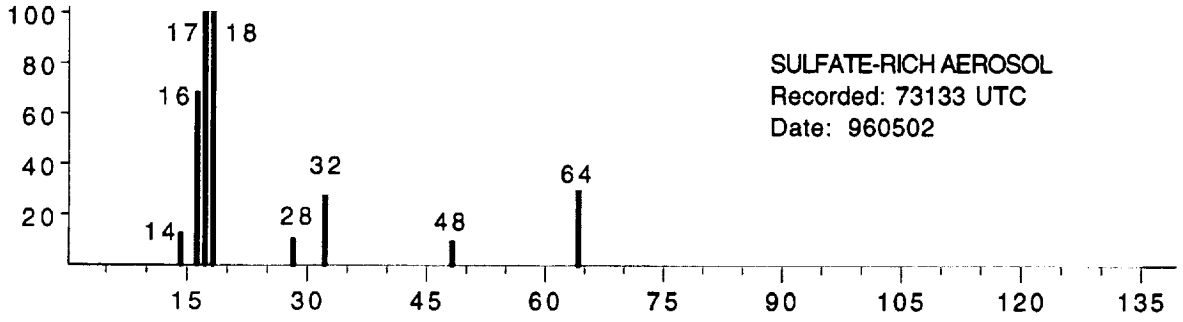

m/z	Rel. Abund.	m/z	Rel. Abund.	m/z	Rel. Abund.
14	13	16	69	17	100
18	100	28	10	32	27
48	10	64	29		

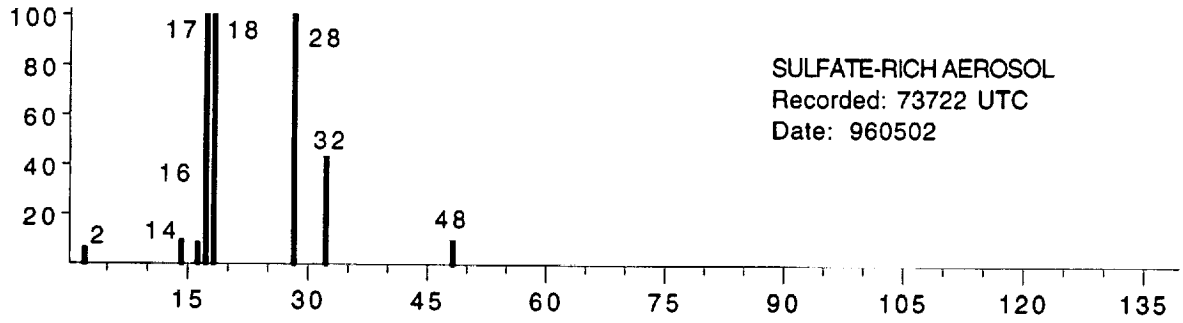

SULFATE-RICH AEROSOL
Recorded: 73722 UTC
Date: 960502

m/z	Rel. Abund.	m/z	Rel. Abund.	m/z	Rel. Abund.
2	6	14	9	16	8
17	100	18	100	28	100
32	43	48	10		

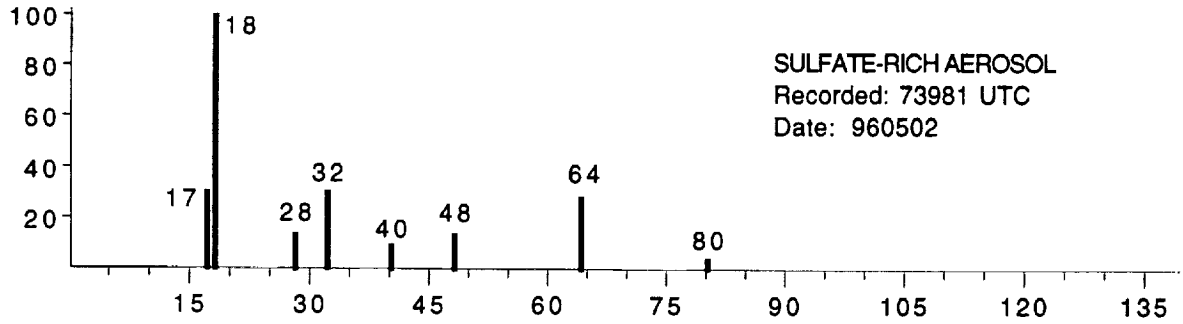

SULFATE-RICH AEROSOL
Recorded: 73981 UTC
Date: 960502

m/z	Rel. Abund.	m/z	Rel. Abund.	m/z	Rel. Abund.
17	30	18	100	28	13
32	30	40	9	48	13
64	29	80	5		

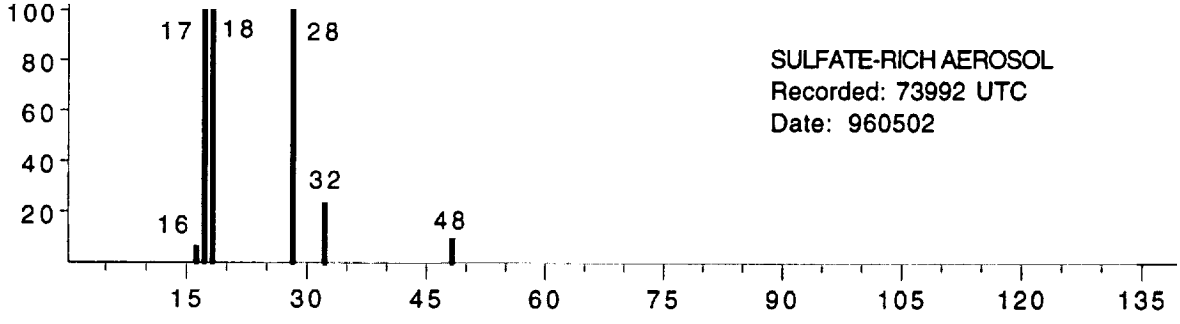

SULFATE-RICH AEROSOL
Recorded: 73992 UTC
Date: 960502

m/z	Rel. Abund.	m/z	Rel. Abund.	m/z	Rel. Abund.
16	7	17	100	18	100
28	100	32	24	48	9

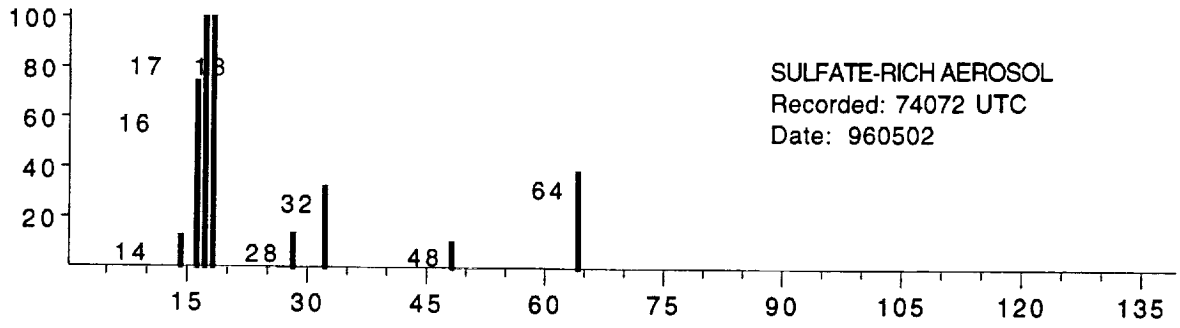

SULFATE-RICH AEROSOL
Recorded: 74072 UTC
Date: 960502

m/z	Rel. Abund.	m/z	Rel. Abund.	m/z	Rel. Abund.
14	12	16	75	17	100
18	100	28	13	32	33
48	11	64	39		

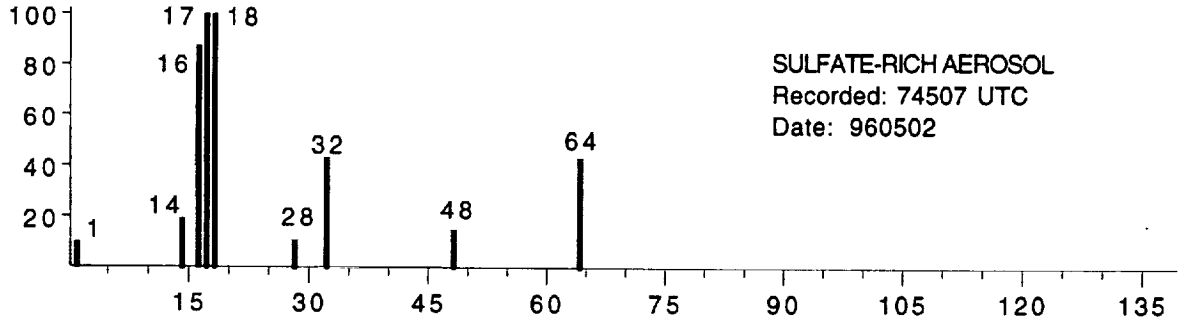

SULFATE-RICH AEROSOL
Recorded: 74507 UTC
Date: 960502

m/z	Rel. Abund.	m/z	Rel. Abund.	m/z	Rel. Abund.
1	9	14	19	16	88
17	100	18	100	28	11
32	43	48	15	64	43

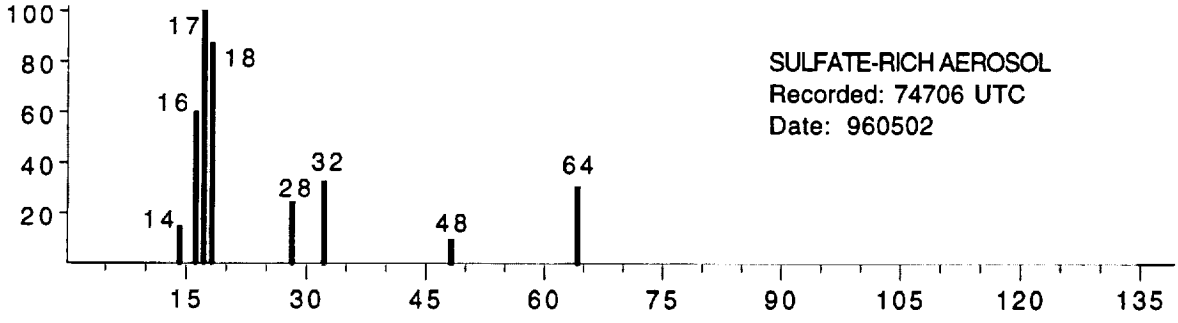

SULFATE-RICH AEROSOL
Recorded: 74706 UTC
Date: 960502

m/z	Rel. Abund.	m/z	Rel. Abund.	m/z	Rel. Abund.
14	15	16	60	17	100
18	87	28	25	32	32
48	10	64	31		

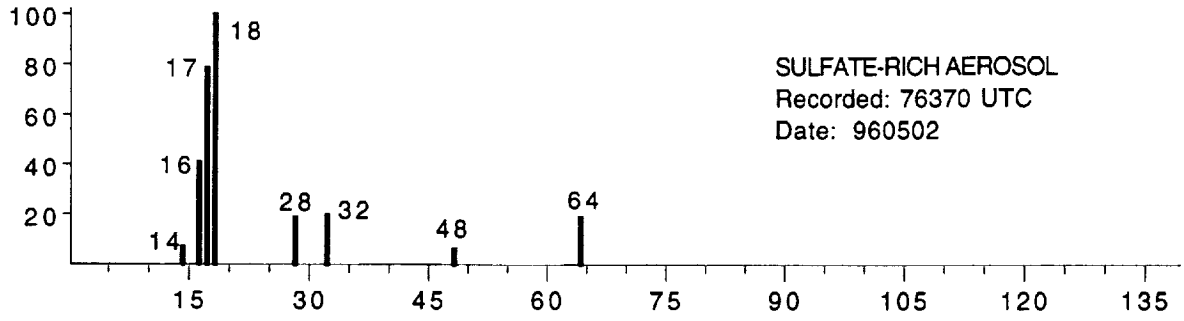

SULFATE-RICH AEROSOL
Recorded: 76370 UTC
Date: 960502

m/z	Rel. Abund.	m/z	Rel. Abund.	m/z	Rel. Abund.
14	8	16	41	17	79
18	100	28	19	32	21
48	6	64	19		

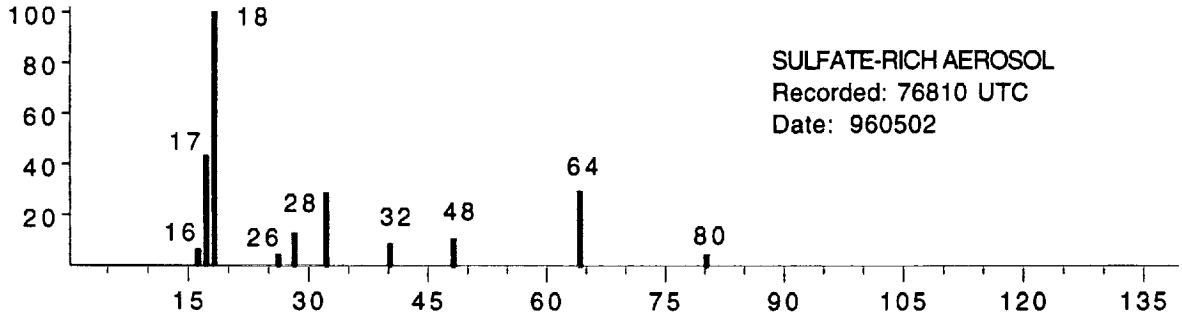

SULFATE-RICH AEROSOL
Recorded: 76810 UTC
Date: 960502

m/z	Rel. Abund.	m/z	Rel. Abund.	m/z	Rel. Abund.
16	6	17	43	18	100
26	5	28	13	32	28
40	8	48	10	64	29
80	4				

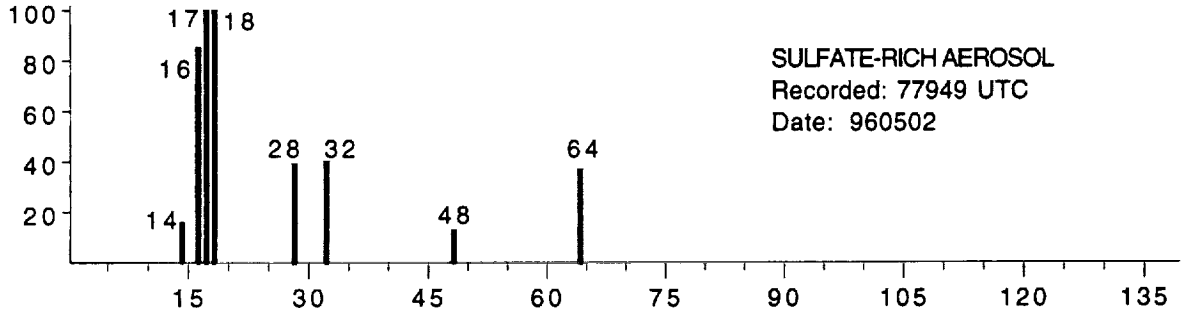

SULFATE-RICH AEROSOL
Recorded: 77949 UTC
Date: 960502

m/z	Rel. Abund.	m/z	Rel. Abund.	m/z	Rel. Abund.
14	16	16	85	17	100
18	100	28	39	32	40
48	13	64	37		

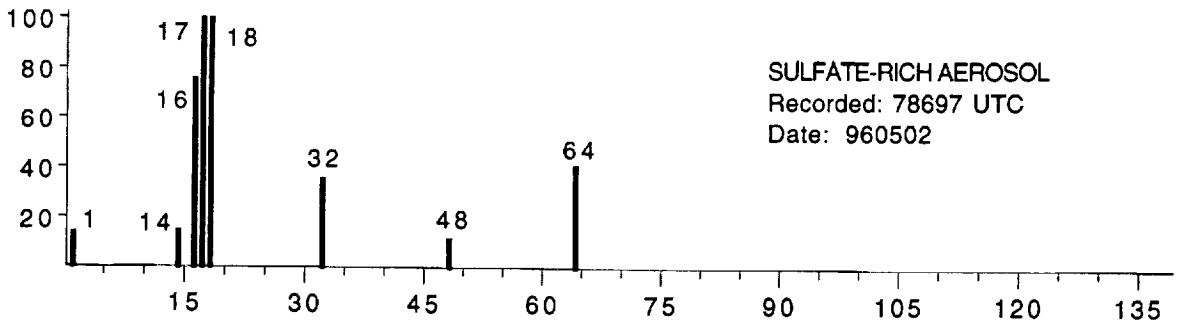

m/z	Rel. Abund.	m/z	Rel. Abund.	m/z	Rel. Abund.
1	14	14	15	16	75
17	100	18	100	32	35
48	12	64	41		

APPENDIX B

SELECTED AEROSOL MASS SPECTRA FROM SUCCESS MISSION

FLIGHT 09213

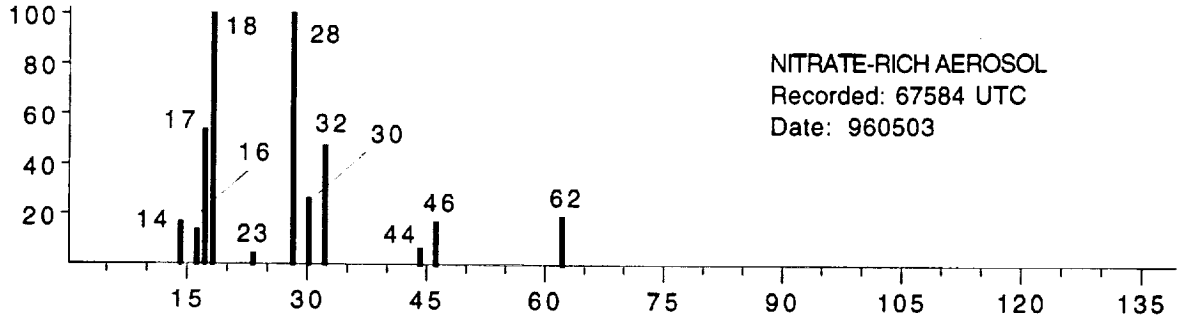

NITRATE-RICH AEROSOL
Recorded: 67584 UTC
Date: 960503

m/z	Rel. Abund.	m/z	Rel. Abund.	m/z	Rel. Abund.
14	17	16	14	17	53
18	100	23	5	28	100
30	26	32	48	44	6
46	17	62	18		

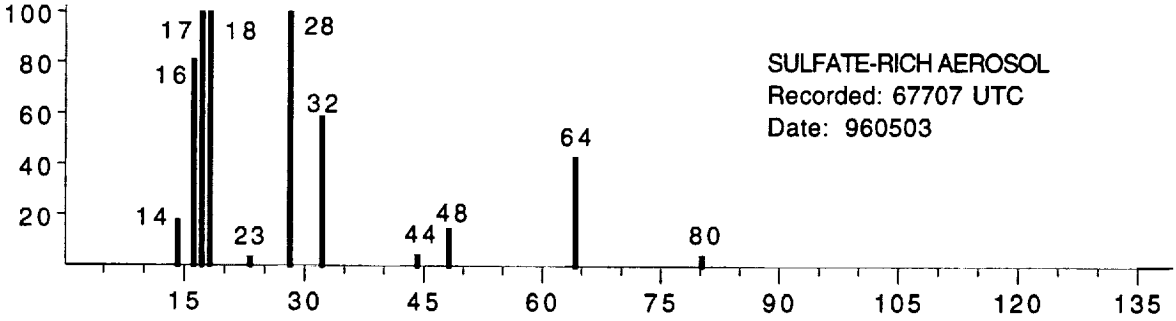

SULFATE-RICH AEROSOL
Recorded: 67707 UTC
Date: 960503

m/z	Rel. Abund.	m/z	Rel. Abund.	m/z	Rel. Abund.
14	18	16	82	17	100
18	100	23	3	28	100
32	58	44	5	48	15
64	43	80	4		

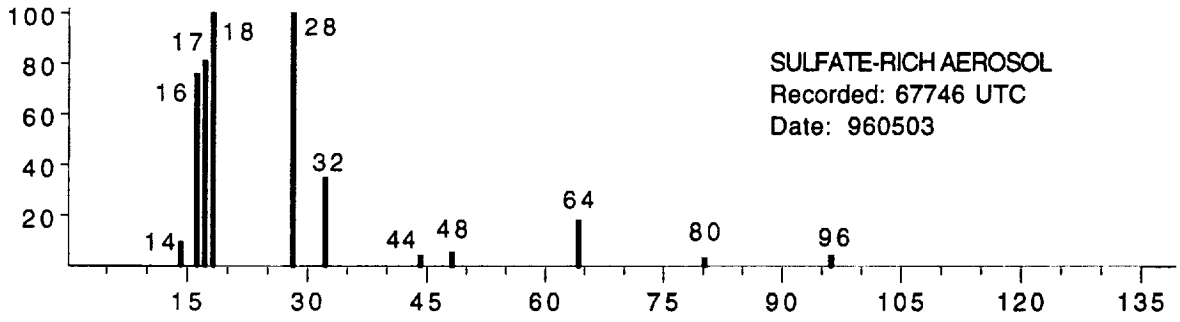

SULFATE-RICH AEROSOL
Recorded: 67746 UTC
Date: 960503

m/z	Rel. Abund.	m/z	Rel. Abund.	m/z	Rel. Abund.
14	9	16	75	17	81
18	100	28	100	32	35
44	4	48	5	64	18
80	3	96	4		

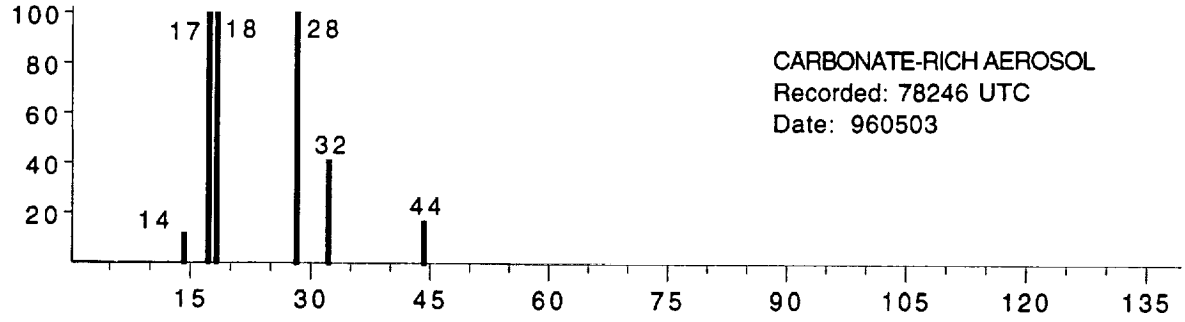

CARBONATE-RICH AEROSOL
Recorded: 78246 UTC
Date: 960503

m/z	Rel. Abund.	m/z	Rel. Abund.	m/z	Rel. Abund.
14	11	17	100	18	100
28	100	32	41	44	16

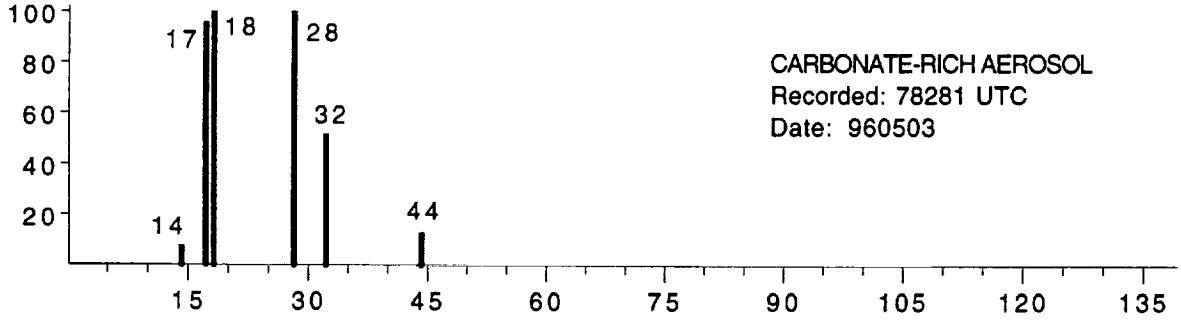

CARBONATE-RICH AEROSOL
Recorded: 78281 UTC
Date: 960503

m/z	Rel. Abund.	m/z	Rel. Abund.	m/z	Rel. Abund.
14	7	17	95	18	100
28	100	32	51	44	13

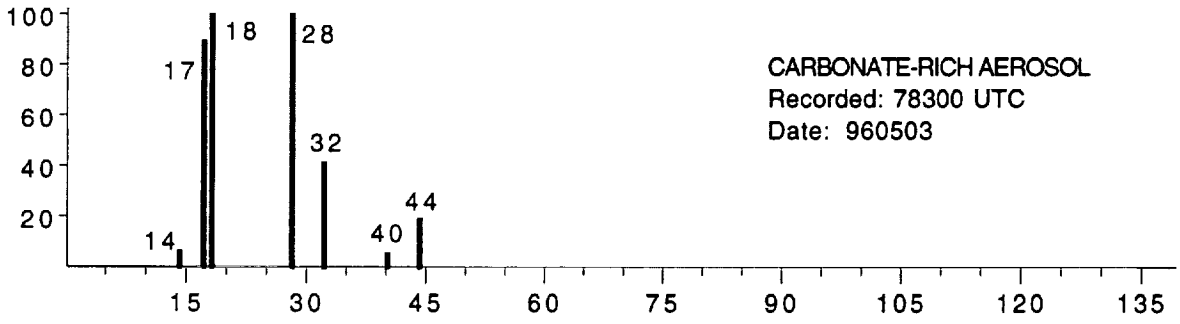

CARBONATE-RICH AEROSOL
Recorded: 78300 UTC
Date: 960503

m/z	Rel. Abund.	m/z	Rel. Abund.	m/z	Rel. Abund.
14	6	17	89	18	100
28	100	32	42	40	5
44	19				

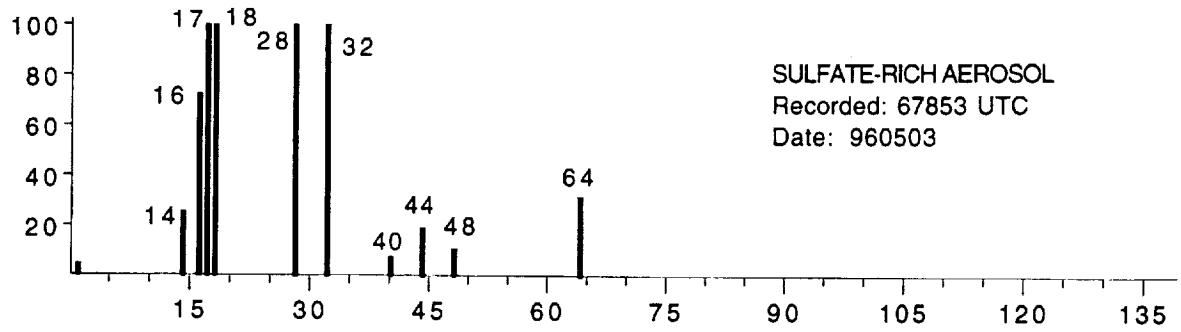

SULFATE-RICH AEROSOL
Recorded: 67853 UTC
Date: 960503

m/z	Rel. Abund.	m/z	Rel. Abund.	m/z	Rel. Abund.
1	4	14	25	16	73
17	100	18	100	28	100
32	100	40	7	44	19
48	11	64	32		

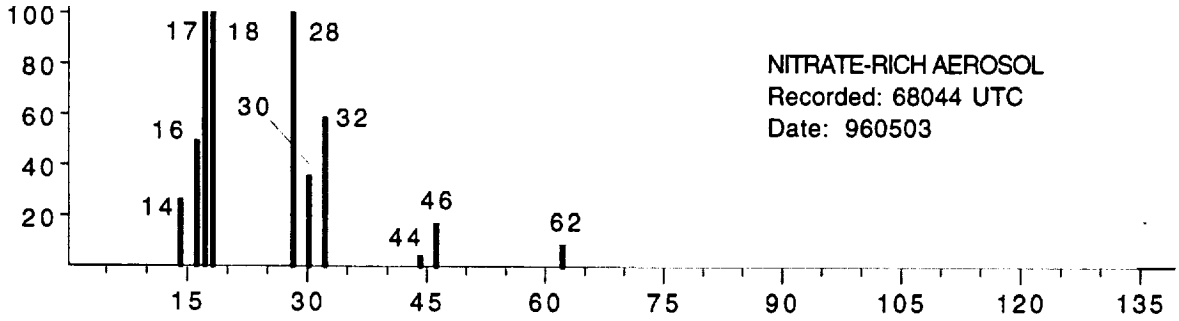

NITRATE-RICH AEROSOL
Recorded: 68044 UTC
Date: 960503

m/z	Rel. Abund.	m/z	Rel. Abund.	m/z	Rel. Abund.
14	26	16	50	17	100
18	100	28	100	30	35
32	59	44	4	46	17
62	8				

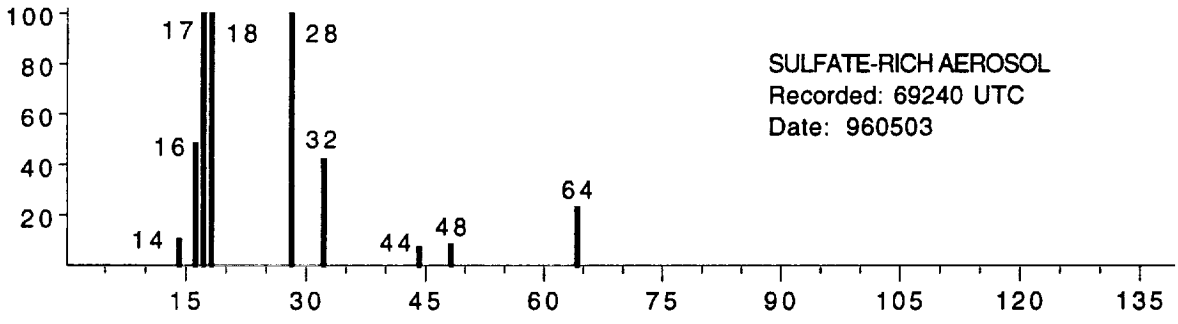

SULFATE-RICH AEROSOL
Recorded: 69240 UTC
Date: 960503

m/z	Rel. Abund.	m/z	Rel. Abund.	m/z	Rel. Abund.
14	11	16	48	17	100
18	100	28	100	32	42
44	7	48	9	64	24

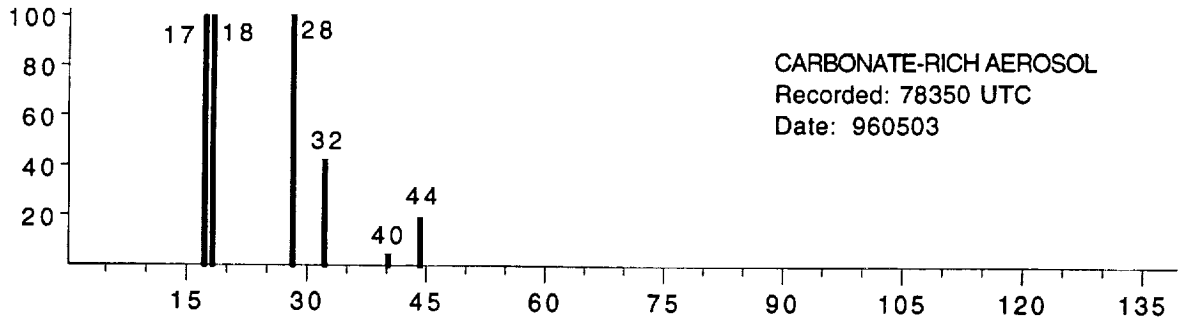

CARBONATE-RICH AEROSOL
Recorded: 78350 UTC
Date: 960503

m/z	Rel. Abund.	m/z	Rel. Abund.	m/z	Rel. Abund.
17	100	18	100	28	100
32	42	40	5	44	18

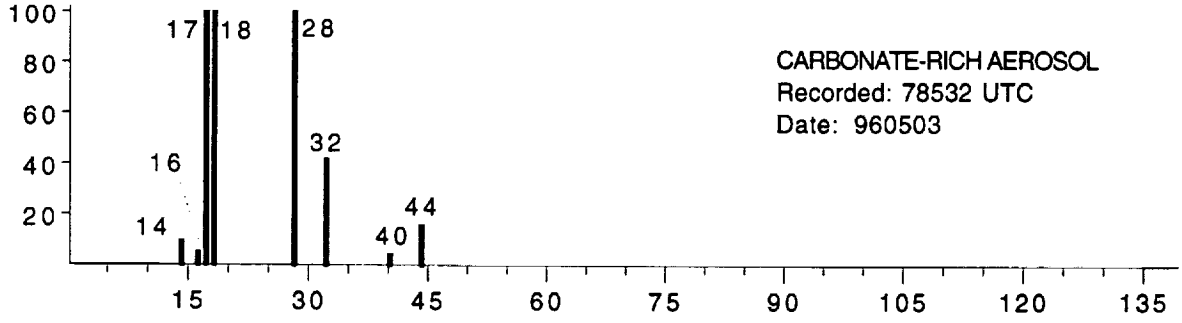

CARBONATE-RICH AEROSOL
Recorded: 78532 UTC
Date: 960503

m/z	Rel. Abund.	m/z	Rel. Abund.	m/z	Rel. Abund.
14	9	16	5	17	100
18	100	28	100	32	42
40	5	44	15		

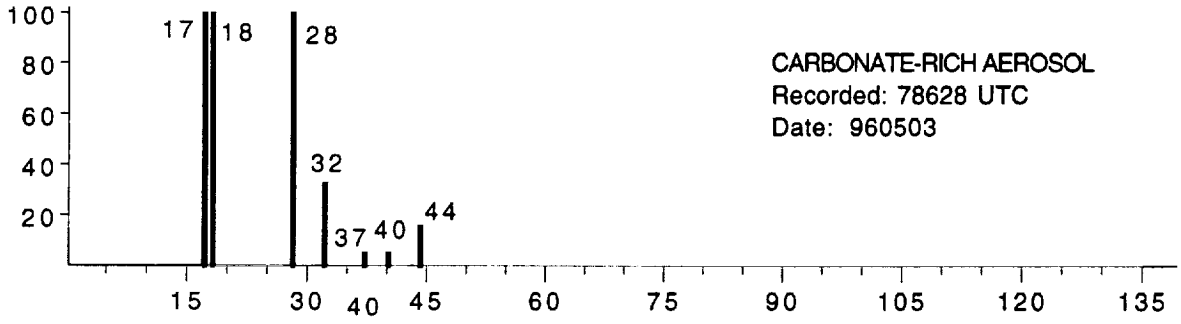

CARBONATE-RICH AEROSOL
Recorded: 78628 UTC
Date: 960503

m/z	Rel. Abund.	m/z	Rel. Abund.	m/z	Rel. Abund.
17	100	18	100	28	100
32	32	37	5	40	5
44	16				

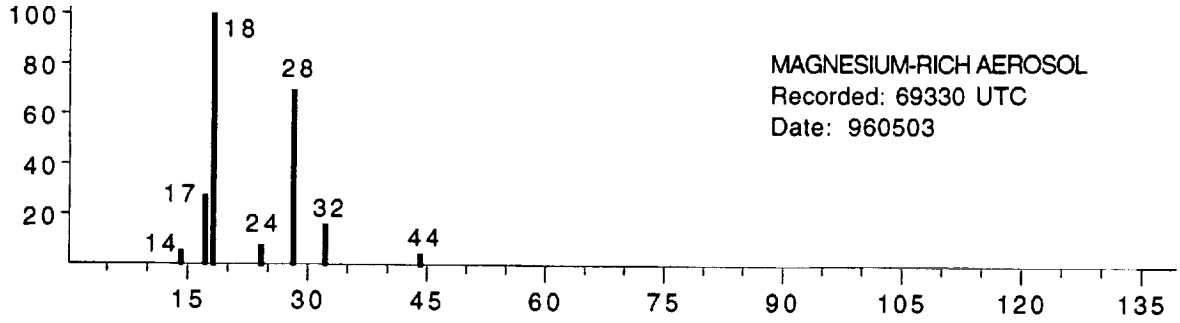

MAGNESIUM-RICH AEROSOL
Recorded: 69330 UTC
Date: 960503

m/z	Rel. Abund.	m/z	Rel. Abund.	m/z	Rel. Abund.
14	5	17	27	18	100
24	7	28	70	32	16
44	4				

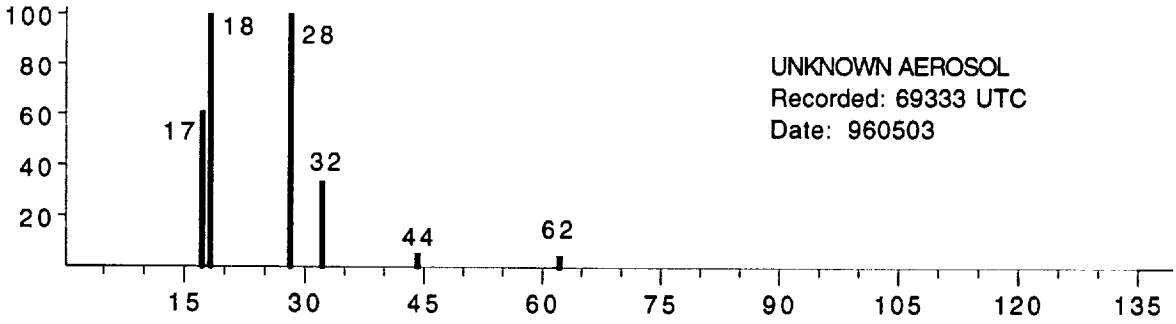

UNKNOWN AEROSOL
Recorded: 69333 UTC
Date: 960503

m/z	Rel. Abund.	m/z	Rel. Abund.	m/z	Rel. Abund.
17	62	18	100	28	100
32	33	44	5	62	4

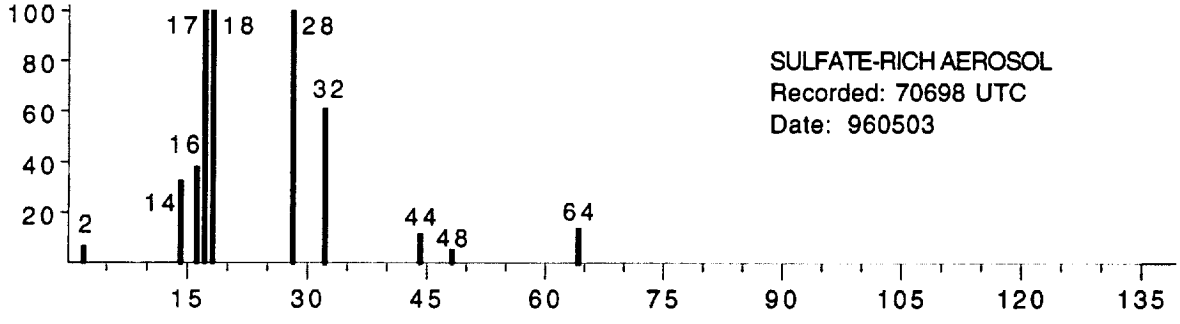

SULFATE-RICH AEROSOL
Recorded: 70698 UTC
Date: 960503

m/z	Rel. Abund.	m/z	Rel. Abund.	m/z	Rel. Abund.
2	6	14	33	16	38
17	100	18	100	28	100
32	62	44	11	48	5
64	14				

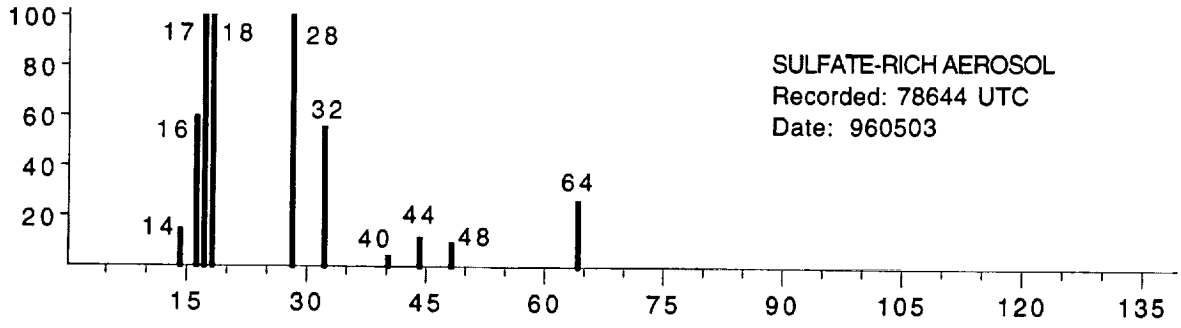

SULFATE-RICH AEROSOL
Recorded: 78644 UTC
Date: 960503

m/z	Rel. Abund.	m/z	Rel. Abund.	m/z	Rel. Abund.
14	15	16	60	17	100
18	100	28	100	32	56
40	4	44	11	48	9
64	27				

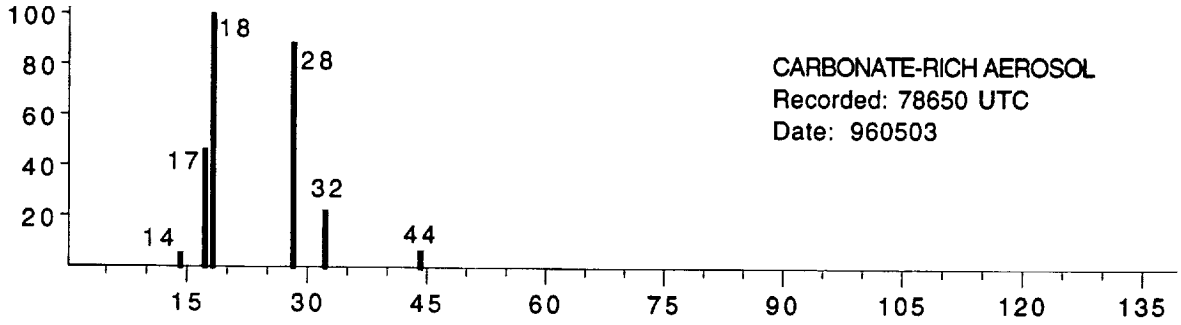

CARBONATE-RICH AEROSOL
Recorded: 78650 UTC
Date: 960503

m/z	Rel. Abund.	m/z	Rel. Abund.	m/z	Rel. Abund.
14	5	17	46	18	100
28	89	32	22	44	7

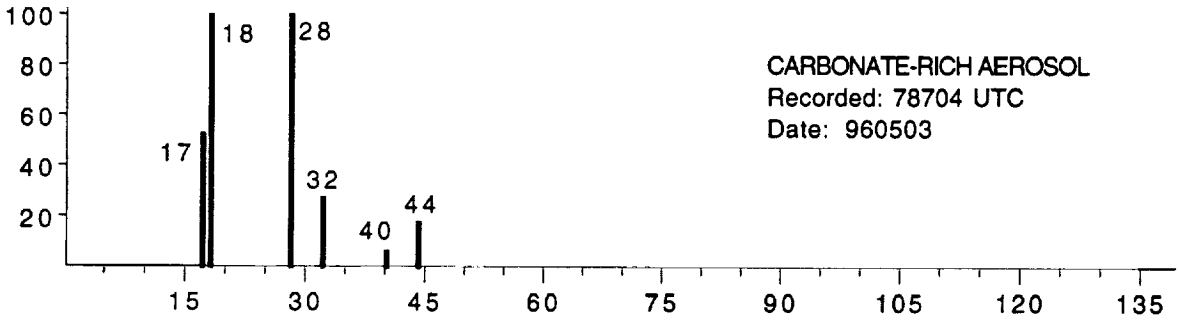

CARBONATE-RICH AEROSOL
Recorded: 78704 UTC
Date: 960503

m/z	Rel. Abund.	m/z	Rel. Abund.	m/z	Rel. Abund.
17	53	18	100	28	100
32	27	40	6	44	18

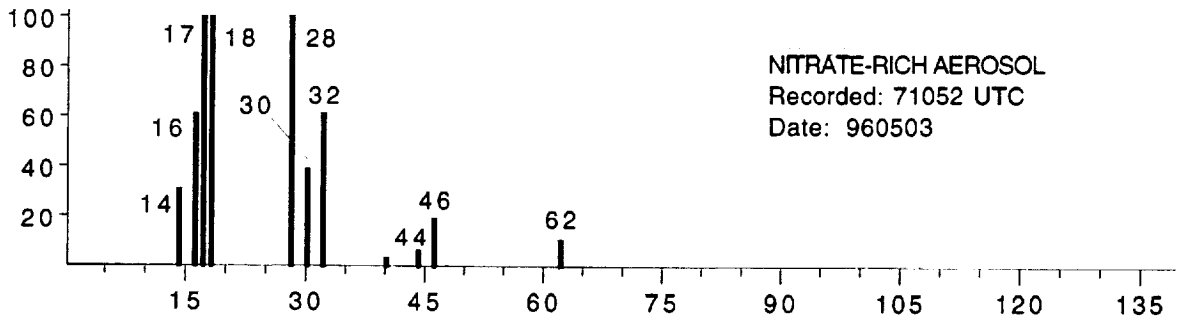

NITRATE-RICH AEROSOL
Recorded: 71052 UTC
Date: 960503

m/z	Rel. Abund.	m/z	Rel. Abund.	m/z	Rel. Abund.
14	30	16	61	17	100
18	100	28	100	30	39
32	61	40	4	44	6
46	19	62	11		

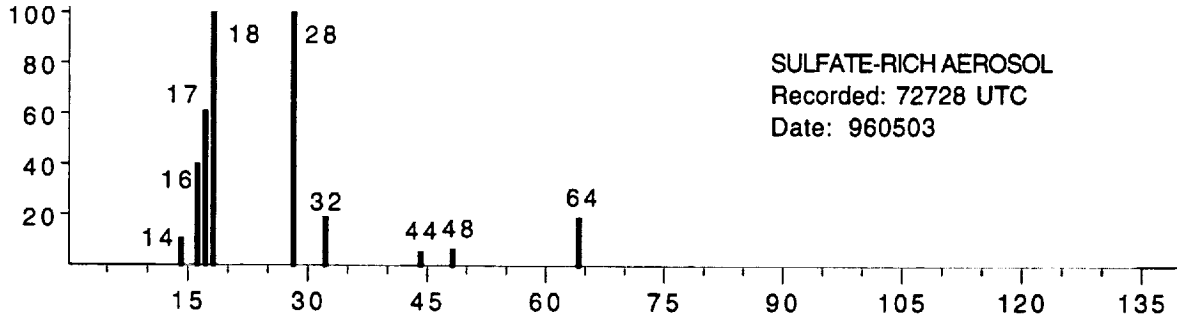

SULFATE-RICH AEROSOL
Recorded: 72728 UTC
Date: 960503

m/z	Rel. Abund.	m/z	Rel. Abund.	m/z	Rel. Abund.
14	10	16	40	17	61
18	100	28	100	32	19
44	5	48	7	64	19

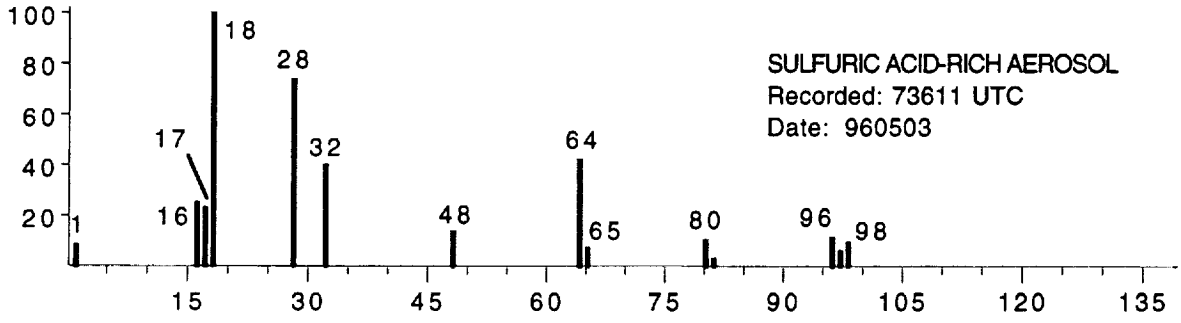

SULFURIC ACID-RICH AEROSOL
Recorded: 73611 UTC
Date: 960503

m/z	Rel. Abund.	m/z	Rel. Abund.	m/z	Rel. Abund.
1	9	16	25	17	24
18	100	28	73	32	40
48	14	64	42	65	8
80	10	81	3	96	12
97	6	98	9		

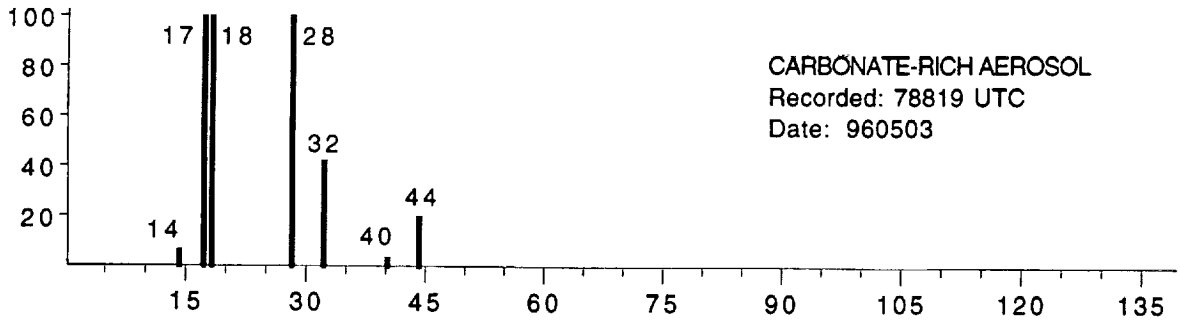

CARBONATE-RICH AEROSOL
Recorded: 78819 UTC
Date: 960503

m/z	Rel. Abund.	m/z	Rel. Abund.	m/z	Rel. Abund.
14	7	17	100	18	100
28	100	32	42	40	4
44	20				

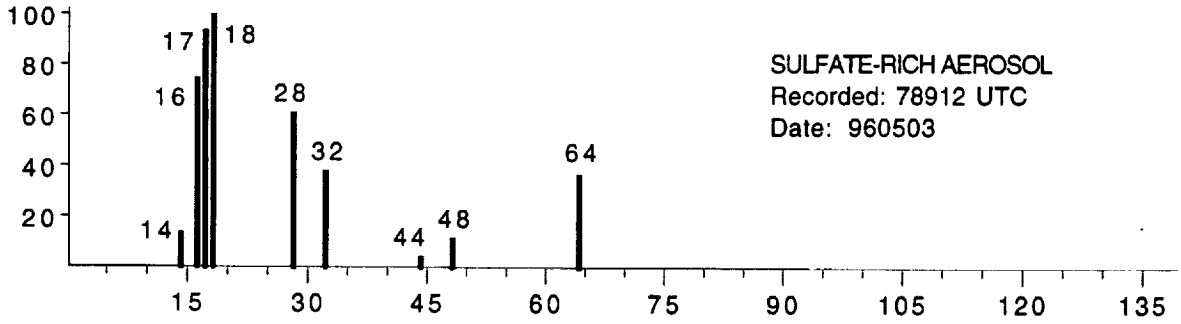

SULFATE-RICH AEROSOL
Recorded: 78912 UTC
Date: 960503

m/z	Rel. Abund.	m/z	Rel. Abund.	m/z	Rel. Abund.
14	14	16	75	17	94
18	100	28	62	32	38
44	4	48	12	64	37

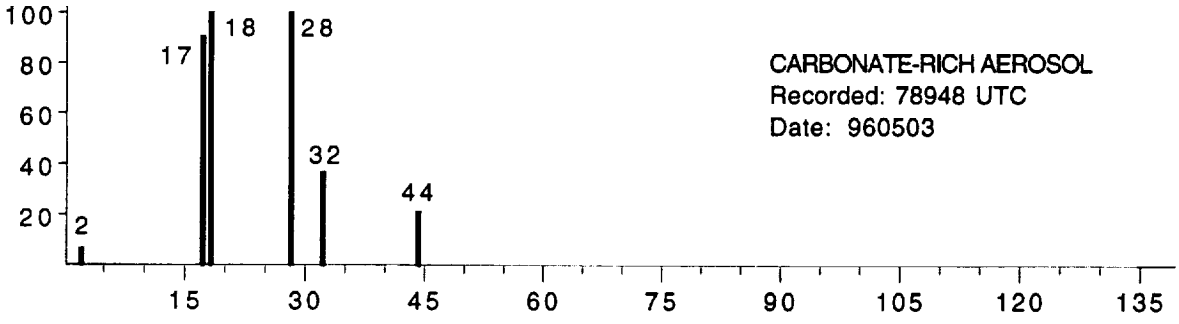

CARBONATE-RICH AEROSOL
Recorded: 78948 UTC
Date: 960503

m/z	Rel. Abund.	m/z	Rel. Abund.	m/z	Rel. Abund.
2	7	17	90	18	100
28	100	32	36	44	22

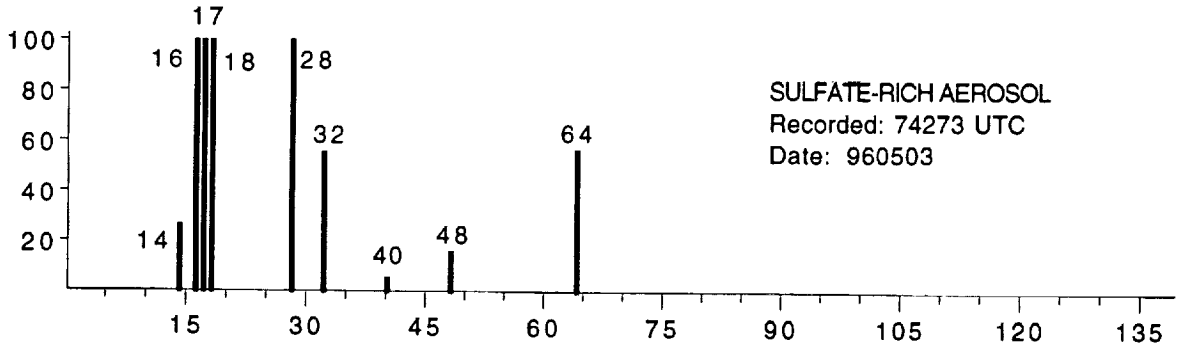

SULFATE-RICH AEROSOL
Recorded: 74273 UTC
Date: 960503

m/z	Rel. Abund.	m/z	Rel. Abund.	m/z	Rel. Abund.
14	26	16	100	17	100
18	100	28	100	32	55
40	5	48	16	64	56

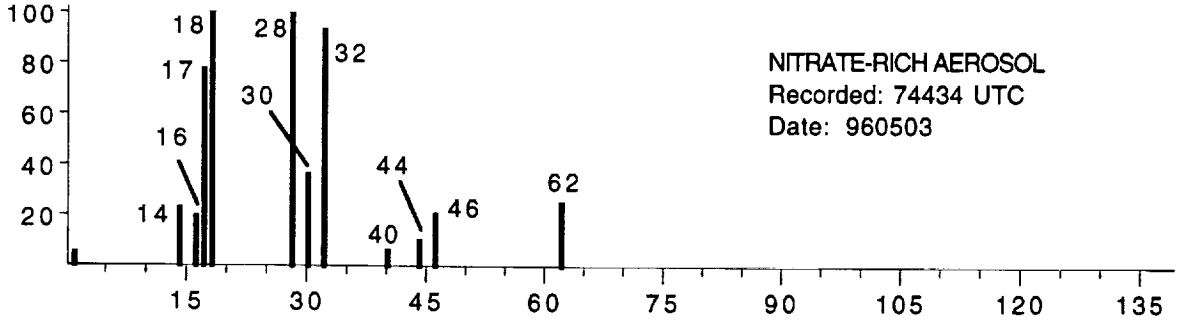

NITRATE-RICH AEROSOL
Recorded: 74434 UTC
Date: 960503

m/z	Rel. Abund.	m/z	Rel. Abund.	m/z	Rel. Abund.
1	5	14	23	16	20
17	78	18	100	28	100
30	37	32	94	40	6
44	11	46	21	62	25

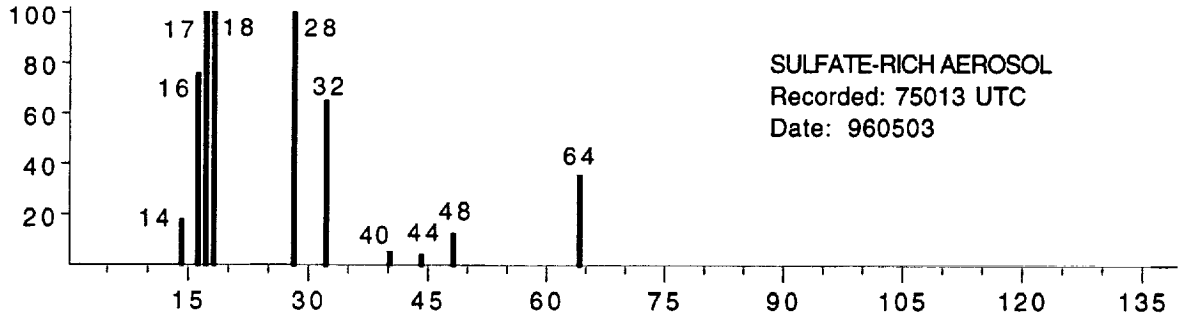

SULFATE-RICH AEROSOL
Recorded: 75013 UTC
Date: 960503

m/z	Rel. Abund.	m/z	Rel. Abund.	m/z	Rel. Abund.
14	18	16	75	17	100
18	100	28	100	32	65
40	5	44	4	48	12
64	35				

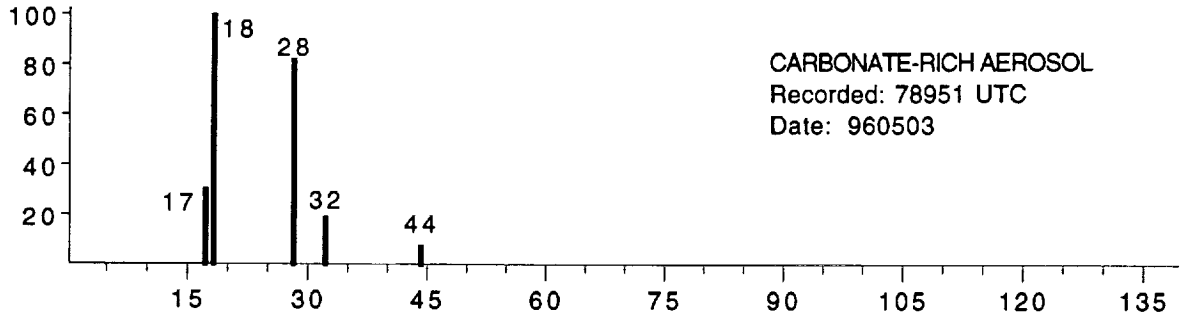

CARBONATE-RICH AEROSOL
Recorded: 78951 UTC
Date: 960503

m/z	Rel. Abund.	m/z	Rel. Abund.	m/z	Rel. Abund.
17	31	18	100	28	82
32	19	44	7		

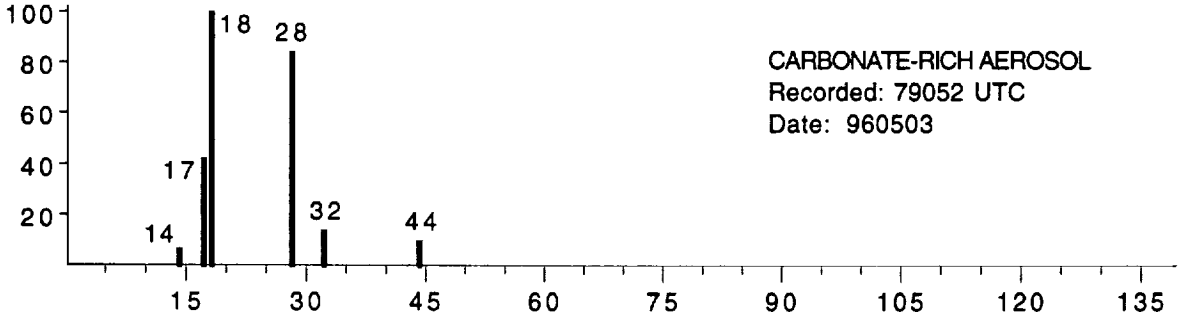

CARBONATE-RICH AEROSOL
Recorded: 79052 UTC
Date: 960503

m/z	Rel. Abund.	m/z	Rel. Abund.	m/z	Rel. Abund.
14	6	17	42	18	100
28	84	32	13	44	9

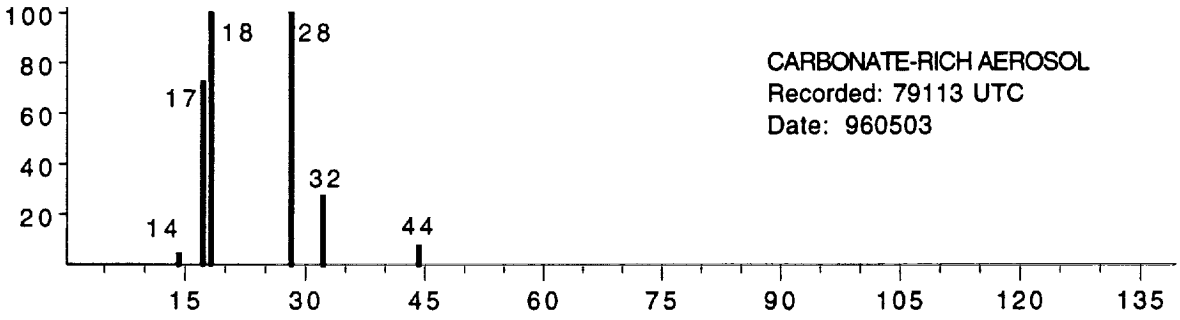

CARBONATE-RICH AEROSOL
Recorded: 79113 UTC
Date: 960503

m/z	Rel. Abund.	m/z	Rel. Abund.	m/z	Rel. Abund.
14	4	17	72	18	100
28	100	32	27	44	7

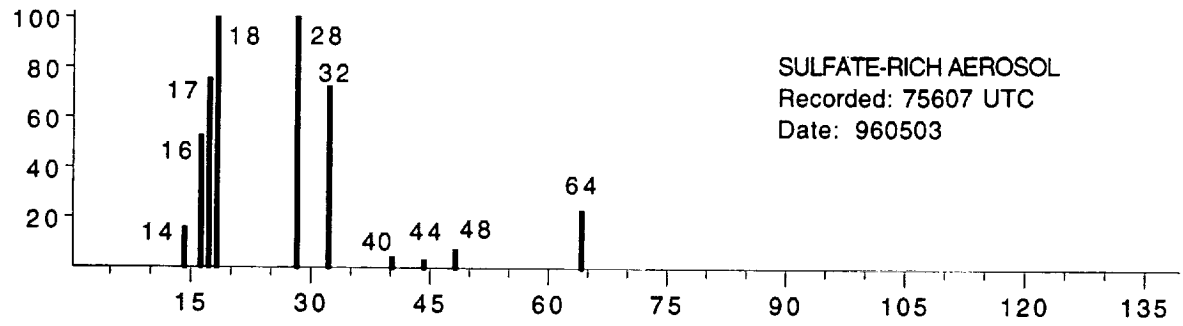

SULFATE-RICH AEROSOL
Recorded: 75607 UTC
Date: 960503

m/z	Rel. Abund.	m/z	Rel. Abund.	m/z	Rel. Abund.
14	16	16	53	17	76
18	100	28	100	32	72
40	5	44	4	48	8
64	23				

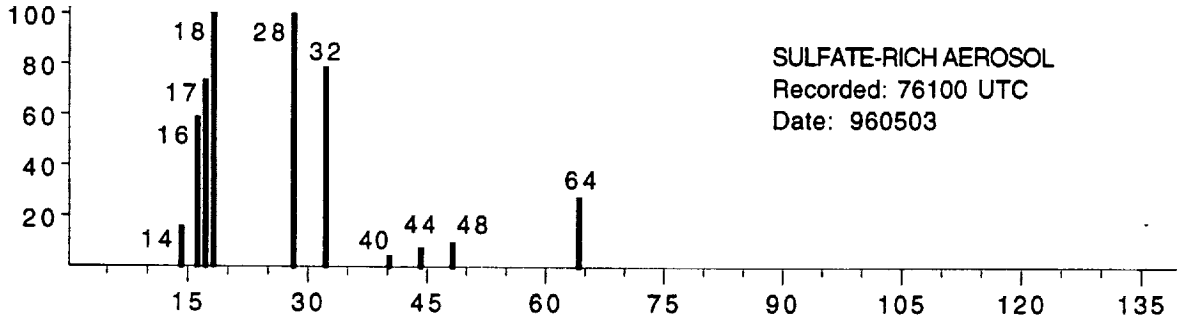

SULFATE-RICH AEROSOL
Recorded: 76100 UTC
Date: 960503

m/z	Rel. Abund.	m/z	Rel. Abund.	m/z	Rel. Abund.
14	15	16	58	17	73
18	100	28	100	32	78
40	4	44	7	48	9
64	28				

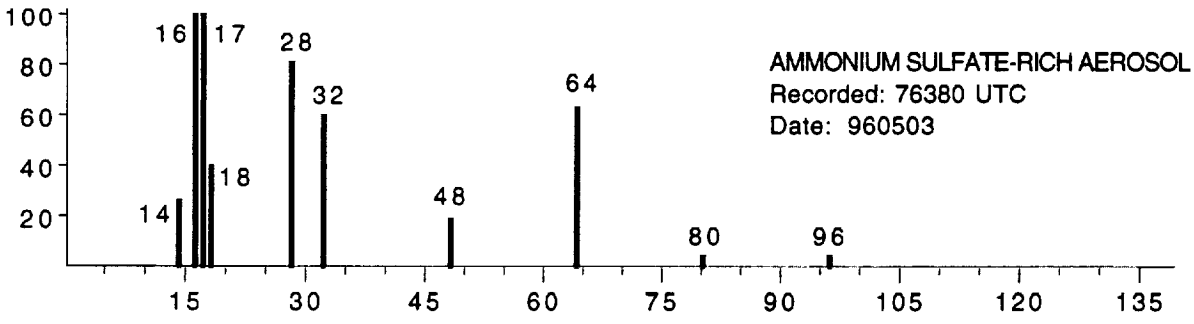

AMMONIUM SULFATE-RICH AEROSOL
Recorded: 76380 UTC
Date: 960503

m/z	Rel. Abund.	m/z	Rel. Abund.	m/z	Rel. Abund.
14	27	16	100	17	100
18	40	28	82	32	60
48	19	64	64	80	5
96	4				

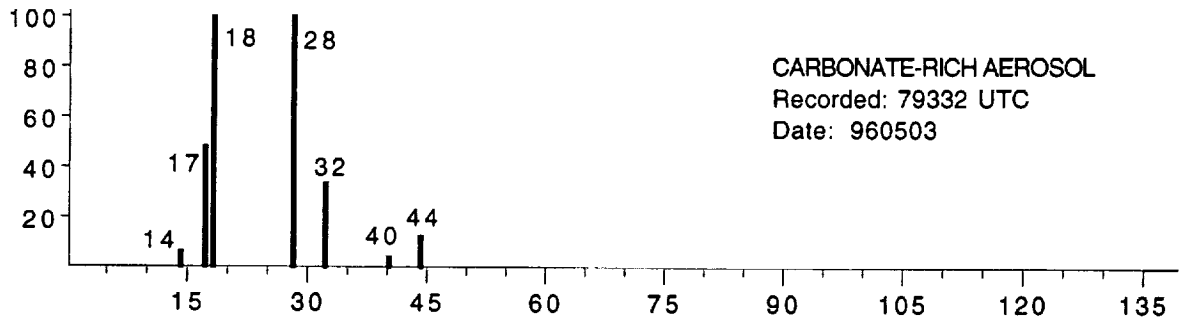

CARBONATE-RICH AEROSOL
Recorded: 79332 UTC
Date: 960503

m/z	Rel. Abund.	m/z	Rel. Abund.	m/z	Rel. Abund.
14	6	17	48	18	100
28	100	32	33	40	4
44	13				

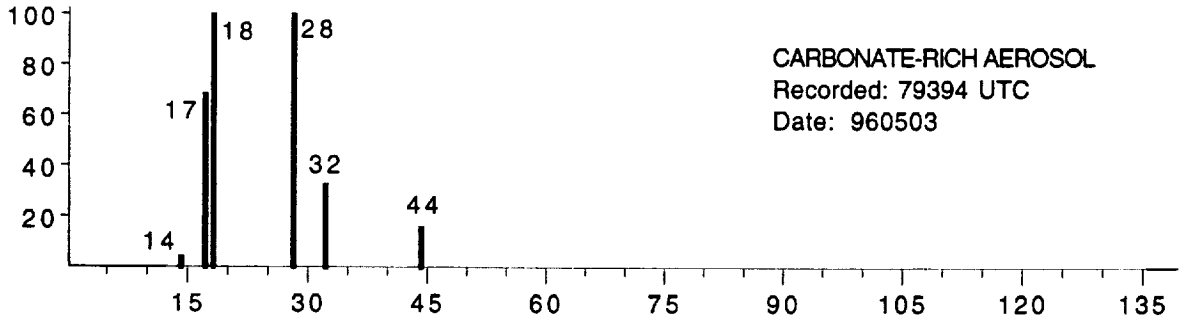

CARBONATE-RICH AEROSOL
Recorded: 79394 UTC
Date: 960503

m/z	Rel. Abund.	m/z	Rel. Abund.	m/z	Rel. Abund.
14	4	17	68	18	100
28	100	32	32	44	16

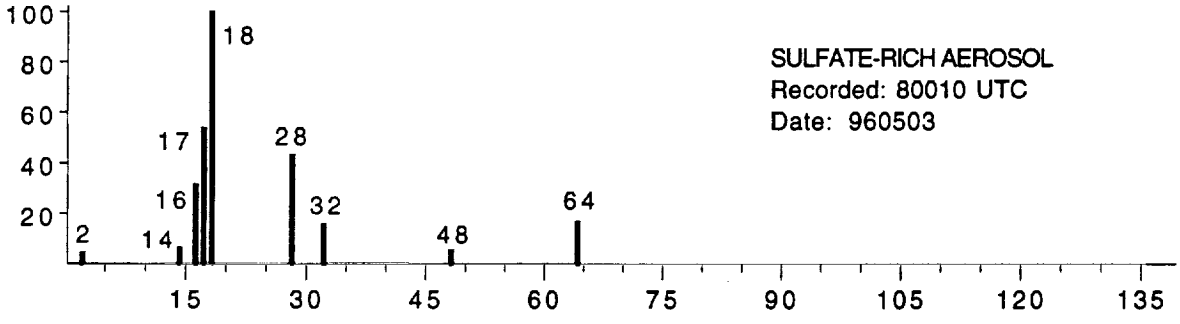

SULFATE-RICH AEROSOL
Recorded: 80010 UTC
Date: 960503

m/z	Rel. Abund.	m/z	Rel. Abund.	m/z	Rel. Abund.
2	4	14	7	16	32
17	54	18	100	28	43
32	16	48	5	64	17

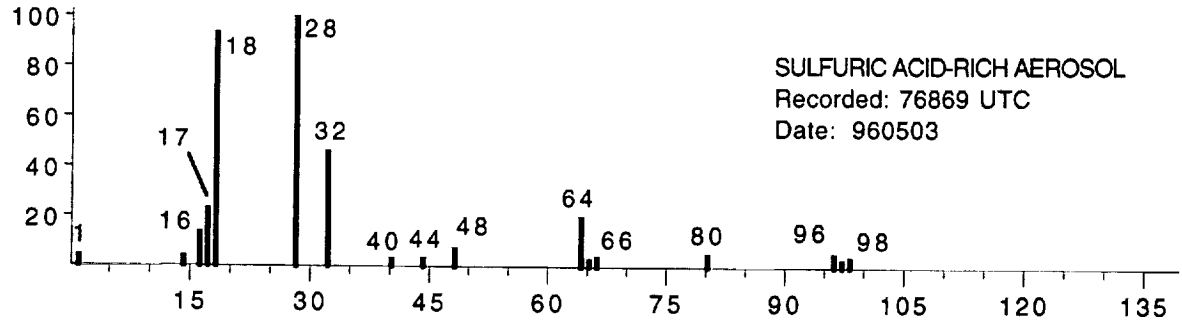

SULFURIC ACID-RICH AEROSOL
Recorded: 76869 UTC
Date: 960503

m/z	Rel. Abund.	m/z	Rel. Abund.	m/z	Rel. Abund.
1	4	14	5	16	14
17	23	18	93	28	100
32	47	40	3	44	4
48	7	64	20	65	3
66	4	80	5	96	5
97	3	98	5		

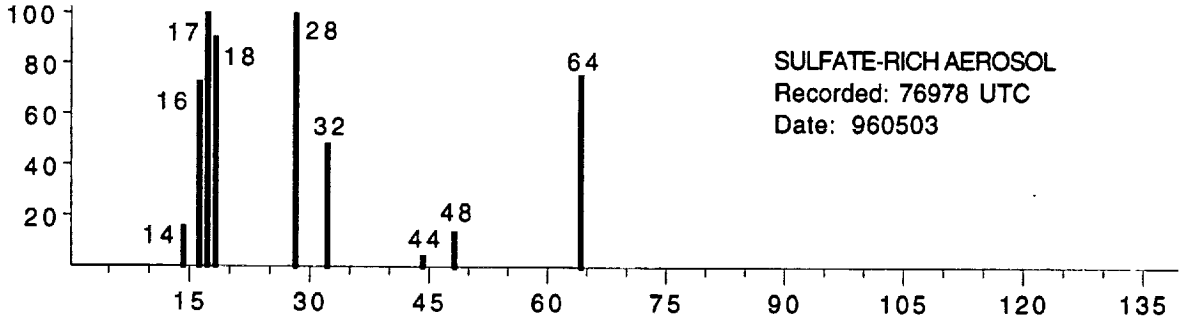

SULFATE-RICH AEROSOL
Recorded: 76978 UTC
Date: 960503

m/z	Rel. Abund.	m/z	Rel. Abund.	m/z	Rel. Abund.
14	16	16	73	17	100
18	91	28	100	32	48
44	4	48	14	64	75

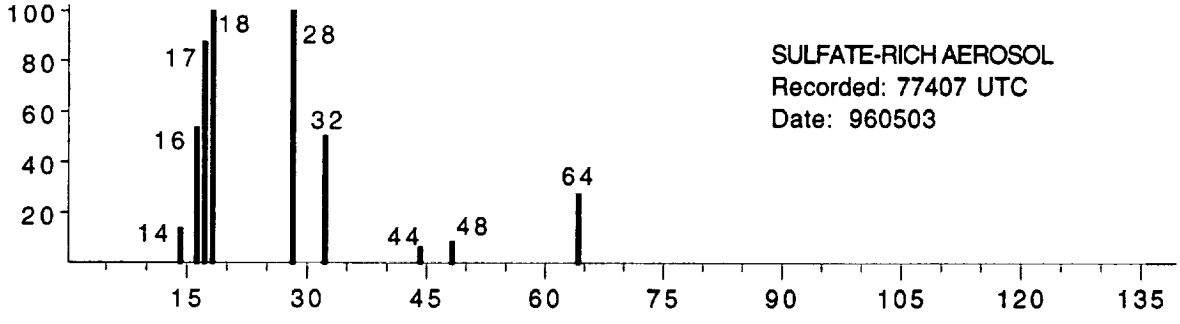

SULFATE-RICH AEROSOL
Recorded: 77407 UTC
Date: 960503

m/z	Rel. Abund.	m/z	Rel. Abund.	m/z	Rel. Abund.
14	14	16	54	17	87
18	100	28	100	32	51
44	6	48	9	64	27

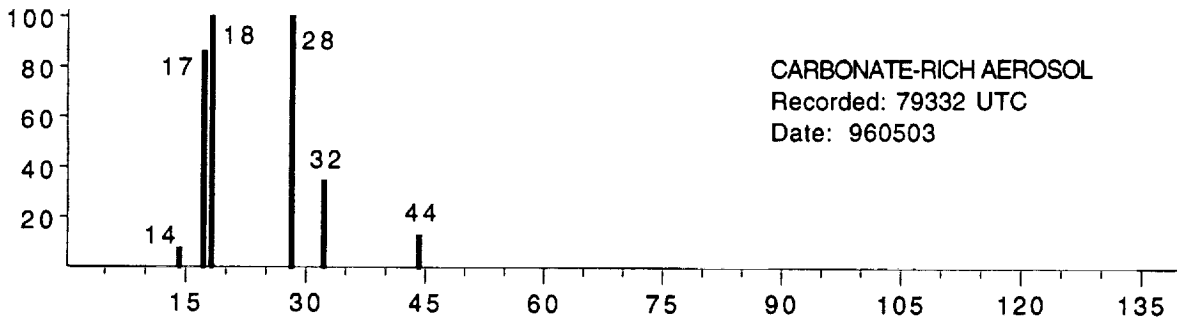

m/z	Rel. Abund.	m/z	Rel. Abund.	m/z	Rel. Abund.
14	7	17	86	18	100
28	100	32	35	44	13

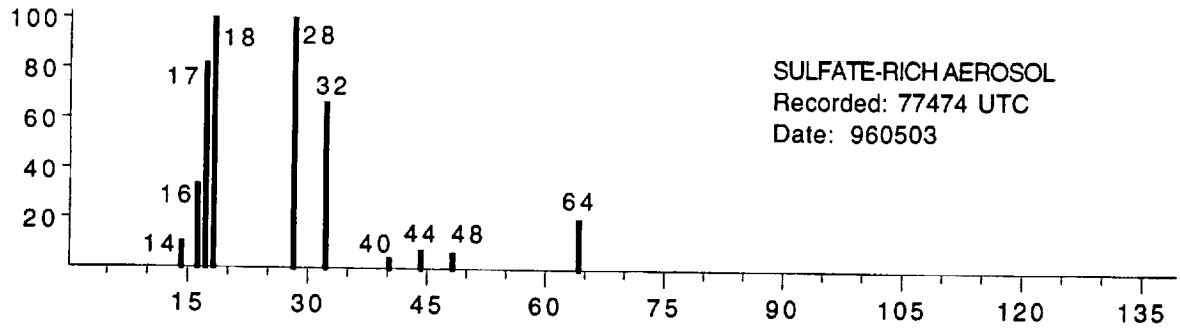

SULFATE-RICH AEROSOL
Recorded: 77474 UTC
Date: 960503

m/z	Rel. Abund.	m/z	Rel. Abund.	m/z	Rel. Abund.
14	10	16	34	17	82
18	100	28	100	32	67
40	4	44	8	48	6
64	20				

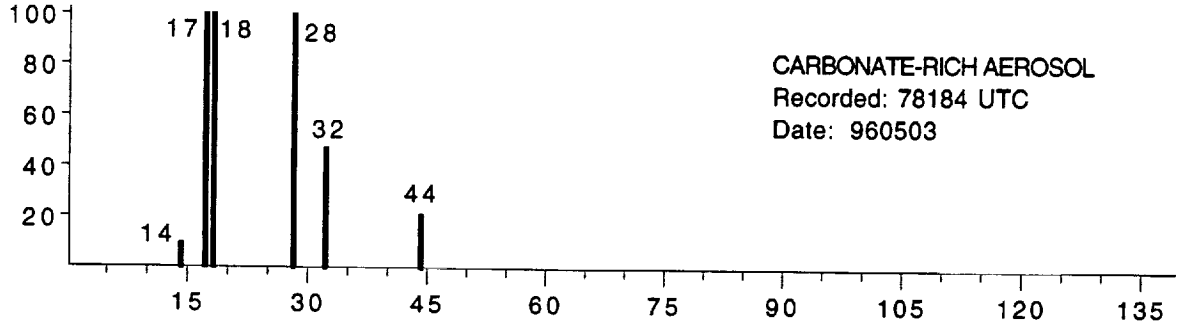

CARBONATE-RICH AEROSOL
Recorded: 78184 UTC
Date: 960503

m/z	Rel. Abund.	m/z	Rel. Abund.	m/z	Rel. Abund.
14	9	17	100	18	100
28	100	32	47	44	22

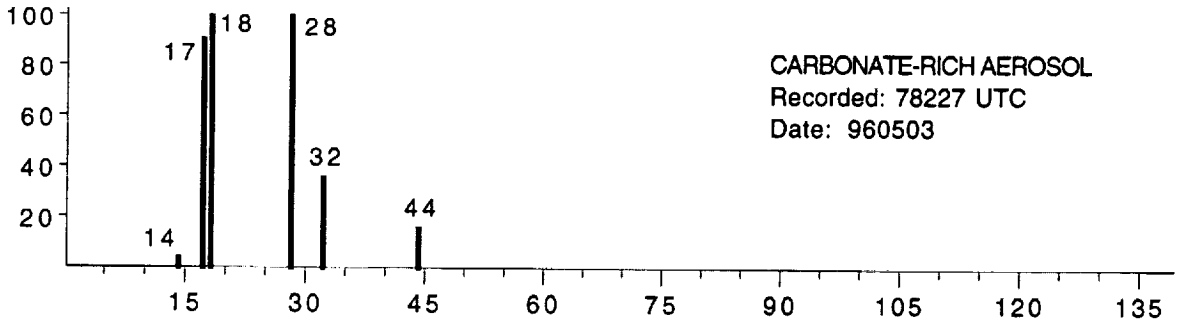

CARBONATE-RICH AEROSOL
Recorded: 78227 UTC
Date: 960503

m/z	Rel. Abund.	m/z	Rel. Abund.	m/z	Rel. Abund.
14	5	17	91	18	100
28	100	32	35	44	16

APPENDIX C

SELECTED AEROSOL MASS SPECTRA FROM SUCCESS MISSION

FLIGHT 09214

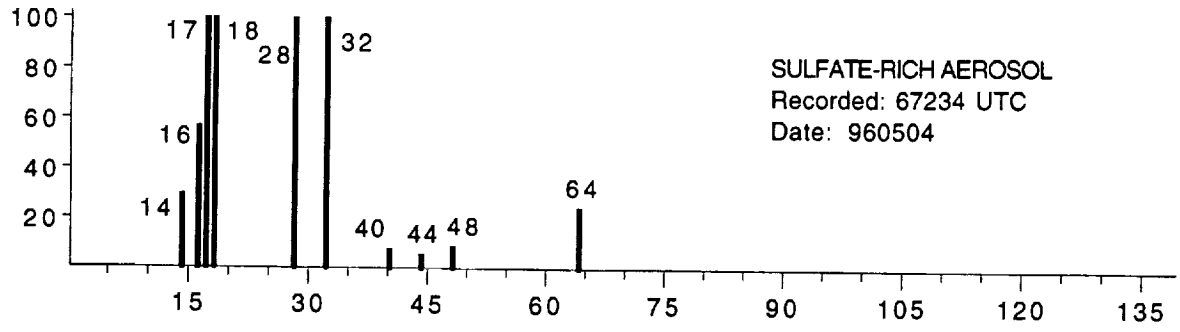

SULFATE-RICH AEROSOL
Recorded: 67234 UTC
Date: 960504

m/z	Rel. Abund.	m/z	Rel. Abund.	m/z	Rel. Abund.
14	29	16	57	17	100
18	100	28	100	32	100
40	7	44	5	48	9
64	24				

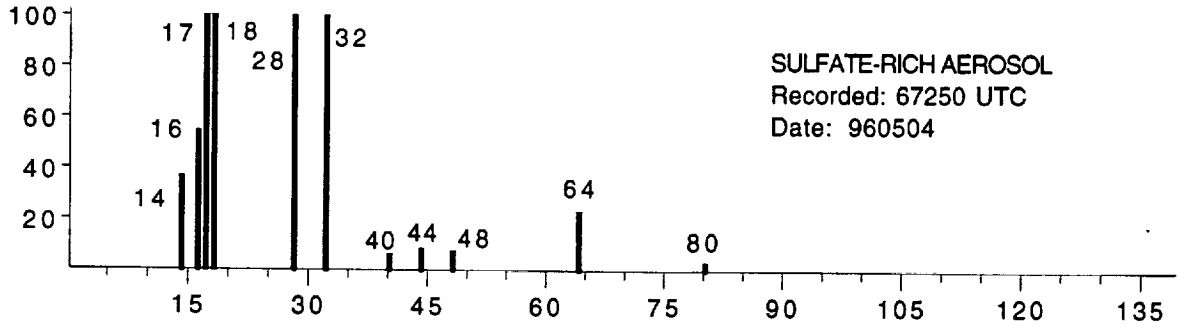

SULFATE-RICH AEROSOL
Recorded: 67250 UTC
Date: 960504

m/z	Rel. Abund.	m/z	Rel. Abund.	m/z	Rel. Abund.
14	37	16	55	17	100
18	100	28	100	32	100
40	7	44	9	48	7
64	23	80	3		

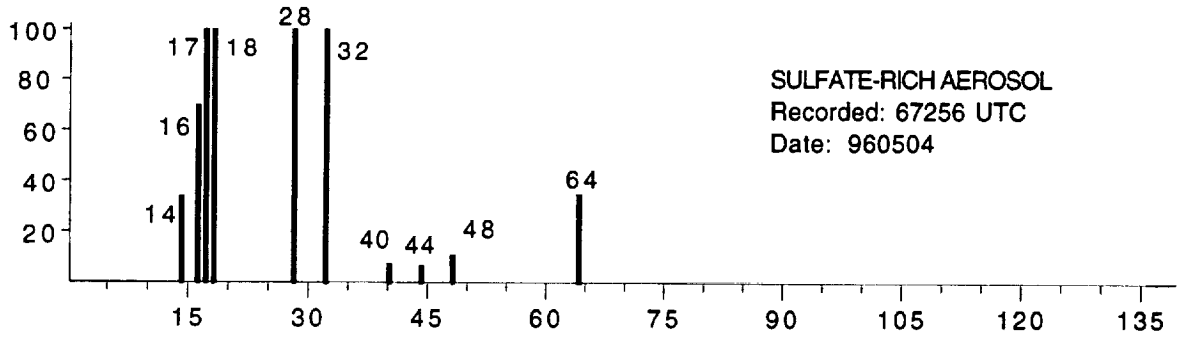

SULFATE-RICH AEROSOL
Recorded: 67256 UTC
Date: 960504

m/z	Rel. Abund.	m/z	Rel. Abund.	m/z	Rel. Abund.
14	34	16	69	17	100
18	100	28	100	32	100
40	7	44	6	48	11
64	35				

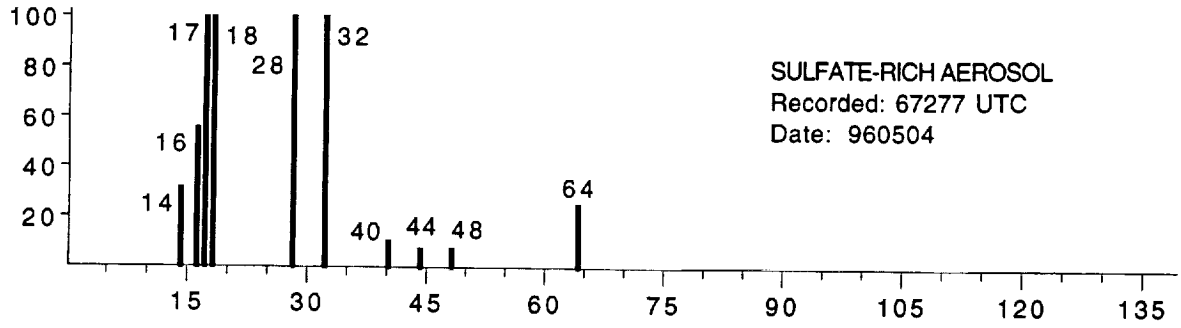

SULFATE-RICH AEROSOL
Recorded: 67277 UTC
Date: 960504

m/z	Rel. Abund.	m/z	Rel. Abund.	m/z	Rel. Abund.
14	31	16	55	17	100
18	100	28	100	32	100
40	11	44	7	48	8
64	25				

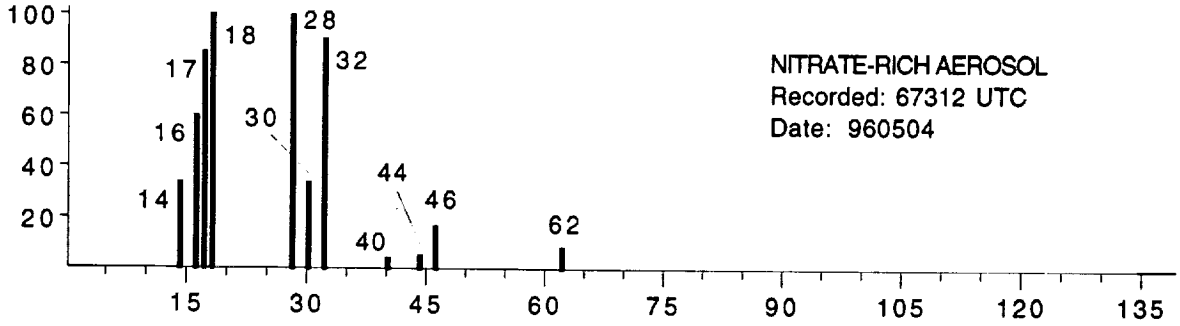

NITRATE-RICH AEROSOL
Recorded: 67312 UTC
Date: 960504

m/z	Rel. Abund.	m/z	Rel. Abund.	m/z	Rel. Abund.
14	34	16	60	17	85
18	100	28	100	30	34
32	91	40	4	44	5
46	17	62	9		

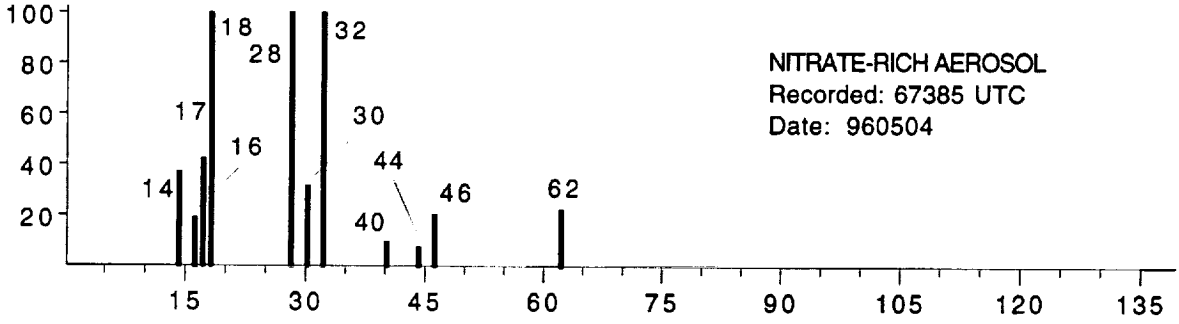

NITRATE-RICH AEROSOL
Recorded: 67385 UTC
Date: 960504

m/z	Rel. Abund.	m/z	Rel. Abund.	m/z	Rel. Abund.
14	36	16	19	17	42
18	100	28	100	30	31
32	100	40	10	44	7
46	20	62	22		

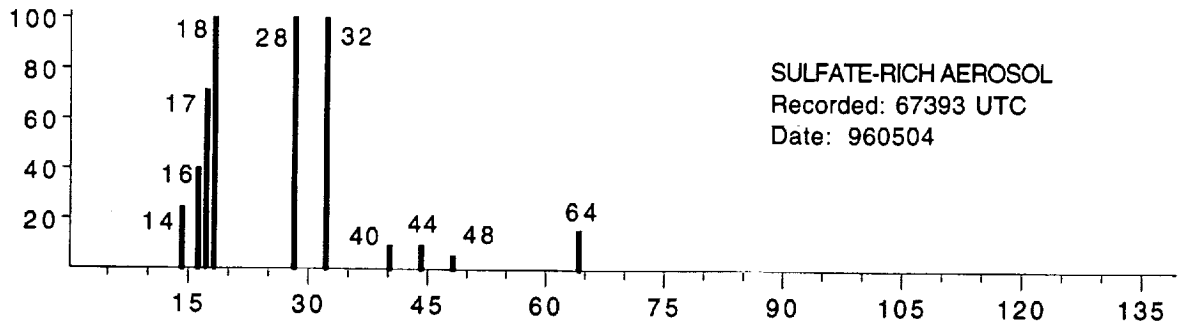

SULFATE-RICH AEROSOL
Recorded: 67393 UTC
Date: 960504

m/z	Rel. Abund.	m/z	Rel. Abund.	m/z	Rel. Abund.
14	25	16	40	17	72
18	100	28	100	32	100
40	10	44	9	48	5
64	15				

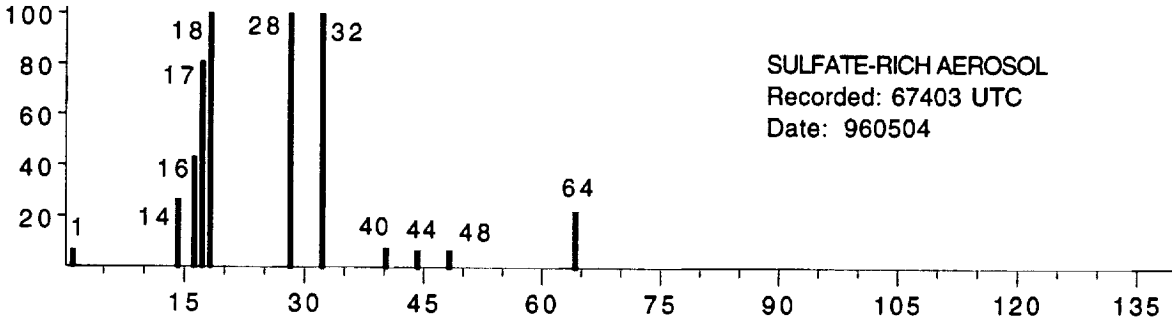

SULFATE-RICH AEROSOL
Recorded: 67403 UTC
Date: 960504

m/z	Rel. Abund.	m/z	Rel. Abund.	m/z	Rel. Abund.
1	6	14	27	16	43
17	81	18	100	28	100
32	100	40	7	44	6
48	7	64	22		

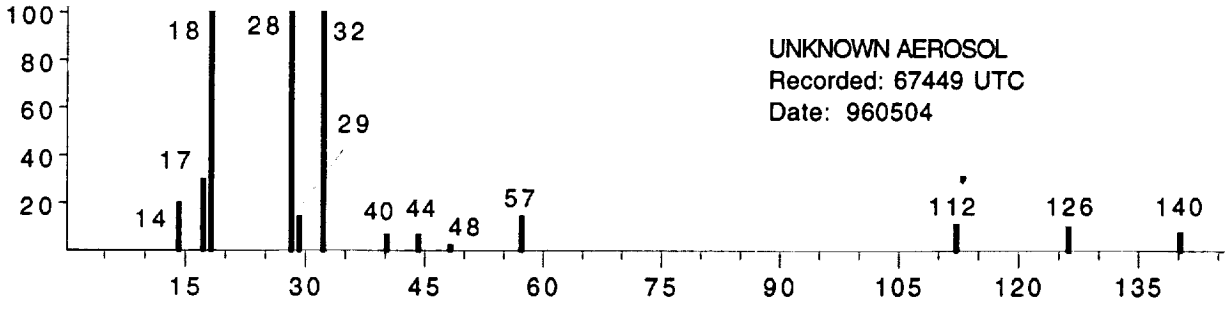

UNKNOWN AEROSOL
Recorded: 67449 UTC
Date: 960504

m/z	Rel. Abund.	m/z	Rel. Abund.	m/z	Rel. Abund.
14	20	17	30	18	100
28	100	29	14	32	100
40	7	44	7	48	3
57	15	112	11	126	10
140	7				

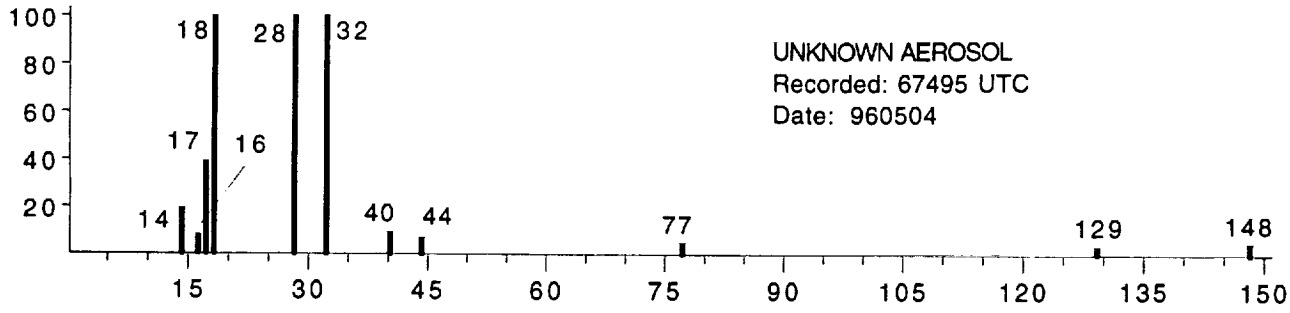

m/z	Rel. Abund.	m/z	Rel. Abund.	m/z	Rel. Abund.
14	19	16	7	17	38
18	100	28	100	32	100
40	9	44	7	77	4
129	3	148	5		

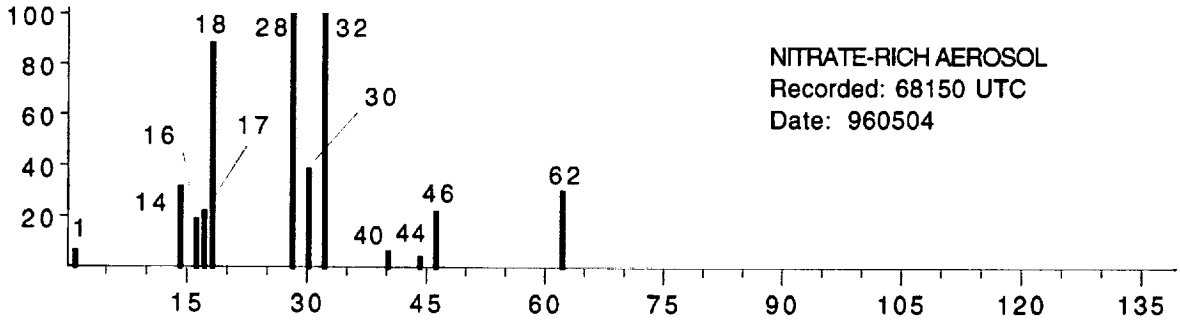

m/z	Rel. Abund.	m/z	Rel. Abund.	m/z	Rel. Abund.
1	6	14	32	16	18
17	22	18	89	28	100
30	38	32	100	40	7
44	4	46	22	62	31

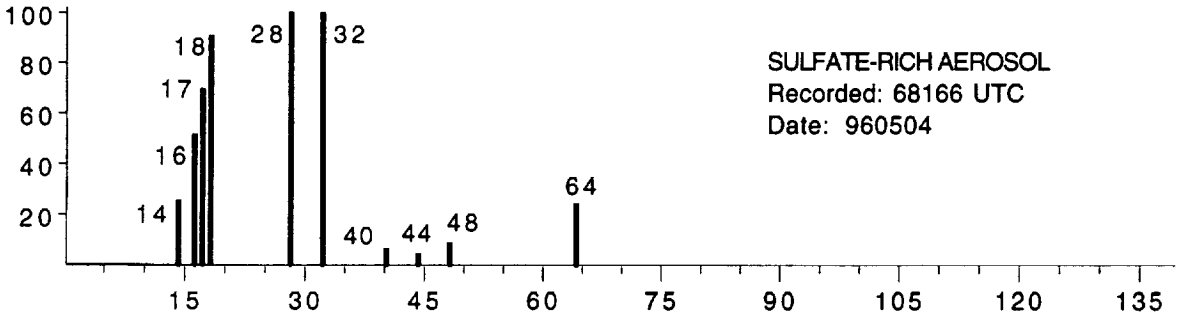

m/z	Rel. Abund.	m/z	Rel. Abund.	m/z	Rel. Abund.
14	25	16	51	17	69
18	90	28	100	32	100
40	7	44	5	48	8
64	24				

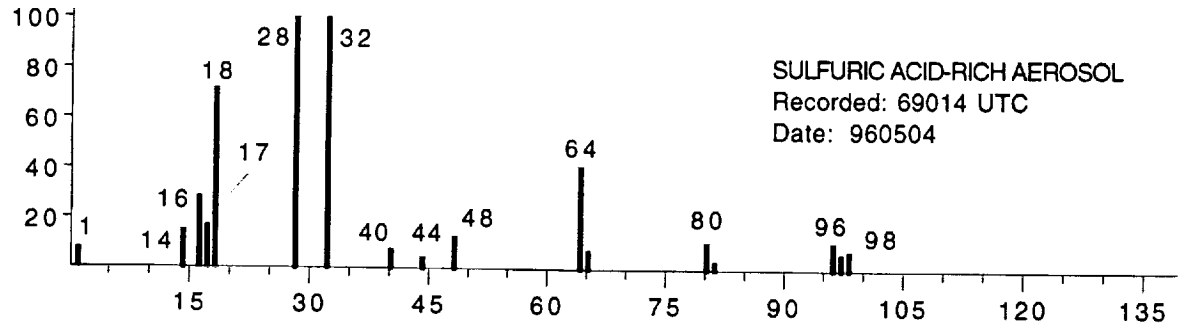

SULFURIC ACID-RICH AEROSOL
Recorded: 69014 UTC
Date: 960504

m/z	Rel. Abund.	m/z	Rel. Abund.	m/z	Rel. Abund.
1	7	14	15	16	28
17	17	18	71	28	100
32	100	40	7	44	4
48	12	64	41	65	7
80	10	81	4	96	11
97	6	98	7		

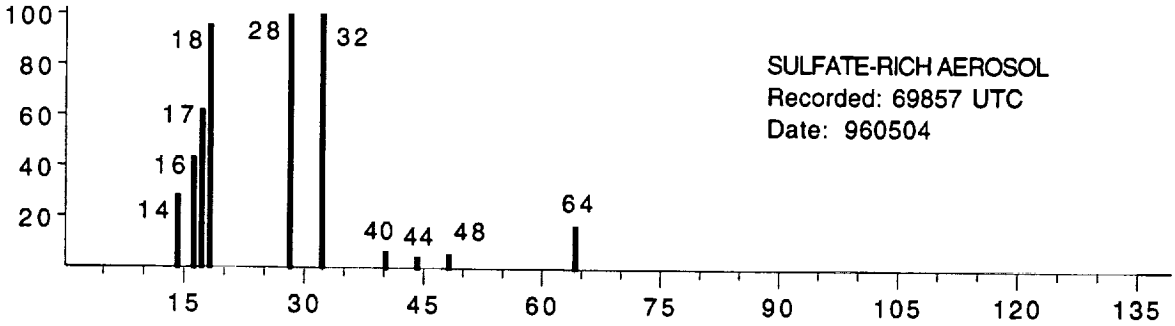

SULFATE-RICH AEROSOL
Recorded: 69857 UTC
Date: 960504

m/z	Rel. Abund.	m/z	Rel. Abund.	m/z	Rel. Abund.
14	29	16	43	17	62
18	95	28	100	32	100
40	7	44	4	48	5
64	17				

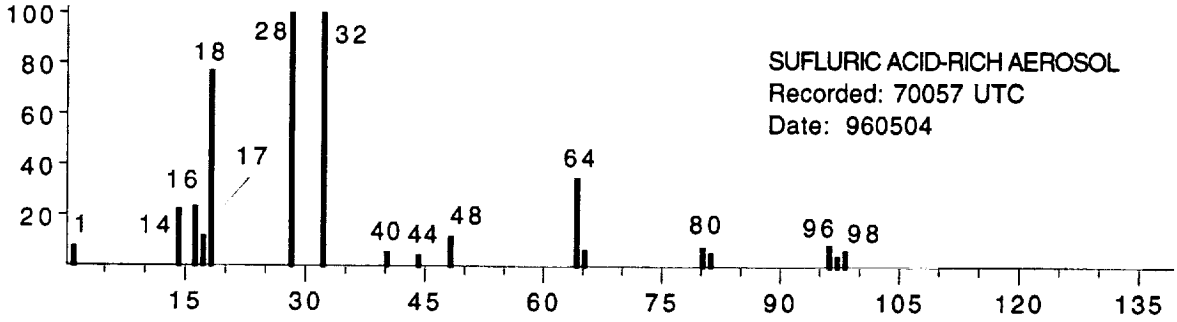

SUFLURIC ACID-RICH AEROSOL
Recorded: 70057 UTC
Date: 960504

m/z	Rel. Abund.	m/z	Rel. Abund.	m/z	Rel. Abund.
1	8	14	22	16	24
17	12	18	76	28	100
32	100	40	5	44	5
48	11	64	35	65	6
80	7	81	5	96	8
97	5	98	6		

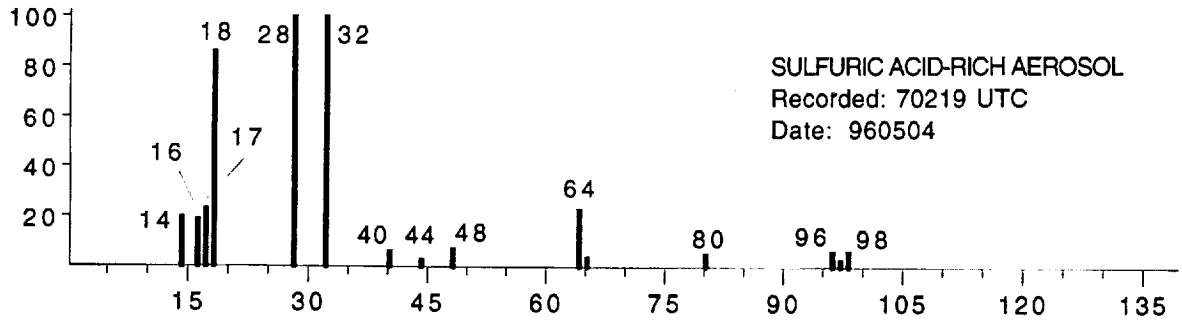

m/z	Rel. Abund.	m/z	Rel. Abund.	m/z	Rel. Abund.
14	20	16	19	17	24
18	87	28	100	32	100
40	6	44	3	48	8
64	23	65	4	80	5
96	6	97	4	98	6

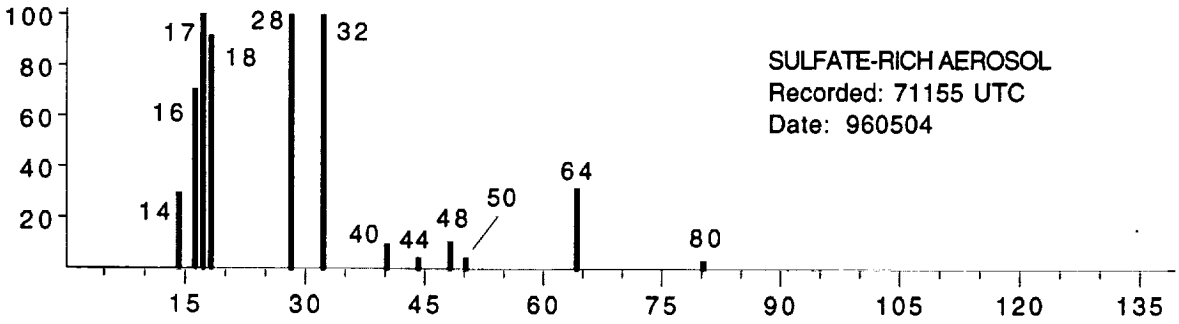

m/z	Rel. Abund.	m/z	Rel. Abund.	m/z	Rel. Abund.
14	29	16	71	17	100
18	91	28	100	32	100
40	9	44	5	48	11
50	4	64	31	80	3

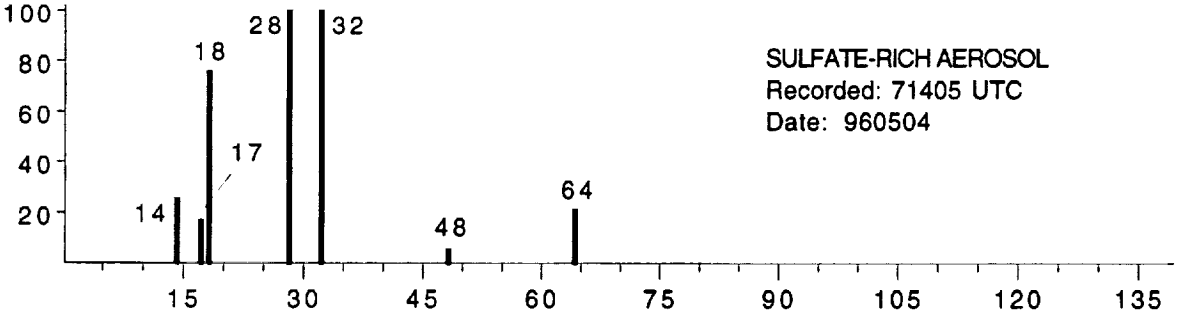

m/z	Rel. Abund.	m/z	Rel. Abund.	m/z	Rel. Abund.
14	25	17	17	18	76
28	100	32	100	48	5
64	22				

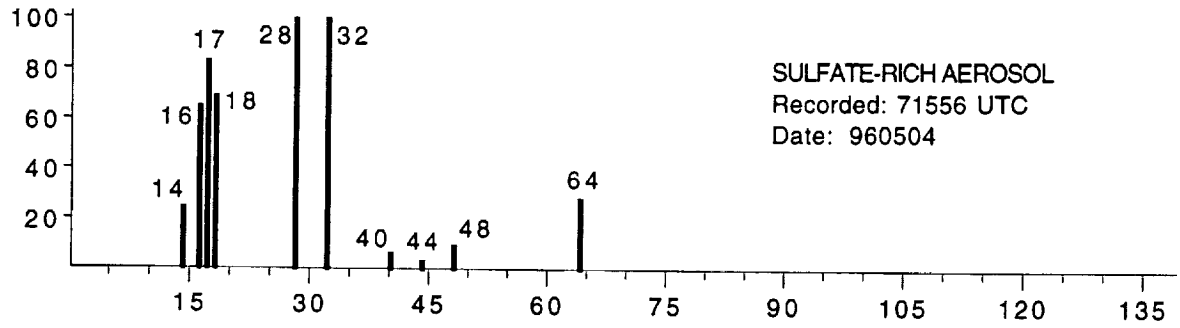

m/z	Rel. Abund.	m/z	Rel. Abund.	m/z	Rel. Abund.
14	25	16	65	17	84
18	69	28	100	32	100
40	6	44	3	48	9
64	29				

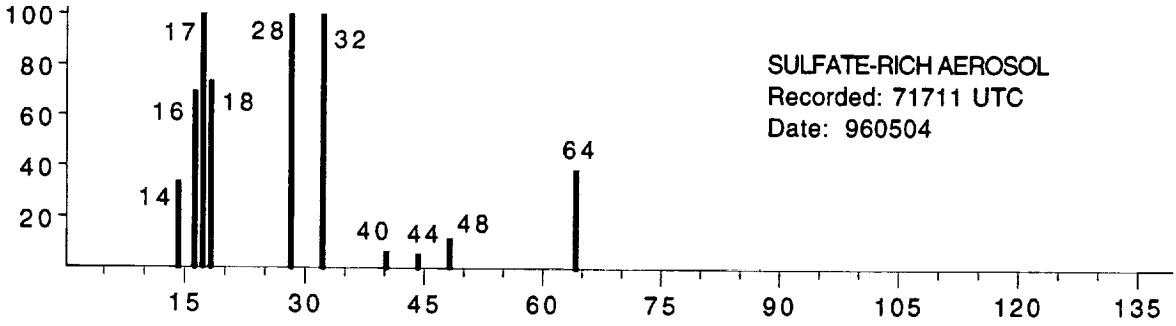

m/z	Rel. Abund.	m/z	Rel. Abund.	m/z	Rel. Abund.
14	34	16	69	17	100
18	74	28	100	32	100
40	6	44	5	48	12
64	39				

APPENDIX D

SELECTED AEROSOL MASS SPECTRA FROM SUCCESS MISSION

FLIGHT 09215

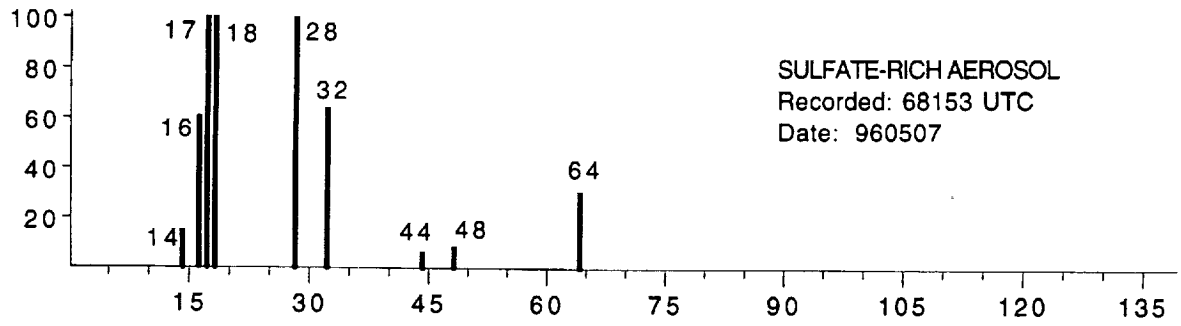

SULFATE-RICH AEROSOL
Recorded: 68153 UTC
Date: 960507

m/z	Rel. Abund.	m/z	Rel. Abund.	m/z	Rel. Abund.
14	15	16	61	17	100
18	100	28	100	32	64
44	6	48	8	64	30

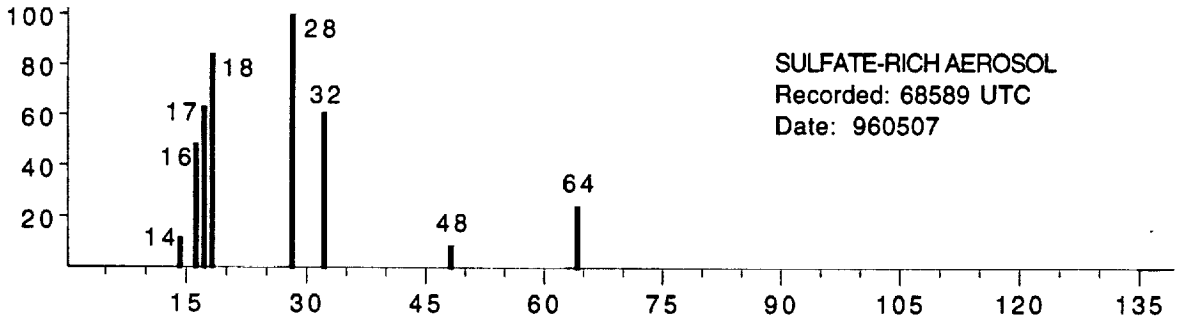

SULFATE-RICH AEROSOL
Recorded: 68589 UTC
Date: 960507

m/z	Rel. Abund.	m/z	Rel. Abund.	m/z	Rel. Abund.
14	11	16	48	17	63
18	84	28	100	32	62
48	8	64	25		

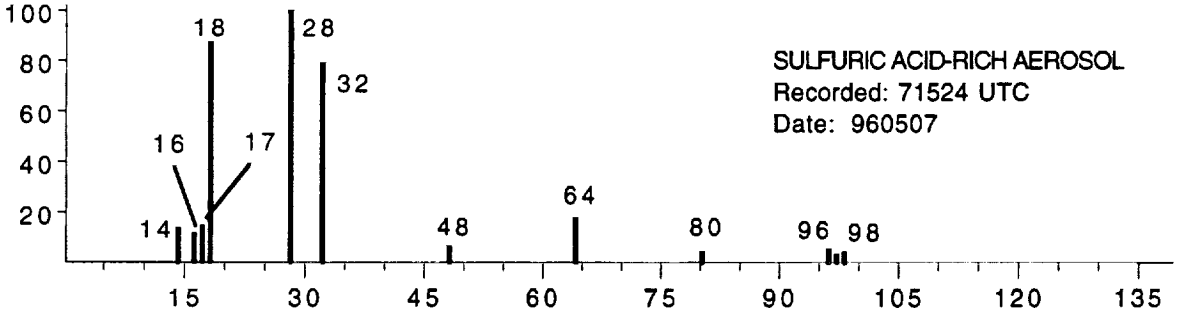

SULFURIC ACID-RICH AEROSOL
Recorded: 71524 UTC
Date: 960507

m/z	Rel. Abund.	m/z	Rel. Abund.	m/z	Rel. Abund.
14	14	16	12	17	15
18	87	28	100	32	79
48	7	64	18	80	5
96	5	97	3	98	5

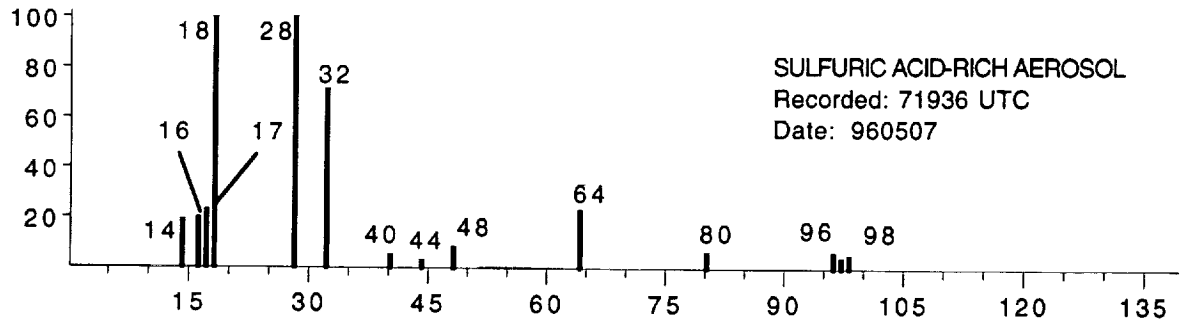

SULFURIC ACID-RICH AEROSOL
Recorded: 71936 UTC
Date: 960507

m/z	Rel. Abund.	m/z	Rel. Abund.	m/z	Rel. Abund.
14	18	16	20	17	23
18	100	28	100	32	72
40	5	44	4	48	9
64	23	80	6	96	6
97	4	98	5		

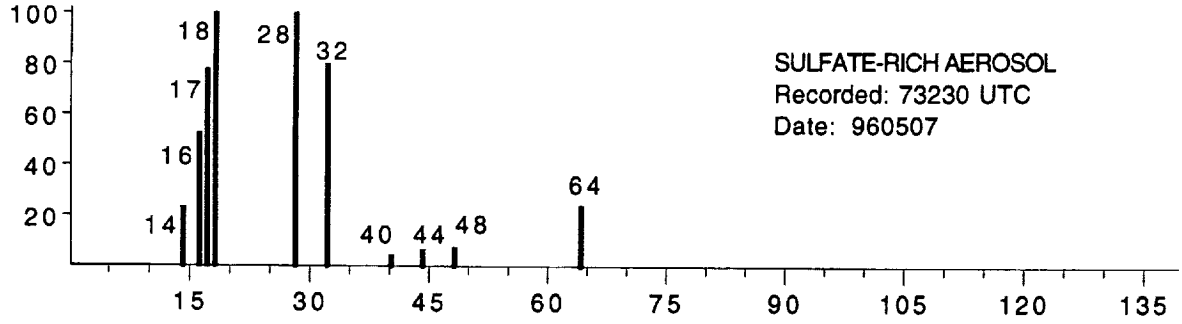

SULFATE-RICH AEROSOL
Recorded: 73230 UTC
Date: 960507

m/z	Rel. Abund.	m/z	Rel. Abund.	m/z	Rel. Abund.
14	23	16	53	17	78
18	100	28	100	32	80
40	5	44	6	48	7
64	24				

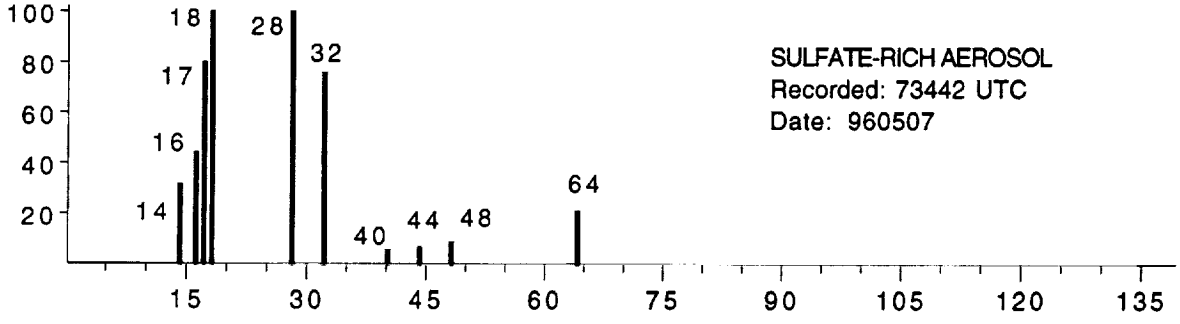

SULFATE-RICH AEROSOL
Recorded: 73442 UTC
Date: 960507

m/z	Rel. Abund.	m/z	Rel. Abund.	m/z	Rel. Abund.
14	31	16	45	17	80
18	100	28	100	32	75
40	5	44	6	48	8
64	21				

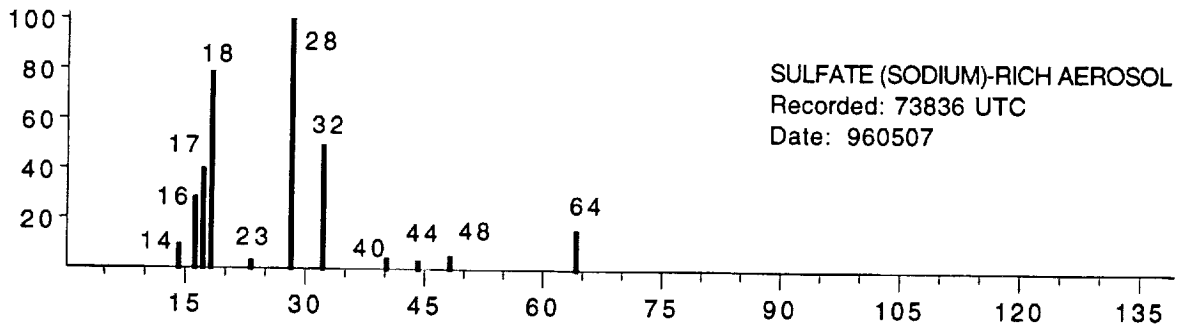

SULFATE (SODIUM)-RICH AEROSOL
Recorded: 73836 UTC
Date: 960507

m/z	Rel. Abund.	m/z	Rel. Abund.	m/z	Rel. Abund.
14	9	16	28	17	40
18	79	23	3	28	100
32	49	40	4	44	4
48	5	64	15		

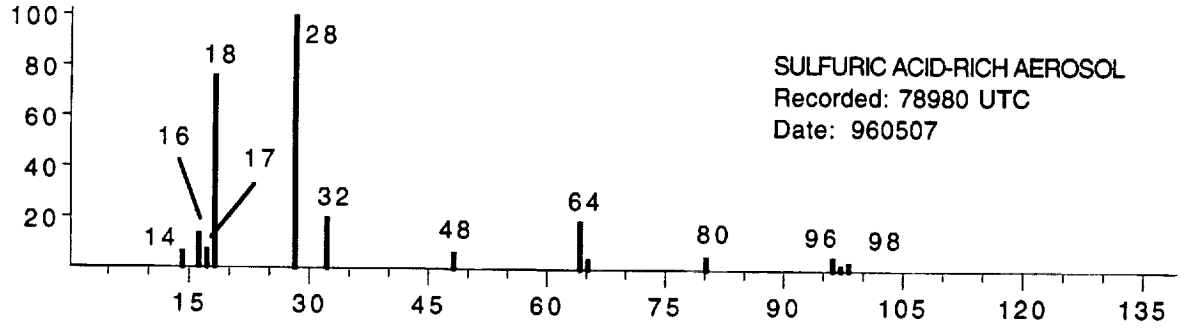

SULFURIC ACID-RICH AEROSOL
Recorded: 78980 UTC
Date: 960507

m/z	Rel. Abund.	m/z	Rel. Abund.	m/z	Rel. Abund.
14	6	16	13	17	8
18	75	28	100	32	20
48	7	64	19	65	4
80	5	96	5	97	2
98	3				

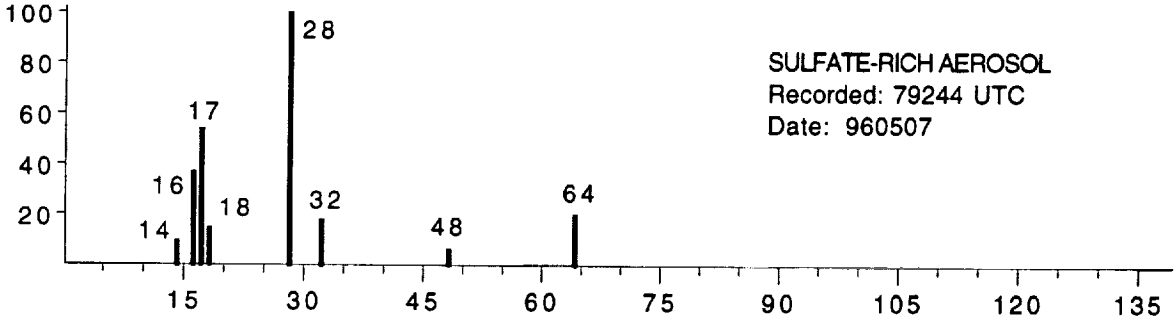

SULFATE-RICH AEROSOL
Recorded: 79244 UTC
Date: 960507

m/z	Rel. Abund.	m/z	Rel. Abund.	m/z	Rel. Abund.
14	9	16	37	17	53
18	15	28	100	32	18
48	7	64	20		

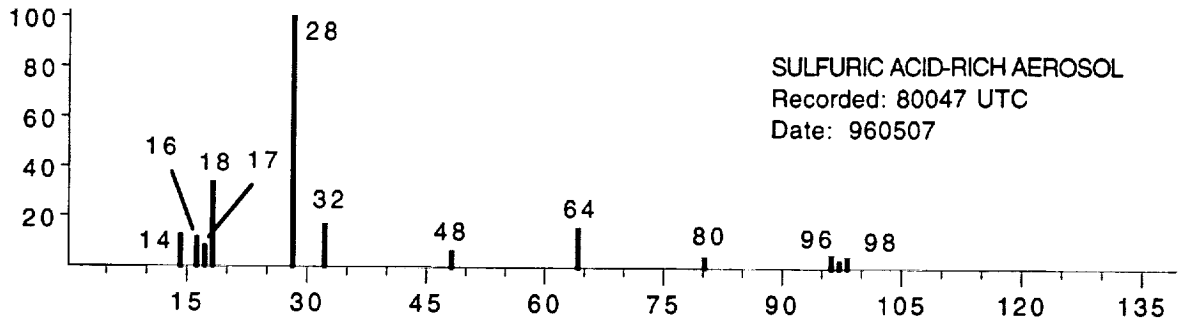

SULFURIC ACID-RICH AEROSOL
Recorded: 80047 UTC
Date: 960507

m/z	Rel. Abund.	m/z	Rel. Abund.	m/z	Rel. Abund.
14	13	16	11	17	8
18	33	28	100	32	16
48	7	64	16	80	5
96	5	97	3	98	4

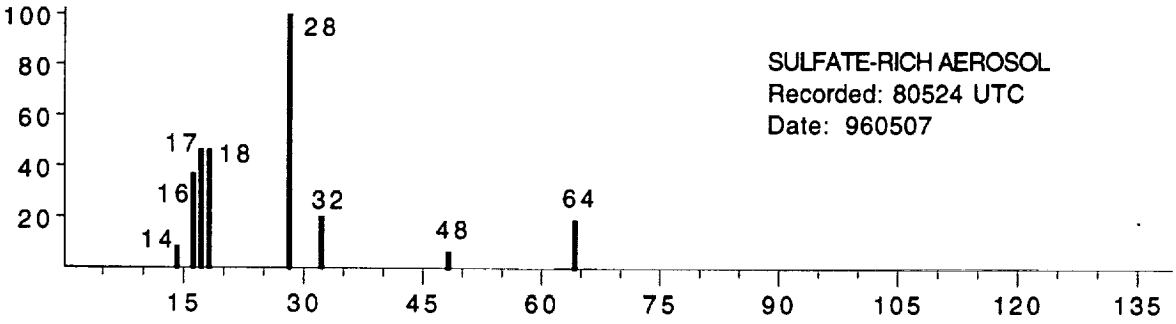

SULFATE-RICH AEROSOL
Recorded: 80524 UTC
Date: 960507

m/z	Rel. Abund.	m/z	Rel. Abund.	m/z	Rel. Abund.
14	8	16	36	17	46
18	46	28	100	32	20
48	6	64	19		

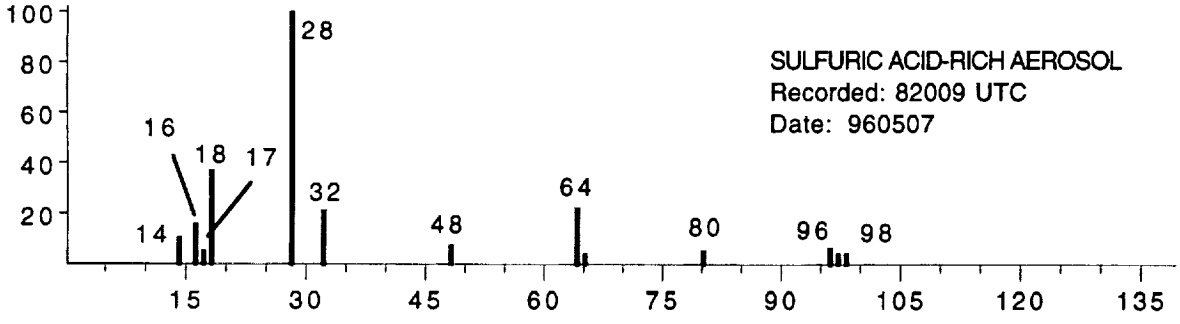

SULFURIC ACID-RICH AEROSOL
Recorded: 82009 UTC
Date: 960507

m/z	Rel. Abund.	m/z	Rel. Abund.	m/z	Rel. Abund.
14	11	16	15	17	5
18	36	28	100	32	21
48	7	64	22	65	5
80	5	96	7	97	4
98	5				